Zaitri
Mohamed Abdelaziz

Controlo Ótimo e Biomatemática: Modelação, Controlo e Otimização

Optimal Control and Biomathematics: Modeling, Control and Optimization

Zaitri
Mohamed Abdelaziz

Controlo Ótimo e Biomatemática: Modelação, Controlo e Otimização

Optimal Control and Biomathematics: Modeling, Control and Optimization

"*The measure of intelligence is the ability to change*"

— Albert Einstein

Universidade de Aveiro
2023

Zaitri
Mohamed Abdelaziz

Controlo Ótimo e Biomatemática: Modelação, Controlo e Otimização

Optimal Control and Biomathematics: Modeling, Control and Optimization

Tese apresentada à Universidade de Aveiro para cumprimento dos requisitos necessários à obtenção do grau de Doutor em Matemática, Programa Doutoral em Matemática (PDMat-UA), realizada sob a orientação científica do Doutor Delfim Fernando Marado Torres, Professor Catedrático do Departamento de Matemática da Universidade de Aveiro, e da Doutora Cristiana João Soares da Silva, Professor Auxiliar do Departamento de Matemática ISCTE–Instituto Universitário de Lisboa

Ph.D. thesis submitted to the University of Aveiro in fulfilment of the requirements for the degree of Doctor of Philosophy in Mathematics, Doctoral Programme in Mathematics (PDMat-UA), under the scientific supervision of Professor Delfim Fernando Marado Torres, Full Professor of Department of Mathematics, University of Aveiro, and Professor Cristiana João Soares da Silva, Assistant Professor of the Department of Mathematics, ISCTE–University Institute of Lisbon.

I dedicate this work to my father Slimane, my mother Naouia, my wife Nadia, my children Iyad and Lina, and my niece Ritaj, for the unwavering support you have provided me.

o júri / the jury

presidente / president

Prof. Doutor José Carlos Esteves Duarte Pedro
Professor Catedrático, Universidade de Aveiro

vogais / examiners committee

Prof. Doutor Delfim Fernando Marado Torres (Orientador)
Professor Catedrático, Universidade de Aveiro

Prof. Doutora Cristiana João Soares Da Silva (Co-orientador)
Professora Auxiliar, ISCTE – Instituto Universitário de Lisboa

Prof. Doutor Jorge das Neves Duarte
Professor Coordenador com Agregação, Instituto Superior de Engenharia de Lisboa

Prof. Doutor Silvério Simões Rosa
Professor Auxiliar, Universidade da Beira Interior

Prof. Doutor Patrícia Andreia da Silva Filipe
Professor Auxiliar, Iscte – Instituto Universitário de Lisboa

Prof. Doutor Ana Pedro Lemos Paião
Professor Adjunto Convidado, ESTGA, Universidade de Aveiro

agradecimentos / acknowledgements

I am deeply grateful and would like to express my sincere thanks to my supervisor, Prof. Delfim F. M. Torres, and my co-supervisor, Prof. Cristiana J. S. Silva, for their unwavering support throughout my PhD study. Their unfailing friendliness, exceptional professionalism, and continuous guidance have played an integral role in my research journey.

I am truly thankful for their generosity in sharing their extensive knowledge with me, providing valuable advice, and keeping me motivated throughout this process. It has been an absolute pleasure working with Prof. Torres, and I am profoundly appreciative of the time he dedicated to me, as well as his exceptional pedagogical and scientific qualities.

I would also like to express my deep gratitude to my parents for the invaluable education they provided me. Their unwavering support and belief in my abilities have been instrumental in my academic and personal growth.

Furthermore, I am grateful to my family for their constant moral and emotional support throughout my life. Their encouragement and understanding of the challenges I faced during my PhD journey have been a source of strength.

Lastly, I would like to extend my thanks to the Center for Research and Development in Mathematics and Applications (CIDMA – University of Aveiro) for their financial support through projects UIDB/04106/2020 and UIDP/04106/2020. Their support has been crucial in enabling me to pursue and successfully complete my research.

Palavras Chave

modelação matemática, equação do calor, sistemas de controlo, sistemas com tempo de atraso, otimização, controlo ótimo, extremos de Pontryagin, cálculo fracionário, modelo SEIR, modelo farmacocinético/farmacodinâmico, pontos de equilíbrio, estabilidade, análise da propagação de doenças, vacinação.

Resumo

Nesta tese de doutoramento, aplicamos a teoria do controlo ótimo a um modelo farmacocinético/farmacodinâmico (PK/PD) e a um modelo epidemiológico do tipo SEIR.

Primeiro, estudamos as propriedades do modelo PK/PD para controlar a infusão de propofol. Começamos por analisar um model matemático para a anestesia e determinamos uma solução analítica para o problema de control ótimo de tempo mínimo para a fase de indução da anestesia, mostrando que esta coincide numericamente com a solução obtida usando o método de tiro. Considerando o princípio do mínimo de Pontryagin, resolvemos o problema de controlo ótimo de tempo mínimo através de um novo método analítico e mostramos que a taxa de infusão contínua ótima do anestésico e o tempo mínimo requerido para passar do estado de vigília para o estado de anesthesia são semelhantes usando os dois métodos. Além disso, analisamos um model fracionário de Anestesia PK/PD via derivadas fracionais de psi-Caputo.

A segunda parte da tese é dedicada ao desenvolvimento de um modelo do tipo SEIR. Primeiramente, analisamos modelos matemáticos para a COVID-19 com tempos de atrasos discretos e vacinação. Mas precisamente, introduzimos um tempo de atraso que representa, matematicamente, o fato de a migração de indivíduos suscetíveis para infetados estar sujeita a tempos de atraso. Um dos resultados mais importantes em sistemas dinâmicos é a estabilidade. Nesta tese demonstramos condições suficientes para a estabilidade local dos pontos de equilíbrio endémico e livre de doença, para qualquer tempo de atraso positive. Para combater a propagação da COVID-19, propomos um modelo com controlo, generalizando o modelo do tipo SEIR. Além disso, introduzimos três controlos ao modelo SEIR e analisamos o problema de controlo ótimo da transmissão da doença usando dados reais de Itália. Os nossos resultados mostram o ajuste do modelo aos dados reais, em particular no que diz respeito ao número de indivíduos em quarentena e recuperados. Considerando os controlos de Pontryagin, mostramos como num mundo perfeito seria possível diminuir drasticamente o número de indivíduos suscetíveis, expostos, infetados, em quarentena/hospitalizados e óbitos, aumentando a população de protegidos. Além disso, apresentamos um modelo para manter a eficácia da vacina para a COVID-19 desde o transporte da área de armazenamento na fábrica até ao destino desejado e introduzir a vacina na população suscetível, a fim de controlar a disseminação da COVID-19.

Mostramos a importância da vacina para o controlo da propagação da COVID-19 e também na melhoria do resultado que poderia ser obtido se o número de vacinas disponíveis satisfizesse as necessidades da população e fossem distribuídas de acordo com a teoria do controlo ótimo.

Classificação de Disciplinas de Matemática 2020: 49K15, 49M05, 49N90, 34C60, 92C45, 92D30.

Keywords mathematical modeling, heat equation, control systems, delayed systems, optimization, optimal control, Pontryagin extremals, fractional calculus, SEIR model, pharmacokinetic/pharmacodynamic model, equilibrium points, stability, analysis of the spread of diseases, vaccination.

Abstract In this Ph.D. thesis, we apply optimal control theory to various mathematical models, including a pharmacokinetic/pharmacodynamic (PK/PD) model, a fractional PK/PD model, and an epidemiological SEIR models.

First, we focus on the PK/PD model to control the infusion of propofol. We begin by analyzing the mathematical model of anesthesia and provide an analytical solution to the time-optimal control problem for the induction phase of anesthesia. Our approach aligns closely with results obtained using the standard shooting method. Utilizing the Pontryagin minimum principle, we propose a new analytical method for solving the time-optimal control problem. Our findings reveal that the optimal continuous infusion rate of the anesthetic and the minimum time required to transition from an awake state to an anesthetized state are consistent between both methods. Furthermore, we extend our analysis to a PK/PD anesthesia model using psi-caputo fractional derivatives.

The second part of the thesis focuses on the development of an SEIR model. Initially, we explore mathematical models for COVID-19 with discrete time delays and vaccination. Specifically, we introduce a time delay to account for the delayed migration of individuals from susceptible to infected states. We establish sufficient conditions for the local stability of both endemic and disease-free equilibrium points in the presence of positive time delays. To address the COVID-19 pandemic, we propose a generalized SEIR-type control model. Additionally, we introduce three time-dependent controls for the SEIR model and analyze the optimal control problem with respect to real data transmission in Italy. Our results demonstrate the effectiveness of the model, particularly concerning the number of quarantined and recovered individuals. By considering Pontryagin controls, we illustrate the potential for significant reductions in susceptible, exposed, infected, quarantined/hospitalized, and deceased individuals through increased population protection. We also present a model for maintaining the efficacy of COVID-19 vaccines during transportation and distribution, emphasizing the importance of vaccination in controlling the pandemic.

2020 Mathematics Subject Classification: 49K15, 49M05, 49N90, 34C60, 92C45, 92D30.

Contents

List of Figures

List of Tables

Glossary

PMP	Pontryagin's Minimum Principle
PK	Pharmacokinetic
PD	Pharmacodynamic
PK/PD	Pharmacokinetic/ Pharmacodynamic
LBM	Lean Body Mass
BIS	Bispectral Index
SIR	Susceptible–Infectious–Recovered
SEIR	Susceptible–Exposed–Infectious–Recovered
SEIQRP	Susceptible–Exposed–Infectious–Quaranted–Recovered–Protected
SEIQRPW	Susceptible–Exposed–Infectious–Quaranted–Recovered–Protected–Vaccinated
DFE	Disease Free Equilibrium Point
EE	Endemic Equilibrium Point
EEG	Electroencephalography

CHAPTER 1

Introduction

1.1 Scope of the study

Optimal control is a mathematical theory that consists of finding a control that optimizes a functional on a domain described by a system of differential equations. This theory is applied in various scientific fields. The Pontryagin's Minimum Principle (PMP) is used to find the necessary conditions for optimal controls [1]. In this thesis, we embark on a comprehensive exploration of various mathematical models and control problems in the fields of anesthesia, infectious diseases, and vaccine distribution. Our research objectives are as follows:

1. To delve into a mathematical model of anesthesia and investigate the time-optimal control problem concerning the induction phase of anesthesia.
2. To analyze the stability of equilibrium points, both endemic and disease-free, within infectious disease models.
3. To extend our mathematical models for infectious diseases by incorporating discrete time delays, enhancing our understanding of real-world dynamics.
4. To forecast the spread of infectious diseases and demonstrate the effectiveness of our epidemic models in capturing real-world scenarios.
5. To apply the principles of optimal control theory to the mathematical models previously developed. Specifically, we employ the Pontryagin minimum/maximum principle to derive essential optimality conditions.
6. To explore mathematical models for the transportation of vaccines, with a particular focus on the heat diffusion equation as a basis for analysis and optimization.

This thesis aims to contribute to the fields of mathematical modeling and control theory, offering valuable insights and practical applications in the domains of anesthesia, epidemiology, and vaccine logistics.

1.2 Motivation

Presently, the field of modern pharmacotherapy is still under vigorous development. Based on Guedel's classification, the first stage of anesthesia is the induction phase, which begins with the initial administration of anesthesia and ends with loss of consciousness [2]. Millions of people safely receive several types of anesthesia while undergoing medical procedures: local anesthesia, regional anesthesia, general anesthesia, and sedation [3]. However, there may be some potential complications of anesthesia including anesthetic awareness, collapsed lung, malignant hyperthermia, nerve damage, and postoperative delirium. Certain factors make it riskier to receive anesthesia, including advanced age, diabetes, kidney disease, heart disease, high blood pressure and smoking [4]. To avoid the risk, administering anesthesia should be done on a scientific basis, based on modern pharmacotherapy, which relies on both Pharmacokinetic (PK) and Pharmacodynamic (PD) information [5]. PK is used to describe the absorption and distribution of anesthesia in body fluids, resulting from the administration of a certain anesthesia dose. PD is the study of the effect resulting from anesthesia [6]. Multiple mathematical models were already presented to predict the dynamics of the PK/PD models [7]–[10]. Some of these models were implemented following different methods [3], [11], [12]. Some of these models were implemented following different methods [3], [11], [12].

The parameters of PK/PD models were fitted by Schnider et al. in [13]. In [7], the authors study PK models for propofol, comparing Schnider et al. and Marsh et al. models [14]. The authors of [7] conclude that Schnider's model should always be used in effect-site targeting mode, in which larger initial doses are administered but smaller than those obtained from Marsh's model. However, users of the Schnider model should be aware that in the morbidly obese the Lean Body Mass (LBM) equation can generate paradoxical values, resulting in excessive increases in maintenance infusion rates [13]. In [15], a new strategy is presented to develop a robust control of anesthesia for the maintenance phase, taking into account the saturation of the actuator. The authors of [16] address the problem of optimal control of the induction phase. For other related works see [9], [17] and references therein.

On the other hand, multiple mathematical models were already presented to predict the dynamics of infectious disease at a regional and global level, and some of these models were implemented, following different methods [18], to evaluate a strategy for preventive measures: in [19], the classical Susceptible–Infectious–Recovered (SIR) modeling approach [20] was employed to study the parameters of this model for India while considering different governmental lockdown measures; in [21], the length of the incubation period of COVID-19 is estimated using confirmed COVID-19 cases reported

between January 4 and February 24, 2020, from fifty provinces, regions, and counties from China; in [22] a model of the outbreak in Wuhan, with individual reaction and governmental action (holiday extension, city lockdown, hospitalisation and quarantine) is analyzed in the light of the 1918 influenza pandemic in London; in [23], SEIR modeling is considered to forecast the COVID-19 outbreak in Algeria by using real data from March 1 to April 10, 2020; in [24], a modified SEIR model is considered under three intervention scenarios (suppression, mitigation, mildness) and simulated to predict and investigate the realities in several African countries: South Africa, Egypt, Algeria, Nigeria, Senegal and Kenya. The list of such studies is long: see, e.g., [25] for a new compartmental epidemiological model for COVID-19 with a case study of Portugal; [26] for a fractional (non-integer order) model applied to COVID-19 in Galicia, Spain and Portugal; [27] for a stochastic time-delayed COVID-19 model with application to the Moroccan deconfinement strategy; etc.

In [28], a mathematical system, generalizing the SEIR model, is presented to analyze the COVID-19 epidemic based on a dynamic mechanism that incorporates the intrinsic impact of hidden latent and infectious cases on the entire process of the virus transmission. The authors of [28] validate their model by analyzing data correlation on public data of the National Health Commission of China from January 20 to February 9, 2020, and produce reliable estimates and predictions, revealing key parameters of the COVID-19 epidemic.

1.3 Structure

This thesis is organized in the following manner.

In Chapter 2, we study properties of PK/PD model for controlling the infusion of propofol. We start by analyzing a mathematical model of anesthesia and provide an analytical solution to the time-optimal control problem for the induction phase of anesthesia. Moreover, we also solve the time-optimal control problem by the new proposed analytical method and find that the optimal continuous infusion rate of the anesthetic and the minimum time that needs to be chosen to transfer from the awake state to an anesthetized state are similar between both methods. However, the new analytic method has the advantage of not depending on unknown initial conditions for the adjoint variables.

In Chapter 3, we recall several definitions and properties of fractional calculus which will be needed in the sequel. Next, we present a novel PK/PD model for the induction phase of anesthesia, incorporating the ψ-Caputo fractional derivative. By employing the Picard iterative process, we derive a solution for the nonhomogeneous

ψ-Caputo fractional system. To explore the dynamics of the fractional anesthesia model, we perform numerical analysis on solutions involving various functions of ψ and fractional orders. All numerical simulations are conducted using the MATLAB computing environment.

In Chapter 4, we analyze mathematical models for COVID-19 with discrete time delays and vaccination. Sufficient conditions for the local stability of the endemic and disease-free equilibrium points are proved for any positive time delay. The stability results are illustrated through numerical simulations performed in MATLAB.

In Chapter 5, we apply optimal control theory to a generalized SEIR-type model. The proposed system has three controls, representing social distancing, preventive means, and treatment measures to combat the spread of the COVID-19 pandemic. We analyze such optimal control problem with respect to real data transmission in Italy. Our results show the appropriateness of the model, in particular with respect to the number of quarantined/hospitalized (confirmed and infected) and recovered individuals. Considering the Pontryagin controls, we show how in a perfect world one could have drastically diminish the number of susceptible, exposed, infected, quarantined/hospitalized, and death individuals, by increasing the population of insusceptible/protected.

In Chapter 6, we develop a mathematical model for transferring the vaccine BNT162b2 based on the heat diffusion equation. Then, we apply optimal control theory to the proposed generalized SEIR model. We introduce vaccination for the susceptible population to control the spread of the COVID-19 epidemic. For this, we use the Pontryagin minimum principle to find the necessary optimality conditions for the optimal control. The optimal control problem and the heat diffusion equation are solved numerically. Finally, several simulations are done to study and predict the spread of the COVID-19 epidemic in Italy. In particular, we compare the model in the presence and absence of vaccination.

1.4 Contributions

The following sections list the key contributions associated with this work.

1.4.1 Communications in international conferences and seminars

[1] M. A. Zaitri, C. J. Silva, and D. F. M. Torres, "Stability analysis of a delayed COVID-19 model," The Cape Verde International Days on Mathematics 2021, Praia, Cape Verde, 2021.

[2] M. A. Zaitri, M. O. Bibi, and D. F. M. Torres, "Contrôle optimal pour limiter la propagation de COVID-19," Séminaire Mathématique de Béjaia, LaMOS, University of Bejaia, Algeria, 2022.

1.4.2 Book chapter

[1] M. A. Zaitri, M. O. Bibi, and D. F. M. Torres, *Transport and optimal control of vaccination dynamics for COVID-19*. Chapter of Book : Mathematical Analysis of Infectious Diseases, 1 st Edition, ELSEVIER, 2022, pp. 27–39. DOI: https://doi.org/10.1016/B978-0-32-390504-6.00007-3.

1.4.3 Publications in international journals

[1] M. A. Zaitri, C. J. Silva, and D. Torres, "Stability analysis of delayed COVID-19 models," *Axioms*, vol. 11, no. 8, pp. 1–21, 2022. DOI: https://doi.org/10.3390/axioms11080400.

[2] M. A. Zaitri, M. O. Bibi, and D. F. M. Torres, "Optimal control to limit the spread of COVID-19 in italy," *Kuwait J. Sci.*, vol. Special issue, pp. 1–14, 2021. DOI: https://doi.org/10.48129/kjs.splcov.13961.

[3] M. A. Zaitri, C. J. Silva, and D. F. M. Torres, "An analytic method to determine the optimal time for the induction phase of anesthesia," *Axioms*, vol. 9, no. 12, pp. 1–15, 2023. DOI: https://doi.org/10.3390/axioms12090867.

Two more articles are submitted for possible publication in international journals and wait for the necessary review reports.

CHAPTER 2

An Analytic Method to Determine the Optimal Time for the Induction Phase of Anesthesia

2.1 Introduction

Pharmacokinetic/Pharmacodynamic modeling is a mathematical approach used in pharmacology to study the relationship between drug concentrations (PK) and their effects on the body (PD). The PK/PD models help researchers and clinicians to understand how drugs are absorbed, distributed, metabolized, and eliminated from the body [5].

The PK/PD models integrate PK and PD data to characterize the time course of drug action [6]. These models can be simple or complex, depending on the drug's characteristics and the purpose of the modeling. The parameters of these models were fitted by Schnider et al. in [13].

In this chapter, we consider the problem proposed in [16], to transfer a patient from consciousness to unconsciousness. We apply the shooting method using the PMP [1], correcting some inconsistencies found in [16] related with the stop criteria of the algorithm and the numerical computation of the equilibrium point. Secondly, we provide a new different analytical method to the time-optimal control problem for the induction phase of anesthesia. To compare the methods, we perform numerical simulations to compute the minimum time to anesthetize a man of 53 years, 77 Kg, 177 cm, as considered in [16]. We find the optimal continuous infusion rate of the anesthetic and the minimum time that needs to be chosen for treatment, showing that both the shooting method of [16] and the one proposed here coincide. This chapter is organized

as follows. In Section 2.2, we recall the PK/PD model of Bailey and Haddad [29], the Schnider model [13], the BIS, and the equilibrium point [15]. Then, in Section 2.3, a time-optimal control problem for the induction phase of anesthesia is posed and solved both by the shooting and analytical methods. Finally, in Section 2.4, we compute the parameters of the model, using the Schnider model [13], and we illustrate the results of the time-optimal control problem through numerical simulations. We conclude that the optimal continuous infusion rate for anesthesia and the minimum time that should be chosen for this treatment can be found by both shooting and analytical methods. The advantage of the new method proposed here is that it does not depend on the concrete initial conditions, while the shooting method is very sensitive to the choice of the initial conditions of the state and adjoint variables. We end with Section 2.5 of conclusions, pointing also some directions for future research.

2.2 The PK/PD model

The PK/PD model consists of four compartments: intravascular blood ($x_1(t)$), muscle ($x_2(t)$), fat ($x_3(t)$), and effect site ($x_4(t)$). The effect site compartment (brain) is introduced to account for the finite equilibration time between the central compartment and central nervous system concentrations [29]. This model is used to describe the circulation of drugs in a patient's body, being expressed by a four-dimensional dynamical system as follows:

$$\begin{cases} \dot{x}_1(t) = -(a_{1\,0} + a_{1\,2} + a_{1\,3})\, x_1(t) + a_{2\,1}\, x_2(t) + a_{3\,1}\, x_3(t) + u(t), \\ \dot{x}_2(t) = a_{1\,2}\, x_1(t) - a_{2\,1}\, x_2(t), \\ \dot{x}_3(t) = a_{1\,3}\, x_1(t) - a_{3\,1}\, x_3(t), \\ \dot{x}_4(t) = \frac{a_{e\,0}}{v_1}\, x_1(t) - a_{e\,0}\, x_4(t). \end{cases} \tag{2.1}$$

The state variables for system (2.1) are subject to the following initial conditions:

$$x(0) = (x_1(0), x_2(0), x_3(0), x_4(0)) = (0, 0, 0, 0)\,, \tag{2.2}$$

where $x_1(t), x_2(t), x_3(t)$ and $x_4(t)$ represent, respectively, the masses of the propofol in the compartments of blood, muscle, fat, and effect site at time t. The control $u(t)$ is the continuous infusion rate of the anesthetic. The parameters $a_{1\,0}$ and $a_{e\,0}$ represent, respectively, the rate of clearance from the central compartment and the effect site. The parameters $a_{1\,2}$, $a_{1\,3}$, $a_{2\,1}$, $a_{3\,1}$ and $a_{e\,0}/v_1$ are the transfer rates of the drug between compartments. A schematic diagram of the dynamical control system (2.1) is given in Figure 2.1.

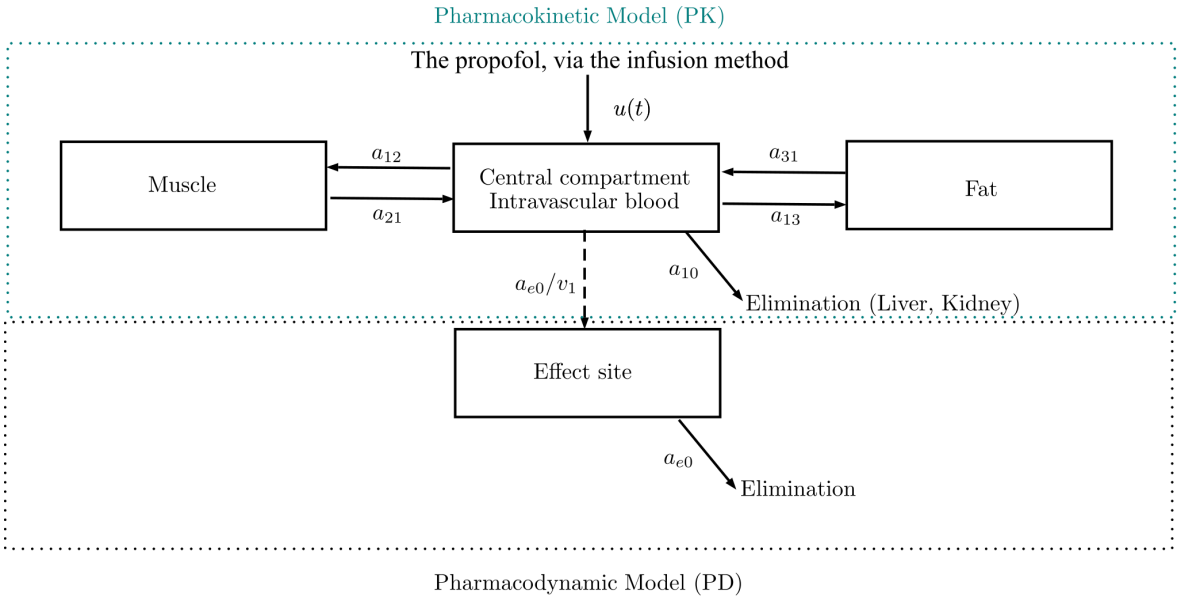

Figure 2.1: Schematic diagram of the PK/PD model with the effect site compartment of Bailey and Haddad [29].

2.2.1 Schnider's model

Following Schnider et al. [13], the LBM is calculated using the James formula, which performs satisfactorily in normal and moderately obese patients, but not so well for severely obese cases [30]. The James formula calculates (LBM) as follows:

$$\text{for Male, LBM} = 1.1 \times \text{weight} - 128 \times \left(\frac{\text{weight}}{\text{height}}\right)^2, \tag{2.3}$$

$$\text{for Female, LBM} = 1.07 \times \text{weight} - 148 \times \left(\frac{\text{weight}}{\text{height}}\right)^2. \tag{2.4}$$

The parameters of the PK/PD model (2.1) are then estimated according with Table 2.1.

Parameter	Estimation
$a_{10}\,(\text{min}^{-1})$	$0.443 + 0.0107\,(\text{weight} - 77) - 0.0159\,(\text{LBM} - 59) + 0.0062\,(\text{height} - 177)$
$a_{12}\,(\text{min}^{-1})$	$0.302 - 0.0056\,(\text{age} - 53)$
$a_{13}\,(\text{min}^{-1})$	0.196
$a_{21}\,(\text{min}^{-1})$	$(1.29 - 0.024\,(\text{age} - 53))\,/\,(18.9 - 0.391\,(\text{age} - 53))$
$a_{31}\,(\text{min}^{-1})$	0.0035
$a_{e0}\,(\text{min}^{-1})$	0.456
$v_1\,(l)$	4.27

Table 2.1: Parameter values for model (2.1) according with Schnider model [13].

2.2.2 The Bispectral Index (BIS)

The BIS is the depth of anesthesia indicator, which is a signal derived from the Electroencephalography (EEG) analysis and directly related to the effect site concen-

tration of $x_4(t)$. It quantifies the level of consciousness of a patient from 0 (no cerebral activity) to 100 (fully awake patient), and can be described empirically by a decreasing sigmoid function [29]:

$$BIS(x_4(t)) = BIS_0 \left(1 - \frac{x_4(t)^\gamma}{x_4(t)^\gamma + EC_{50}^\gamma}\right), \tag{2.5}$$

where BIS_0 is the BIS value of an awake patient typically set to 100, EC_{50} corresponds to the drug concentration associated with 50% of the maximum effect, and γ is a parameter modeling the degree of nonlinearity. According with [31], typical values for these parameters are $EC_{50} = 3.4\, mg/l$ and $\gamma = 3$.

2.2.3 The equilibrium point

Following [15], the equilibrium point is obtained by equating the right hand side of (2.1) to zero,

$$\begin{cases} 0 = -(a_{1\,0} + a_{1\,2} + a_{1\,3})\, x_1 + a_{2\,1}\, x_2 + a_{3\,1}\, x_3 + u, \\ 0 = a_{1\,2}\, x_1 - a_{2\,1}\, x_2, \\ 0 = a_{1\,3}\, x_1 - a_{3\,1}\, x_3, \\ 0 = \frac{a_{e\,0}}{v_1}\, x_1 - a_{e\,0}\, x_4, \end{cases} \tag{2.6}$$

with the condition

$$x_4 = EC_{50}. \tag{2.7}$$

It results that the equilibrium point $x_e = (x_{e\,1}, x_{e\,2}, x_{e\,3}, x_{e\,4})$ is given by

$$x_{e\,1} = v_1\, EC_{50}, \quad x_{e\,2} = \frac{a_{1\,2}\, v_1\, EC_{50}}{a_{2\,1}}, \quad x_{e\,3} = \frac{a_{1\,3}\, v_1\, EC_{50}}{a_{3\,1}}, \quad x_{e\,4} = EC_{50}, \tag{2.8}$$

and the value of the continuous infusion rate for this equilibrium is

$$u_e = a_{1\,0}\, v_1\, EC_{50}. \tag{2.9}$$

The fast state is defined by

$$x_{eF}(t) = (x_1(t), x_4(t)). \tag{2.10}$$

The control of the fast dynamics is crucial, because the BIS is a direct function of the concentration at the effect site.

2.3 Time-optimal control problem

Let $x(t) = (x_1(t), x_2(t), x_3(t), x_4(t)) \in \mathbb{R}^4$. We can write the dynamical system (2.1) in a matrix form as follows:

$$\dot{x}(t) = A\, x(t) + B\, u(t), \tag{2.11}$$

where

$$A = \begin{pmatrix} -(a_{10}+a_{12}+a_{13}) & a_{21} & a_{31} & 0 \\ a_{12} & -a_{21} & 0 & 0 \\ a_{13} & 0 & -a_{31} & 0 \\ \frac{a_{e0}}{v_1} & 0 & 0 & -a_{e0} \end{pmatrix} \quad \text{and} \quad B = \begin{pmatrix} 1 \\ 0 \\ 0 \\ 0 \end{pmatrix}. \tag{2.12}$$

Here, the continuous infusion rate $u(t)$ is to be chosen so as to transfer the system (2.1) from the initial state (wake state) to the fast final state (anesthetized state) in the shortest possible time. Mathematically, we have the following time-optimal control problem [16]:

$$\begin{cases} \min\limits_{u(t)} J = \int\limits_0^{t_f} dt, \\ \dot{x}(t) = A\,x(t) + B\,u(t), \quad x(0) = (0,0,0,0), \\ C\,x_{eF}(t_f) = x_{eF}, \\ 0 \le u(t) \le U_{max}, \quad t \in [0, t_f], \quad t_f \text{ is free}, \end{cases} \tag{2.13}$$

where t_f is the first instant of time that the desired state is reached, C and x_{eF} are given by

$$C = \begin{pmatrix} 1 & 0 \\ 0 & 1 \end{pmatrix}, \quad x_{eF} = (x_{e1},\, x_{e4}), \tag{2.14}$$

with

$$x_{eF}(t_f) = (x_1(t_f), x_2(t_f)). \tag{2.15}$$

2.3.1 The Pontryagin's Minimum Principle (PMP)

According to the PMP [1], if $\tilde{u} \in L^1$ is optimal for problem (2.13) and the final time t_f is free, then there exists

$$\psi(t) = (\psi_1(t), \ldots, \psi_4(t)),\ t \in [0, t_f],\ \psi \in AC([0, t_f]; \mathbb{R}^4),$$

called the adjoint vector, such that

$$\begin{cases} \dot{x}(t) = \dfrac{\partial H}{\partial \psi}(t, x, u, \psi), \\ \dot{\psi}(t) = -\dfrac{\partial H}{\partial x}(t, x, u, \psi), \end{cases} \tag{2.16}$$

where the Hamiltonian H is defined by

$$H(t, x, u, \psi) = 1 + \psi^T\,(A\,x + B\,u). \tag{2.17}$$

Moreover, the minimality condition

$$H(t, \tilde{x}(t), \tilde{u}(t), \tilde{\psi}(t)) = \min_{0 \le u \le U_{max}} H(t, \tilde{x}(t), u, \tilde{\psi}(t)) \tag{2.18}$$

holds almost everywhere on $t \in [0, t_f]$.

Since the final time t_f is free, according to the transversality condition of PMP, we get:

$$H(t_f, x(t_f), u(t_f), \psi(t_f)) = 0. \tag{2.19}$$

Solving the minimality condition (2.18) on the interior of the set of admissible controls gives the necessary condition

$$\tilde{u}(t) = \begin{cases} 0 & \text{if } \tilde{\psi}_1(t) > 0, \\ U_{max} & \text{if } \tilde{\psi}_1(t) < 0. \end{cases} \tag{2.20}$$

2.3.2 Shooting method

The shooting method is a numerical technique used to solve boundary value problems, specifically in the realm of differential equations and optimal control. It transforms the problem into an initial value problem by estimating the unknown boundary conditions. Through iterative adjustments to these estimates, the boundary conditions are gradually satisfied. In [32], the authors propose an algorithm that addresses numerical solutions for parameterized optimal control problems. This algorithm incorporates multiple shooting and recursive quadratic programming, introducing a condensing algorithm for linearly constrained quadratic subproblems and high-rank update procedures. The algorithm's implementation leads to significant improvements in convergence behavior, computing time, and storage requirements. For more on numerical approaches to solve optimal control problems, we refer the reader to [33] and references therein.

Using (2.16), (2.17), (2.19) and (2.20), we consider the following problem:

$$\begin{cases} \dot{x}(t) = A\,x(t) + B\ \times \max\left(0, -U_{max}\, sign(\psi_1(t))\right), \\ \dot{\psi}(t) = -A^T\,\psi(t), \\ x(0) = (0,0,0,0),\ x_1(t_f) = x_{e1},\ x_4(t_f) = x_{e4}, \\ \psi(0) \text{ is free, } H(t_f, x(t_f), \max\left(0, -U_{max}\, sign(\psi_1(t_f))\right), \psi(t_f)) = 0. \end{cases} \tag{2.21}$$

Let $z(t) = (x(t), \psi(t))$. Then we get the following two points boundary value problem:

$$\begin{cases} \dot{z}(t) = A^* z(t) + B^*, \\ R(z(0), z(t_f)) = 0, \end{cases} \tag{2.22}$$

where $A^* \in M_{8\times 8}(\mathbb{R})$ is the matrix given by

$$A^* = \begin{pmatrix} A & 0_{4\times 4} \\ 0_{4\times 4} & -A^T \end{pmatrix}, \tag{2.23}$$

$B^* \in \mathbb{R}^8$ is the vector given by

$$B^* = \begin{cases} (0\,0\,0\,0\,0\,0\,0\,0)^T & \text{if } \psi_1(t) > 0, \\ (U_{max}\,0\,0\,0\,0\,0\,0\,0)^T & \text{if } \psi_1(t) < 0, \end{cases} \tag{2.24}$$

and $R(z(0), z(t_f))$ is given by (2.2), (2.15), and (2.19). We consider the following Cauchy problem:

$$\begin{cases} \dot{z}(t) = A^* z(t) + B^*, \\ z(0) = z_0. \end{cases} \tag{2.25}$$

If we define the shooting function $S\colon \mathbb{R}^8 \longrightarrow \mathbb{R}^3$ by

$$S(z_0) = R(t_f, z(t_f, z_0)), \tag{2.26}$$

where $z(t, z_0)$ represents the solution of Cauchy's problem (2.25), then the two points boundary value problem (2.21) is equivalent to

$$S(z_0) = 0. \tag{2.27}$$

To solve (2.27), we use Newton's method [34].

2.3.3 Analytical method

We now propose a different method to choose the optimal control. If the pair (A, B) satisfies the Kalman condition and all eigenvalues of matrix $A \in n \times n$ are real, then any extremal control has at most $n-1$ commutations on $\mathbb{R}^+$ (at most $n-1$ switching times). We consider the following eight possible strategies:
Strategy 1 (zero switching times)

$$u(t) = U_{max},\ \forall t \in [0, t_f]. \tag{2.28}$$

Strategy 2 (zero switching times)

$$u(t) = 0,\ \forall t \in [0, t_f]. \tag{2.29}$$

Strategy 3 (one switching time)

$$u(t) = \begin{cases} U_{max} & \text{if } 0 \le t < t_c, \\ 0 & \text{if } t_c < t \le t_f, \end{cases} \tag{2.30}$$

where t_c is a switching time.
Strategy 4 (one switching time)

$$u(t) = \begin{cases} 0 & \text{if } 0 \le t < t_c, \\ U_{max} & \text{if } t_c < t \le t_f. \end{cases} \tag{2.31}$$

Strategy 5 (two switching times)

$$u(t) = \begin{cases} U_{max} & \text{if } 0 < t < t_{c1}, \\ 0 & \text{if } t_{c1} < t < t_{c2}. \\ U_{max} & \text{if } t_{c2} < t \leq t_f, \end{cases} \tag{2.32}$$

where t_{c1} and t_{c2} represent two switching times.
Strategy 6 (two switching times)

$$u(t) = \begin{cases} 0 & \text{if } 0 < t < t_{c1}, \\ U_{max} & \text{if } t_{c1} < t < t_{c2}. \\ 0 & \text{if } t_{c2} < t \leq t_f. \end{cases} \tag{2.33}$$

Strategy 7 (three switching times)

$$u(t) = \begin{cases} U_{max} & \text{if } 0 < t < t_{c1}, \\ 0 & \text{if } t_{c1} < t < t_{c2}. \\ U_{max} & \text{if } t_{c2} < t \leq t_{c3}. \\ 0 & \text{if } t_{c3} < t < t_f, \end{cases} \tag{2.34}$$

where t_{c1}, t_{c2} and t_{c3} represent three switching times.
Strategy 8 (three switching times)

$$u(t) = \begin{cases} 0 & \text{if } 0 < t < t_{c1}, \\ U_{max} & \text{if } t_{c1} < t < t_{c2}. \\ 0 & \text{if } t_{c2} < t \leq t_{c3}. \\ U_{max} & \text{if } t_{c3} < t < t_f. \end{cases} \tag{2.35}$$

Let $x(t)$ be the trajectory associated with the control $u(t)$, given by the relation

$$x(t) = exp(A\,t)\,x(0) + \int_0^t exp(A(t-s))Bu(t)ds, \tag{2.36}$$

where $exp(A)$ is the exponential matrix of A.

To calculate the switching times t_c, t_{c1}, t_{c2}, t_{c3} and the final time t_f, we have to solve the following nonlinear equation:

$$\tilde{x}_{eF}(t_f) = (x_{e1},\, x_{e4}). \tag{2.37}$$

We also solve (2.37) using the Newton method [34].

2.4 Numerical example

In this section, we use the shooting and analytical methods to calculate the minimum time t_f to anesthetize a man of 53 years, 77 Kg, and 177 cm.

The equilibrium point and the flow rate corresponding to a BIS of 50 are:

$$x_e = (14.518\,mg,\ 64.2371\,mg,\ 813.008\,mg,\ 3.4\,mg),\ \ u_e = 6.0907\,mg/min. \tag{2.38}$$

Following the Schnider model, the matrix A of the dynamic system (2.11) is given by:

$$A = \begin{pmatrix} -0.9175 & 0.0683 & 0.0035 & 0 \\ 0.3020 & -0.0683 & 0 & 0 \\ 0.1960 & 0 & -0.0035 & 0 \\ 0.1068 & 0 & 0 & -0.4560 \end{pmatrix} \quad \text{and} \quad B = \begin{pmatrix} 1 \\ 0 \\ 0 \\ 0 \end{pmatrix}. \tag{2.39}$$

We are interested in solving the following minimum-time control problem:

$$\begin{cases} \min\limits_{t_f} J(u) = t_f dt, \\ \dot{x}(t) = A\,x(t) + B\,u(t), \quad x(0) = (0,\,0,\,0,\,0), \\ x_{e1}(t_f) = 14.518\,mg, \quad x_{e4}(t_f) = 3.4\,mg, \\ 0 \le u(t) \le 106.0907, \quad t \in [0, t_f], \quad t_f \text{ is free.} \end{cases} \tag{2.40}$$

2.4.1 Numerical resolution by the shooting method

Let $z(t) = (x(t), \psi(t))$. We consider the following Cauchy problem:

$$\begin{cases} \dot{z}(t) = A^* z(t) + B^*, \\ z(0) = z_0 = (0,\,0,\,0,\,0,\,\psi_{01},\,\psi_{02},\,\psi_{03},\,\psi_{04}), \end{cases} \tag{2.41}$$

where

$$A^* = 10^{-4} \begin{pmatrix} -9175 & 683 & 35 & 0 & 0 & 0 & 0 & 0 \\ 3020 & -683 & 0 & 0 & 0 & 0 & 0 & 0 \\ 196 & 0 & -35 & 0 & 0 & 0 & 0 & 0 \\ 1068 & 0 & 0 & -456 & 0 & 0 & 0 & 0 \\ 0 & 0 & 0 & 0 & 9175 & -3020 & -196 & -1068 \\ 0 & 0 & 0 & 0 & -683 & 683 & 0 & 0 \\ 0 & 0 & 0 & 0 & -35 & 0 & 35 & 0 \\ 0 & 0 & 0 & 0 & 0 & 0 & 0 & 456 \end{pmatrix}, \tag{2.42}$$

$$B^* = \begin{pmatrix} \max\left(0, -106.0907\, sign(\psi_1(t))\right) \\ 0 \\ 0 \\ 0 \\ 0 \\ 0 \\ 0 \\ 0 \end{pmatrix}. \tag{2.43}$$

The shooting function S is given by

$$S(z_0) = (S_1(z_0),\, S_2(z_0),\, S_3(z_0)), \tag{2.44}$$

where

$$\begin{aligned} S_1(z_0) &= x_{e1}(t_f) - 14.518, \\ S_2(z_0) &= x_{e4}(t_f) - 3.4, \\ S_3(z_0) &= 1 + \psi^T(t_f)\left(Ax(t_f) + B\max\left(0, -106.0907\, sing\, \psi_1(t_f)\right)\right). \end{aligned}$$

All computations were performed with the MATLAB numeric computing environment, version R2020b, using the medium order method and the function `ode45` (Runge–Kutta Method) in order to solve the nonstiff differential system (2.22). We have used the variable order method and the function `ode113` (Adams–Bashforth–Moulton method) in order to solve the nonstiff differential system (2.25); and the function `fsolve` in order to solve equation $S(z_0) = 0$. Thus, we get that the minimum time is equal to

$$t_f = 1.8397\, min \tag{2.45}$$

with

$$\psi^T(0) = (-0.0076,\, 0.0031,\, -0.0393,\, -0.0374). \tag{2.46}$$

2.4.2 Numerical resolution by the analytical method

The pair (A, B) satisfies the Kalman condition and the matrix A has four real eigenvalues. Then, the extremal control $u(t)$ has at most three commutations on $\mathbb{R}^+$. Therefore, let's test the eight strategies provided in Section 2.3.3.

Note that the anesthesiologist begins with a bolus injection to transfer the patient state from the consciousness state $x(0)$ to the unconsciousness state

$$x_{eF} = (14.518,\, 3.4),$$

that is,

$$u(0) = U_{max} = 106.0907\, mg/min. \tag{2.47}$$

Thus, Strategies 2, 4, 6 and 8 are not feasible here. Therefore, in the sequel, we investigate Strategies 1, 3, 5, and 7 only.

Strategy 1: Let $u(t) = 106.0907\, mg/min$ for all $t \in [0, t_f]$. The trajectory $x(t)$, associated with this control $u(t)$, is given by the following relation:

$$x(t) = \int_0^t exp(A(t-s))BU_{max}ds,\ \forall t \in [0, t_f], \tag{2.48}$$

where

$$exp(A\,(t-s)) \;\; = \;\; V\,D(t-s)\,V^{-1} \tag{2.49}$$

with

$$V = \begin{pmatrix} 0 & 0.9085 & 0.0720 & -0.0058 \\ 0 & -0.3141 & 0.9377 & -0.0266 \\ 0 & -0.1898 & -0.3395 & -0.9996 \\ 1 & -0.1997 & 0.0187 & -0.0014 \end{pmatrix} \tag{2.50}$$

and

$$D(\tau) = \begin{pmatrix} \exp^{-0.4560\,\tau} & 0 & 0 & 0 \\ 0 & \exp^{-0.9419\,\tau} & 0 & 0 \\ 0 & 0 & \exp^{-0.0451\,\tau} & 0 \\ 0 & 0 & 0 & \exp^{-0.0024\,\tau} \end{pmatrix}. \tag{2.51}$$

The system (2.37) takes the form

$$\begin{cases} x_1(t_f) = 14.518, \\ x_4(t_f) = 3.4, \end{cases} \tag{2.52}$$

and has no solutions. Thus, the Strategy 1 is not feasible.

Strategy 3: Let $u(t)$, $t \in [0, t_f]$, be the control defined by

$$u(t) = \begin{cases} 106.0907\, mg/min & \text{if } 0 \le t < t_c, \\ 0 & \text{if } t_c < t \le t_f. \end{cases} \tag{2.53}$$

The trajectory $x(t)$ associated with this control $u(t)$ is given by

$$x(t) = \begin{cases} \int_0^t exp(A(t-s))BU_{max}ds & \text{if } 0 \le t \le t_c, \\ exp(A\,(t-t_c))\,x(t_c) & \text{if } t_c < t \le t_f, \end{cases} \tag{2.54}$$

where

$$exp(A\,(t-t_c)) \;\; = \;\; V\,D(t-t_c)\,V^{-1}. \tag{2.55}$$

To calculate the switching time t_c and the final time t_f, we have to solve the nonlinear system (2.52) with the new condition

$$t_c < t_f. \tag{2.56}$$

Similarly to Section 2.4.1, all numerical computations were performed with MATLAB R2020b using the command `solve` to solve equation (2.52). The obtained minimum time is equal to

$$t_f = 1.8397\, min \tag{2.57}$$

with the switching time

$$t_c = 0.5467\, min. \tag{2.58}$$

Strategy 5: Let $u(t)$, $t \in [0, t_f]$, be the control defined by the relation

$$u(t) = \begin{cases} 106.0907\, mg/min & \text{if } 0 \leq t < t_{c1}, \\ 0 & \text{if } t_{c1} < t < t_{c2}. \\ 106.0907\, mg/min & \text{if } t_{c2} < t \leq t_f, \end{cases} \tag{2.59}$$

where t_{c1} and t_{c2} are the two switching times. The trajectory $x(t)$ associated with control (2.59) is given by

$$x(t) = \begin{cases} \int_0^t exp(A(t-s))BU_{max}ds & \text{if } 0 \leq t \leq t_{c1}, \\ exp(A\,(t-t_{c1}))\,x(t_{c1}) & \text{if } t_{c1} < t \leq t_{c2}, \\ exp(A\,(t-t_{c2}))\,x(t_{c2}) + \int_{t_{c2}}^t exp(A(t-s))BU_{max}ds & \text{if } t_{c2} < t \leq t_f. \end{cases} \tag{2.60}$$

To compute the two switching times t_{c1} and t_{c2} and the final time t_f, we have to solve the nonlinear system (2.52) with

$$0 \leq t_{c1} \leq t_{c2} \leq t_f. \tag{2.61}$$

It turns out that the system (2.52) subject to condition (2.61) has no solution. Thus, the Strategy 5 is also not feasible.

Strategy 7: Let $u(t)$, $t \in [0, t_f]$, be the control defined by the relation

$$u(t) = \begin{cases} 106.0907\, mg/min & \text{if } 0 \leq t < t_{c1}, \\ 0 & \text{if } t_{c1} < t < t_{c2}. \\ 106.0907\, mg/min & \text{if } t_{c2} < t \leq t_{c3}, \\ 0\, mg/min & \text{if } t_{c3} < t \leq t_f, \end{cases} \tag{2.62}$$

where t_{c1}, t_{c2} and t_{c3} are the three switching times. The trajectory $x(t)$ associated with control (2.62) is given by

$$x(t) = \begin{cases} \int_0^t exp(A(t-s))BU_{max}ds & \text{if } 0 \leq t \leq t_{c1}, \\ exp(A\,(t-t_{c1}))\,x(t_{c1}) & \text{if } t_{c1} < t \leq t_{c2}, \\ exp(A\,(t-t_{c2}))\,x(t_{c2}) + \int_{t_{c2}}^t exp(A(t-s))BU_{max}ds & \text{if } t_{c2} < t \leq t_{c3}, \\ exp(A\,(t-t_{c3}))\,x(t_{c3}) & \text{if } t_{c3} < t \leq t_f. \end{cases} \tag{2.63}$$

To compute the three switching times t_{c1}, t_{c2} and t_{c3} and the final time t_f, we have to solve the nonlinear system (2.52) with

$$0 \leq t_{c1} \leq t_{c2} \leq t_{c3} \leq t_f. \tag{2.64}$$

It turns out that the system (2.52) subject to condition (2.64) has no solution. Thus, the Strategy 7 is also not feasible.

In Figures 2.2 and 2.3, we present the solutions of the linear system of differential equations (2.40) under the optimal control $u(t)$ illustrated in Figure 2.4, where the black curve corresponds to the one obtained by the shooting method, as explained in Section 2.3.2; while the blue curve corresponds to our analytical method, in the sense of Section 2.3.3. In addition, for both figures, we show the controlled BIS Index and the trajectory of fast states corresponding to the optimal continuous infusion rate of the anesthetic $u(t)$ and the minimum time t_f required to transition system (2.40) from the initial state

$$x_0 = (0,\, 0,\, 0,\, 0)$$

to the fast final (anesthetized) state

$$x_{eF} = (14.518,\, 3.4)$$

in the shortest possible time. The minimum time t_f is equal to $t_f = 1.8397\,min$ by the shooting method (black curve in Figure 2.2) and it is equal to $t_f = 1.8397\,min$ by the analytical method (blue curve in Figure 2.3).

By using the shooting method, the black curve in Figure 2.4 shows that the optimal continuous infusion rate of the induction phase of anesthesia $u(t)$ is equal to 106.0907 mg/min until the switching time

$$t_c = 0.5467\,min.$$

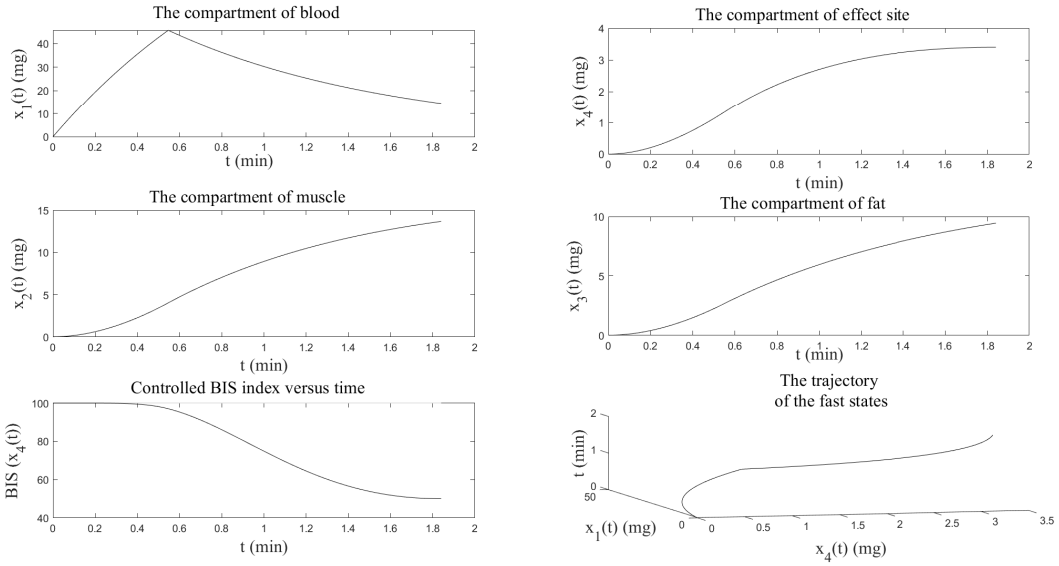

Figure 2.2: The state trajectory, controlled BIS index and trajectry of the fast states corresponding to the optimal control $u(t)$ of Figure 2.4, using the shooting method.

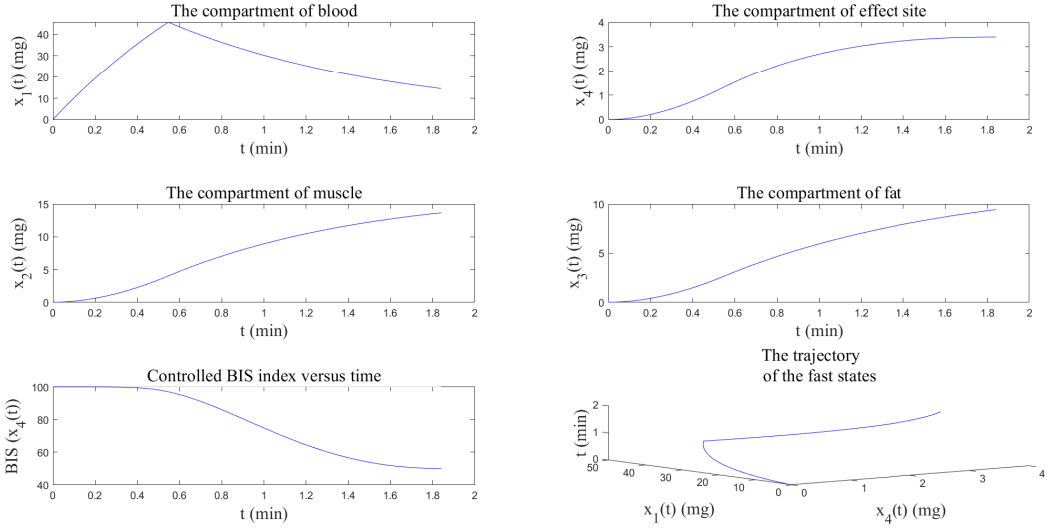

Figure 2.3: The state trajectory, controlled BIS index, and trajectory of the fast states corresponding to the optimal control $u(t)$ of Figure 2.4, using the analytical method.

Then, it is equal to $0\,mg/min$ (Stop-Infusion) until the final time

$$t_f = 1.8397\,min,$$

By using the analytical method, the blue curve in Figure 2.4 shows that the optimal continuous infusion rate of the induction phase of anesthesia $u(t)$ is equal to

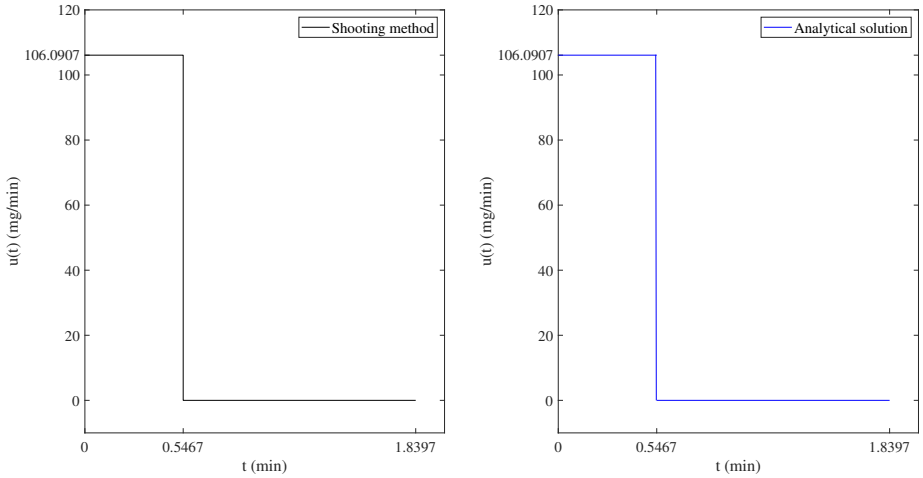

Figure 2.4: The optimal continuous infusion rate $u(t)$ of the induction phase of anesthesia, as obtained by the shooting and analytical methods.

$106.0907\,mg/min$ until the switching time

$$t_c = 0.5467\,min.$$

Then, it is equal to $0\,mg/min$ (Stop-Infusion) until the final time

$$t_f = 1.8397\,min.$$

We conclude that both methods work well and give similar results. However, in general, the shooting method does not always converge, depending on the initial conditions (2.46). To obtain such initial values is not an easy task since no theory is available to find them. For this reason, the proposed analytical method is logic, practical, and more suitable for real applications.

2.5 Conclusion

The approach proposed by the theory of optimal control is very effective. The shooting method was proposed by Zabi et al. [16], which is used to solve the time-optimal control problem and calculate the minimum time. However, this approach is based on Newton's method. The convergence of Newton's method depends on the initial conditions, being necessary to select an appropriate initial value so that the function is differentiable and the derivative does not vanish. This implies that the convergence of the shooting method is attached to the choice of the initial values. Therefore, the difficulty of the shooting method is to find the initial conditions of the adjoint vectors. Here the aim was to propose a different approach, that we call

"the analytical method", that allows to solve the time-optimal control problem for the induction phase of anesthesia without such drawback. Our method is guided by the selection of the optimal strategy, without the need to choose initial values and study the convergence. We claim that our method can also be applied to other PK/PD models, in order to find the optimal time for the drug administration.

In the context of PK/PD modeling, the challenges associated with uncertainties in plant model parameters and controller gains for achieving robust stability and controller non-fragility are significant [35]. These challenges arise from factors like inter-individual variability, measurement errors, and the dynamic nature of patient characteristics and drug response. Further investigation is needed to understand and develop effective strategies to mitigate the impact of these uncertainties in anesthesia-related PK/PD models. This research can lead to the development of robust and non-fragile control techniques that enhance the stability and performance of anesthesia delivery systems. By addressing these challenges, we can improve the precision and safety of drug administration during anesthesia procedures, ultimately benefiting patient outcomes and healthcare practices. In this direction, the recent results of [36] may be useful. Moreover, we plan to investigate PK/PD fractional-order models, which is a subject under strong current research [37]. This is under investigation and will be addressed elsewhere.

CHAPTER 3

Pharmacokinetic/Pharmacodynamic Anesthesia Model via psi-Caputo Fractional Derivatives

3.1 Introduction

In recent years, the field of fractional derivatives has emerged as a promising approach to model and understand complex biological processes characterized by non-integer order dynamics. This unique mathematical framework has found diverse applications in various areas of biology, where traditional integer-order calculus falls short in capturing the intricacies of these systems [38]. One prominent field where fractional derivatives have made significant contributions is Neurobiology. By employing fractional calculus, researchers have been able to delve into the dynamics of neural systems with a greater level of realism. This includes modeling the behavior of neurons, synaptic transmission, and the propagation of nerve impulses. The incorporation of fractional derivatives enables the consideration of memory effects and non-local behavior, providing a more accurate representation of neural processes [39].

In this chapter, we present a novel PK/PD model for the induction phase of anesthesia, incorporating the ψ-Caputo fractional derivative. By employing the Picard iterative process, we derive a solution for the nonhomogeneous ψ-Caputo fractional system. To explore the dynamics of the fractional anesthesia model, we perform numerical analysis on solutions involving various functions of ψ and fractional orders.

The chapter is organized as follows. In Section 3.2, we provide a review of several

definitions and properties of fractional calculus that are essential for our subsequent discussions (Section 3.2.1). Our original contributions are then given in Section 3.3: we obtain a solution to a general linear nonhomogeneous ψ-Caputo fractional system (Section 3.3.1); we introduce a novel PK/PD model for the induction phase of anesthesia based on the ψ-Caputo fractional derivative (Section 3.3.2); and finally, we compute the model parameters using the Schnider model [13], presenting the numerical results of the fractional PK/PD model corresponding to different ψ functions and fractional orders (Section 3.3.3). We conclude with Section 3.4, summarizing our findings and outlining potential directions for future research.

3.2 Preliminaries

In this section, we recall several definitions and properties of fractional calculus that will be used in the sequel.

3.2.1 Fundamental definitions and results

Throughout the chapter, ψ designates a function of class $C^1[a,b]$ such that $\psi'(t) > 0$, for all $t \in [a,b]$.

Definition 3.1 (See [40]). *The left ψ-Riemann-Liouville fractional integral of a function f of order $\alpha \in (0,1)$ is defined by*

$$I_a^{\alpha,\psi} f(t) = \frac{1}{\Gamma(\alpha)} \int_a^t \psi'(s) \left(\psi(t) - \psi(s)\right)^{\alpha-1} f(s) \, \mathrm{d}s,$$

where $\Gamma(\cdot)$ is the Euler Gamma function.

Remark 3.1. *We remark that $\Gamma(x+1) = x\Gamma(x)$, for all $x > 0$, and for any positive integer n we have $\Gamma(n+1) = n!$.*

Definition 3.2 (See [40]). *The ψ-Caputo fractional derivative of a function f of order $\alpha \in (0,1)$ can be defined as follows:*

$${}^{C}D_a^{\alpha,\psi} f(t) = \frac{1}{\Gamma(1-\alpha)} \int_a^t \left(\psi(t) - \psi(a)\right)^{-\alpha} f'(s) \, \mathrm{d}s.$$

We have the following properties of the fractional operators with respect to function ψ.

Lemma 3.1 (See [40]). *Let $\Re(\alpha) > 0$ and $\Re(\beta) > 0$. Then,*

$$I_a^{\alpha,\psi} \left(f(x) - f(a)\right)^{\beta-1}(t) = \frac{\Gamma(\beta)}{\Gamma(\beta+\alpha)} \left(f(t) - f(a)\right)^{\beta-\alpha-1}.$$

Theorem 3.1 (See [41]). *Let $\alpha \in (0,1)$ and $f \in C^1(a,b)$. Then,*

$$I_a^{\alpha,\psi} {}^C D_a^{\alpha,\psi} f(t) = f(t) - f(a).$$

The Mittag–Leffler function appears naturally in the solution of fractional differential equations and in its various applications: see [42], [43] and references therein.

Definition 3.3 (See [42]). *The Mittag–Leffler function of one parameter, of a matrix A, is defined as*

$$E_\alpha(A) = \sum_{l=0}^{+\infty} \frac{A^l}{\Gamma(\alpha l + 1)}, \quad Re(\alpha) > 0. \tag{3.1}$$

Definition 3.4 (See [42]). *The Mittag–Leffler function of two parameters, of a matrix A, is defined as*

$$E_{\alpha,\alpha'}(A) = \sum_{l=0}^{+\infty} \frac{A^l}{\Gamma(\alpha l + \alpha')}, \quad Re(\alpha) > 0,\ \alpha' > 0. \tag{3.2}$$

Remark 3.2. *The matrix exponential function is a special case of the matrix Mittag–Leffler function [43]. For $\alpha' = 1$, we have $E_{\alpha,1}(A) = E_\alpha(A)$ and $E_{1,1}(A) = e^A$.*

Definition 3.5 (See [44]). *Let f and g be two functions which are piecewise continuous at any interval $[a,b]$ and of exponential order. The generalized convolution of f and g is defined by*

$$(f *_\psi g)(t) = \int_a^t f(s) g\left(\psi^{-1}(\psi(t) + \psi(a) - \psi(s))\right) \psi'(s)\, \mathrm{d}s.$$

3.3 Main Results

We begin by using the Picard iterative process to prove a series solution to a linear nonhomogeneous ψ-Caputo fractional system: see Theorem 3.2, in Section 3.3.1. Then, we generalize the state-of-the-art PK/PD model (2.1) by introducing in Section 3.3.2 a more general ψ-Caputo fractional PK/PD model that is covered by our Theorem 3.2. We finish our new results in Section 3.3.3, by investigating numerically the new fractional model and comparing the efficacy of function ψ.

3.3.1 Solution of linear non homogeneous ψ-Caputo fractional systems

Consider the following linear nonhomogeneous fractional equation:

$${}^C D_a^{\alpha,\psi} y(t) = Ay(t) + u(t), \quad t > a, \tag{3.3}$$

subject to the initial condition

$$y(a) = y_0, \tag{3.4}$$

where ${}^{C}D_{a}^{\alpha,\psi}$ is the ψ-Caputo fractional derivative of order $\alpha \in (0,1]$, such that

$$ {}^{C}D_{a}^{\alpha,\psi} y(t) = \left[{}^{C}D_{a}^{\alpha,\psi} y_1(t), {}^{C}D_{a}^{\alpha,\psi} y_2(t), \ldots, {}^{C}D_{a}^{\alpha,\psi} y_n(t) \right]^T,$$

A is a $n \times n$ matrix, $u(t) = [u_1(t), u_2(t), \ldots, u_n(t)]^T$ is a piecewise continuous integrable function on $[a, +\infty)$, and the initial condition is $y(a) = [y_1(a), y_2(a), \ldots, y_n(a)]^T$.

Lemma 3.2. *Let $p \in \mathbb{N}$, $\alpha \in (0,1]$, and f be a piecewise continuous function of exponential order at any interval $[a,b]$. Then,*

$$ I_{a}^{(p+1)\alpha,\psi} f(t) = \frac{(\psi(t) - \psi(a))^{p\alpha+\alpha-1}}{\Gamma(p\alpha+\alpha)} *_{\psi} f(t).$$

Proof. Follows by using the change of variable $z = \psi^{-1}(\psi(t) + \psi(a) - \psi(s))$, Definition 3.5, and performing direct calculations. □

Lemma 3.3. *Let $\alpha \in (0,1]$ and C be a constant. Then, one has*

$$ I_{a}^{\alpha,\psi} C = \frac{C}{\Gamma(\alpha+1)} (\psi(t) - \psi(a))^{\alpha}.$$

Proof. From Definition 3.1, we have

$$\begin{aligned} I_{a}^{\alpha,\psi} C &= \frac{C}{\Gamma(\alpha)} \int_{a}^{t} \psi'(s) (\psi(t) - \psi(s))^{\alpha-1} \, \mathrm{d}s \\ &= \frac{C}{\Gamma(\alpha)} [\alpha^{-1} (\psi(t) - \psi(s))]_{a}^{t} \\ &= \frac{C}{\Gamma(\alpha+1)} (\psi(t) - \psi(a))^{\alpha}, \end{aligned}$$

and the proof is complete. □

Now, we shall utilize the Picard iterative process [45] to formulate a series solution to (3.3)–(3.4).

Theorem 3.2. *The solution of the initial value problem* (3.3)–(3.4) *can be given in series form as*

$$ y(t) = \sum_{l=0}^{\infty} \frac{A^l (\psi(t) - \psi(a))^{l\alpha}}{\Gamma(l\alpha+1)} y(a) + \sum_{l=0}^{\infty} \frac{A^l (\psi(t) - \psi(a))^{l\alpha+\alpha-1}}{\Gamma(l\alpha+\alpha)} *_{\psi} u(t). \tag{3.5}$$

Proof. Applying the fractional integration operator $I_{a}^{\alpha,\psi}$ to both sides of equation (3.3), and using Theorem 3.1, we obtain the following expression:

$$ y(t) = y(a) + A I_{a}^{\alpha,\psi} y(t) + I_{a}^{\alpha,\psi} u(t).$$

Let ϕ_k be the kth approximate solution with the initial one given by

$$\phi_0(a) = y(a)$$

and, for $k \geq 1$, the recurrent formula

$$\phi_k(t) = y(a) + AI_a^{\alpha,\psi}\phi_{k-1}(t) + I_a^{\alpha,\psi}u(t) \tag{3.6}$$

being satisfied. From formula (3.6) and Lemma 3.3, one has

$$\begin{aligned}
\phi_1(t) &= y(a) + \frac{A\left(\psi(t)-\psi(a)\right)^{\alpha}}{\Gamma(\alpha+1)}y(a) + I_a^{\alpha,\psi}u(t),\\
\phi_2(t) &= y(a) + \frac{A\left(\psi(t)-\psi(a)\right)^{\alpha}}{\Gamma(\alpha+1)}y(a) + \frac{A^2\left(\psi(t)-\psi(a)\right)^{2\alpha}}{\Gamma(2\alpha+1)}y(a) + AI_a^{2(\alpha,\psi)}u(t) + I_a^{\alpha,\psi}u(t),\\
&\vdots\\
\phi_k(t) &= \sum_{l=0}^{k}\frac{A^l\left(\psi(t)-\psi(a)\right)^{l\alpha}}{\Gamma(l\alpha+1)}y(a) + \sum_{l=0}^{k-1}A^l I_a^{(l+1)(\alpha,\psi)}u(t).
\end{aligned}$$

By virtue of Lemma 3.2 and by taking the limit $k \longrightarrow \infty$ for $\phi_k(\cdot)$, we obtain the series formula (3.5) for the solution of (3.3)–(3.4). □

Note that, in terms of the matrix Mittag–Leffler functions (3.1) and (3.2), the solution (3.5) may be written as

$$y(t) = E_{\alpha}\left(A(\psi(t)-\psi(a))^{\alpha}\right)y(a) + (\psi(t)-\psi(a))^{\alpha-1}E_{\alpha,\alpha}\left(A(\psi(t)-\psi(a))^{\alpha}\right) *_{\psi} u(t). \tag{3.7}$$

3.3.2 A fractional PK/PD model

Motivated by system (2.1), we introduce here our ψ-Caputo fractional Pharmacokinetic/Pharmacodynamic model, which is obtained by replacing each ordinary derivative in the system by the ψ-Caputo fractional derivative of order $\alpha \in (0,1]$. Then, our proposed PK/PD model can be expressed by the following four-dimensional fractional dynamical system:

$$\begin{cases}
{}^{C}D_0^{\alpha,\psi}y_1(t) = -(a_{1\,0} + a_{1\,2} + a_{1\,3})\,y_1(t) + a_{2\,1}\,y_2(t) + a_{3\,1}\,y_3(t) + u_1(t),\\
{}^{C}D_0^{\alpha,\psi}y_2(t) = a_{1\,2}\,y_1(t) - a_{2\,1}\,y_2(t),\\
{}^{C}D_0^{\alpha,\psi}y_3(t) = a_{1\,3}\,y_1(t) - a_{3\,1}\,y_3(t),\\
{}^{C}D_0^{\alpha,\psi}y_4(t) = \frac{a_{e\,0}}{v_1}\,y_1(t) - a_{e\,0}\,y_4(t),
\end{cases} \tag{3.8}$$

subject to the initial conditions

$$y_1(0) = y_2(0) = y_3(0) = y_4(0) = 0. \tag{3.9}$$

According to the dynamical system (3.3), one may write system (3.8)–(3.9) in a matrix form as follows:

$$ {}^{C}D_{0}^{\alpha,\psi} y(t) = A\, y(t) + B\, u_1(t) \tag{3.10} $$

with $y(t) = [y_1(t), y_2(t), y_3(t), y_4(t)]^T \in \mathbb{R}^4$, $y(0) = [0,0,0,0]^T$,

$$ A = \begin{pmatrix} -(a_{1\,0} + a_{1\,2} + a_{1\,3}) & a_{2\,1} & a_{3\,1} & 0 \\ a_{1\,2} & -a_{2\,1} & 0 & 0 \\ a_{1\,3} & 0 & -a_{3\,1} & 0 \\ \frac{a_{e\,0}}{v_1} & 0 & 0 & -a_{e\,0} \end{pmatrix} \quad \text{and} \quad B = \begin{pmatrix} 1 \\ 0 \\ 0 \\ 0 \end{pmatrix}. $$

One mentions that the continuous infusion rate $u_1(t)$ is to be chosen in such a way to transfer the system (3.8) from the initial state (wake state) to the fast final state (anesthetized state).

Remark 3.3. *If $\psi(t) = t$ and $\alpha = 1$, then the fractional system* (3.8) *reduces to the classical PK/PD model* (2.1).

3.3.3 Numerical simulations

To administer anesthesia to a 53-year-old man weighing 77 Kg and measuring 177 cm, we utilize our proposed fractional PK/PD system described by:

$$ \begin{cases} {}^{C}D_{0}^{\alpha,\psi} y(t) = A\, y(t) + B\, u_1(t), \\ y(0) = (0,\, 0,\, 0,\, 0)^T, \end{cases} \tag{3.11} $$

where, according with Table 2.1 and [46], the matrix A is taken as

$$ A = \begin{pmatrix} -0.9175 & 0.0683 & 0.0035 & 0 \\ 0.3020 & -0.0683 & 0 & 0 \\ 0.1960 & 0 & -0.0035 & 0 \\ 0.1068 & 0 & 0 & -0.4560 \end{pmatrix} \quad \text{and} \quad B = \begin{pmatrix} 1 \\ 0 \\ 0 \\ 0 \end{pmatrix}, \tag{3.12} $$

with

$$ u_1(t) = \begin{cases} 106.0907\, mg/min & \text{if } 0 \leq t < 0.5467, \\ 0 & \text{if } 0.5467 < t \leq 1.8397. \end{cases} \tag{3.13} $$

From Theorem 3.2 of Section 3.3.1, written in form (3.7), the solution of system (3.11) is given by

$$ y(t) = E_{\alpha}\left(A(\psi(t) - \psi(0))^{\alpha}\right) y(0) + (\psi(t) - \psi(0))^{\alpha-1} E_{\alpha,\alpha}\left(A(\psi(t) - \psi(0))^{\alpha}\right) *_{\psi} u(t) \tag{3.14} $$

with $u(t) = Bu_1(t) = [u_1(t), 0, 0, 0]^T$.

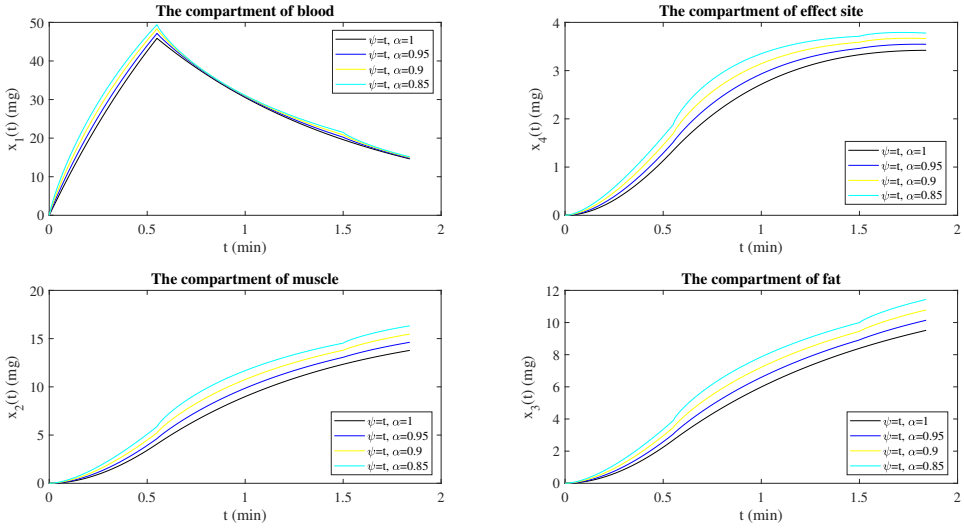

Figure 3.1: Analysis of the fractional PK/PD model (3.11) with functions $\psi(t) = t$ for fractional orders $\alpha = 1$, $\alpha = 0.95$, $\alpha = 0.9$ and $\alpha = 0.85$.

Figure 3.1 showcases the solutions derived from the fractional PK/PD model (3.11), considering the function $\psi(t) = t$ and exploring different fractional order values: $\alpha = 1$, $\alpha = 0.95$, $\alpha = 0.9$, and $\alpha = 0.85$. In Figure 3.2, the curves represent the controlled BIS (Bispectral Index) associated with the optimal continuous infusion rate of the administered anesthetic $u(t)$. It is noteworthy that when the function $\psi(t) = t$ and the fractional order is set to $\alpha = 1$, then the obtained results resemblance those derived from the classical PK/PD model (2.1). However, altering the fractional orders introduces variations in the degree of anesthesia. The recorded values for all fractional orders fell within the range of 40 to 50 (corresponding to the classical model), thus ensuring the condition of anesthesia. Nevertheless, it is crucial to acknowledge that lower fractional order values entail a higher risk of awareness during anesthesia.

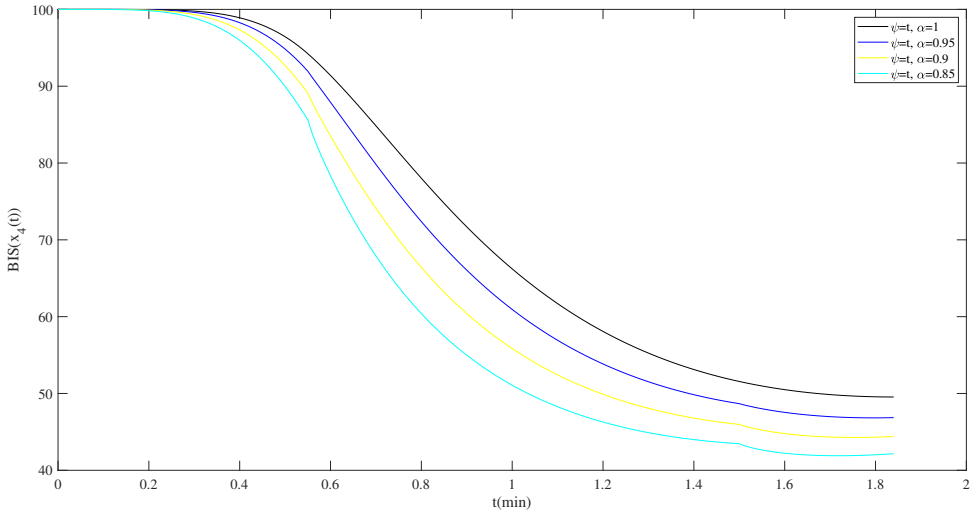

Figure 3.2: Analysis of controlled BIS with functions $\psi(t) = t$ for fractional orders $\alpha = 1$, $\alpha = 0.95$, $\alpha = 0.9$ and $\alpha = 0.85$.

Figure 3.3 illustrates the solutions of the fractional PK/PD model (3.11) associated with the functions $\psi(t) = t$, $\psi(t) = \sqrt{t}$, $\psi(t) = t^2$, and $\psi(t) = t + 0.2$, when considering a fractional order of $\alpha = 1$. The graphs shown in Figure 3.4 depict the controlled BIS corresponding to a specific value of the fractional order $\alpha = 1$, under functions $\psi(t) = t$, $\psi(t) = \sqrt{t}$, $\psi(t) = t^2$ and $\psi(t) = t + 0.2$. It is observed that selecting functions $\psi(t) = \sqrt{t}$ and $\psi(t) = t^2$ does not yield satisfactory anesthesia results. On the other hand, employing the functions $\psi(t) = t$ and $\psi(t) = t + 0.2$ leads to favorable anesthesia outcomes. In subsequent simulations, we will maintain the functions $\psi(t) = t$ and $\psi(t) = t + 0.2$ while altering the fractional orders.

In Figure 3.5, we present the solutions of the fractional PK/PD model (3.11) corresponding to the functions $\psi(t) = t$ and $\psi(t) = t + 0.2$, under the fractional orders $\alpha = 1$, $\alpha = 0.9$, and $\alpha = 0.8$. The curves representing the controlled BIS are displayed in Figure 3.6. It is worth noting that the recorded BIS values for all fractional orders ranged from 50 (resembling the classical model) to 60, thereby satisfying the condition of anesthesia. However, it is crucial to acknowledge that lower fractional order values, specifically with the function $\psi(t) = t + 0.2$, result in a reduced risk of awareness during anesthesia.

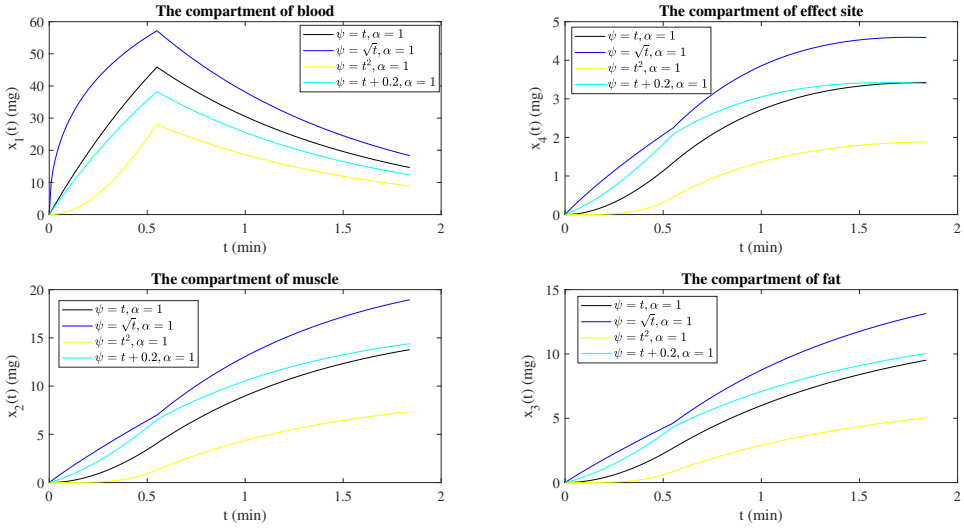

Figure 3.3: Analysis of the fractional PK/PD model (3.11) with functions $\psi(t) = t$, $\psi(t) = \sqrt{t}$, $\psi(t) = t^2$ and $\psi(t) = t + 0.2$ for fractional order $\alpha = 1$.

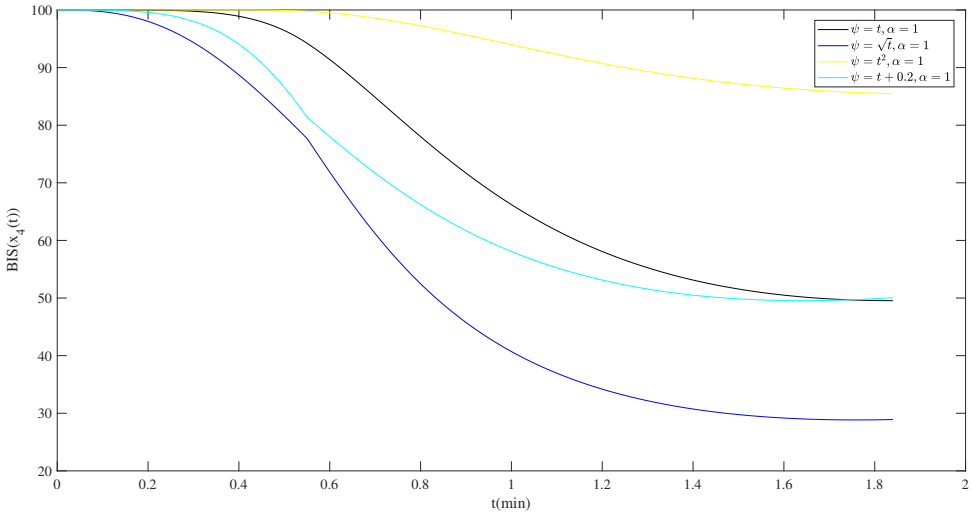

Figure 3.4: Analysis of controlled BIS with functions $\psi(t) = t$, $\psi(t) = \sqrt{t}$, $\psi(t) = t^2$ and $\psi(t) = t + 0.2$ for fractional order $\alpha = 1$.

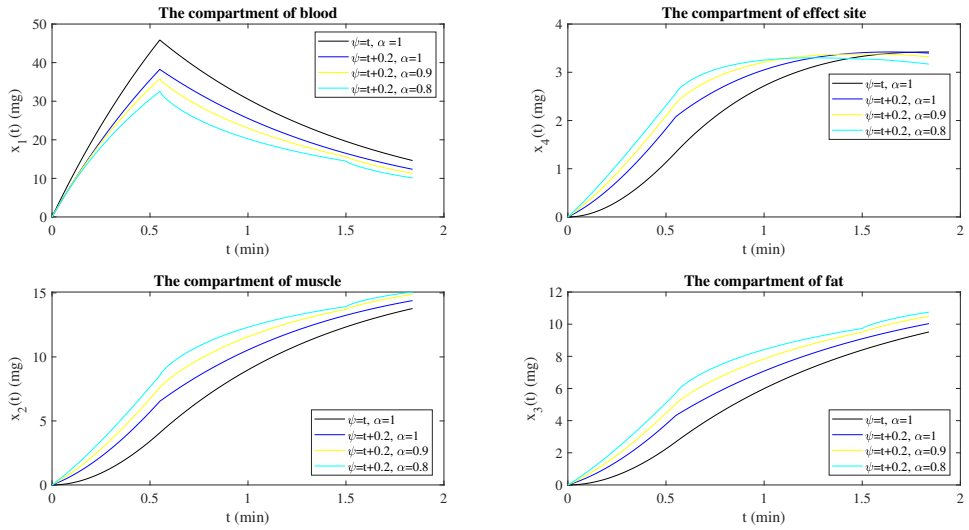

Figure 3.5: Analysis of the fractional PK/PD model (3.11) with functions $\psi(t) = t$ and $\psi(t) = t + 0.2$ for fractional orders $\alpha = 1$, $\alpha = 0.9$, and $\alpha = 0.8$.

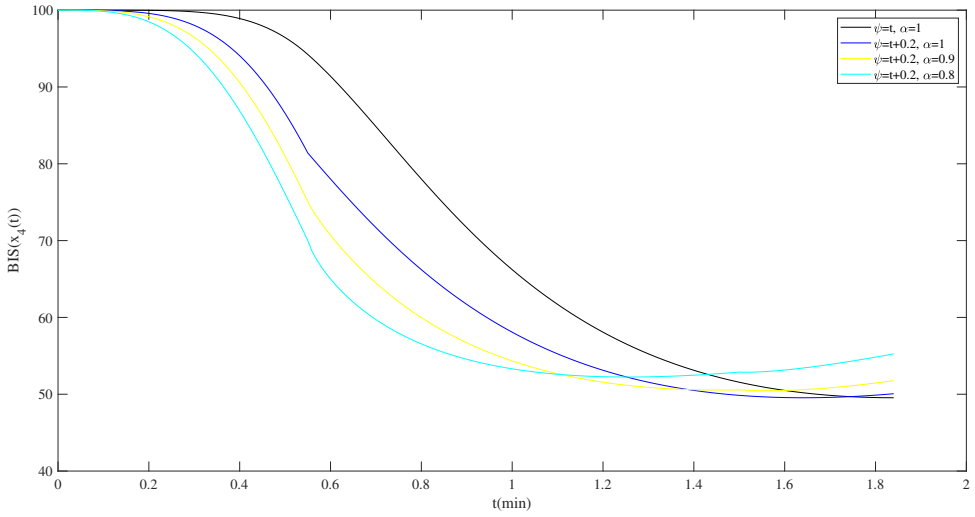

Figure 3.6: Analysis of controlled BIS with functions $\psi(t) = t$ and $\psi(t) = t + 0.2$ for fractional orders $\alpha = 1$, $\alpha = 0.9$, and $\alpha = 0.8$.

3.4 Conclusion

The incorporation of the ψ-Caputo fractional derivative in Pharmacokinetics and Pharmacodynamics, modeling represents a significant advancement in the field. Indeed, by utilizing fractional-order derivatives, researchers can more accurately capture the complex and non-local behavior observed in drugs within biological systems.

The choice of the function ψ and the fractional order α holds critical importance in modeling the relationship between drug concentrations and pharmacological effects. This approach provides a more realistic representation of drug efficacy and dose-response relationships, allowing for a deeper understanding of the intricate dynamics involved in drug-target interactions.

However, further research is necessary to explore the impact of the chosen function ψ and the fractional order α on time-delayed responses. This area remains open for investigation, and future studies can delve into understanding how different choices of ψ and α influence the temporal aspects of drug responses.

In summary, the incorporation of ψ-Caputo fractional derivatives in Pharmacokinetics and Pharmacodynamics modeling offers valuable insights and advancements. By refining the choice of function ψ and fractional order α, researchers can enhance the accuracy and realism of drug modeling, paving the way for a more comprehensive understanding of drug behavior in biological systems.

CHAPTER 4

Stability Analysis of Delayed COVID-19 Models

4.1 Introduction

The introduction of time delays to mathematical epidemic models has been studied in order to better understand and describe the transmission dynamics of infectious diseases, see, e.g., [27], [47]–[49]. Moreover, time delays may have an important effect on the stability of the equilibrium points, leading, for example, to periodic solutions by Hopf bifurcation, see, e.g., [50] and references cited therein. As in other infectious diseases, the latent and incubation periods have an important role on the spread of COVID-19. The latent period of an infectious disease is the time interval between infection and becoming infectious, whether the incubation period is the time interval between infection and the appearance of clinical symptoms [51]–[53]. Following WHO, the incubation period for COVID-19 is between 2 and 10 days [54]. In [53], the authors estimated the mean latent period to be 5.5 (95% CI: 5.1–5.9) days, shorter than the mean incubation period (6.9 days). However, and differently from other infectious diseases, asymptomatic infected individuals can transmit the infection and this imposes more strict mitigation strategies, see, e.g., [55]. To describe and analyze this biological phenomenon, we generalize here a compartmental mathematical model, first proposed in [28], by considering a system of delayed differential equations with discrete time delays. Here, we modify the model analyzed in [28] in order to consider time delays, birth and death rates. More precisely, we introduce a time delay that represents, mathematically, the fact that the migration of individuals from susceptible to infected is subject to delay. Secondly, we present a normalized version of the SEIR-type model, compute the equilibrium points, and the basic reproduction number, and we prove sufficient

conditions for the stability of the equilibrium points, for any positive time delay. Then, we extend the previous model in order to consider vaccination and perform numerical simulations taking into account the real data of the spread of COVID-19 in Italy.

This chapter is organized as follows. In Section 4.2, we propose a delayed SEIQRP mathematical model for COVID-19. Considering the normalized model of the delayed SEIQRP model, we prove sufficient conditions for the stability of the equilibrium points for any time delay. Then, in Section 4.3, we propose a delayed mathematical model for COVID-19 with vaccination. Analogously, we prove sufficient conditions for the stability of the equilibrium points of the normalized SEIQRPW with vaccination, for any time delay. Numerical simulations and a discussion of the results are provided in Section 4.4, illustrating the stability of both delayed models and their practical utility.

The results presented in this chapter have been published in [56].

4.2 The Delayed SEIQRP Model

In this section, we propose a delayed mathematical model for COVID-19, which generalizes the one proposed in [28]. As mentioned in intoduction, there are many different models but, all of them, are approximations of the reality. For example, in [57] the possibility to become susceptible again is ignored, although we know re-infection is possible and occurs; while in [58] deaths are not taken into account.

Our model considers six state variables: susceptible individuals, $S(t)$; exposed individuals, $E(t)$; infected individuals, $I(t)$; quarantined individuals, $Q(t)$; recovered individuals, $R(t)$; and insusceptible/protected individuals, $P(t)$. The total population is denoted by $N(t)$ and is given by

$$N(t) = S(t) + E(t) + I(t) + Q(t) + R(t) + P(t), \quad \text{for all} \quad t \in [0, T]. \tag{4.1}$$

The following assumptions are made to describe the spread of COVID-19: b is the birth rate, μ is the death rate, α is the protection rate, β the infection rate, γ the inverse of the average latent time, δ the rate at which infectious people enter in quarantine, and λ the recovery rate. The time delay $\tau \geq 0$ represents the incubation period, that is, the length of time before the infected individuals become infectious.

We introduce a discrete time delay that represents the transfer delay from the class of susceptible individuals to the class of infected individuals, after the contact of a susceptible individual with an infectious one. Precisely, the model we propose is given

by the following system of six nonlinear ordinary delayed differential equations:

$$\begin{cases} \dot{S}(t) = bN(t) - \frac{\beta S(t-\tau)I(t-\tau)}{N(t)} - (\alpha+\mu)S(t), \\ \dot{E}(t) = \frac{\beta S(t-\tau)I(t-\tau)}{N(t)} - (\gamma+\mu)E(t), \\ \dot{I}(t) = \gamma E(t) - (\delta+\mu)I(t), \\ \dot{Q}(t) = \delta I(t) - (\lambda+\mu)Q(t), \\ \dot{R}(t) = \lambda Q(t) - \mu R(t), \\ \dot{P}(t) = \alpha S(t) - \mu P(t), \end{cases} \tag{4.2}$$

where the state variables are subject to the initial conditions $S(\theta) = S_0$, $\theta \in [-\tau, 0]$, $E(0) = E_0$, $I(\theta) = I_0$, $\theta \in [-\tau, 0]$, $Q(0) = Q_0$, $R(0) = R_0$, and $P(0) = P_0$. We call (4.2) the generalized SEIQRP delayed model. A schematic diagram of our system is given in Figure 4.1.

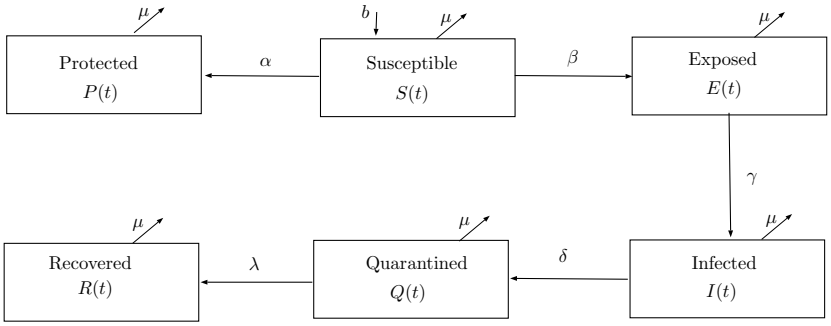

Figure 4.1: Schematic diagram of the generalized SEIQRP delayed model (4.2).

4.2.1 The Normalized SEIQRP Delayed Model

In the situation where the total population size $N(t)$ is not constant over time, it is often convenient to consider the proportions of each compartment of individuals in the population, namely $s(t) = \frac{S(t)}{N(t)}$, $e(t) = \frac{E(t)}{N(t)}$, $i(t) = \frac{I(t)}{N(t)}$, $q(t) = \frac{Q(t)}{N(t)}$, $r(t) = \frac{R(t)}{N(t)}$, and $p(t) = \frac{P(t)}{N(t)}$. According to equality (4.1), we have $\dot{N}(t) = (b-\mu)N(t)$. Therefore, the

normalized SEIQRP delayed model is given by

$$\begin{cases} \dot{s}(t) = b - \beta\, s(t-\tau)\, i(t-\tau) - (\alpha + b)\, s(t)\,, \\ \dot{e}(t) = \beta\, s(t-\tau)\, i(t-\tau) - (\gamma + b)\, e(t)\,, \\ \dot{i}(t) = \gamma\, e(t) - (\delta + b)\, i(t)\,, \\ \dot{q}(t) = \delta\, i(t) - (\lambda + b)\, q(t)\,, \\ \dot{r}(t) = \lambda\, q(t) - b\, r(t)\,, \\ \dot{p}(t) = \alpha\, s(t) - b\, p(t)\,. \end{cases} \tag{4.3}$$

The state variables for system (4.3) are subject to the following initial conditions: $s(\theta) = \dfrac{S_0}{N(0)}$, $\theta \in [-\tau, 0]$, $e(0) = \dfrac{E_0}{N(0)}$, $i(\theta) = \dfrac{I_0}{N(0)}$, $\theta \in [-\tau, 0]$, $q(0) = \dfrac{Q_0}{N(0)}$, $r(0) = \frac{R_0}{N(0)}$, and $p(0) = \dfrac{P_0}{N(0)}$, with $s(t) + e(t) + i(t) + q(t) + r(t) + p(t) = 1$.

In Section 4.2.2 we show that model (4.3) has two equilibrium points: the Disease Free Equilibrium Point (DFE) and the Endemic Equilibrium Point (EE).

4.2.2 Equilibrium Points

The DFE and EE are obtained by solving the right-hand side of equations in (4.3) equal to zero:

$$\begin{aligned} b - \beta\, s(t-\tau)\, i(t-\tau) - (\alpha + b)\, s(t) &= 0\,, \\ \beta\, s(t-\tau)\, i(t-\tau) - (\gamma + b)\, e(t) &= 0\,, \\ \gamma\, e(t) - (\delta + b)\, i(t) &= 0\,, \\ \delta\, i(t) - (\lambda + b)\, q(t) &= 0\,, \\ \lambda\, q(t) - b\, r(t) &= 0\,, \\ \alpha\, s(t) - b\, p(t) &= 0\,, \end{aligned}$$

from which the DFE, Σ_0, is given by

$$\Sigma_0 = (s_0, e_0, i_0, q_0, r_0, p_0) = \left(\frac{b}{\alpha + b}, 0, 0, 0, 0, \frac{\alpha}{\alpha + b}\right), \tag{4.4}$$

while the EE, Σ^+, is given by

$$\Sigma^+ = \left(s^+, e^+, i^+, q^+, r^+, p^+\right) \tag{4.5}$$

with

$$
\begin{aligned}
s^+ &= \frac{(\delta+b)\ (\gamma+b)}{\beta\,\gamma},\\
e^+ &= \frac{\beta\, s^+\, i^+}{(\gamma+b)},\\
i^+ &= \frac{\beta\,\gamma\, b-(\delta+b)\,(\gamma+b)\,(\alpha+b)}{\beta\ (\delta+b)\ (\gamma+b)},\\
q^+ &= \frac{\beta\,\gamma\, b\,\delta-\delta\ (\delta+b)\,(\gamma+b)\,(\alpha+b)}{\beta\ (\lambda+b)\ (\delta+b)\ (\gamma+b)},\\
r^+ &= \frac{\lambda\,\delta\,\beta\,\gamma\, b-\lambda\,\delta\ (\delta+b)\,(\gamma+b)\,(\alpha+b)}{b\,\beta\ (\lambda+b)\ (\delta+b)\ (\gamma+b)},\\
p^+ &= \frac{\alpha\ (\delta+b)\ (\gamma+b)}{b\,\beta\,\gamma}.
\end{aligned}
\tag{4.6}
$$

4.2.3 Basic Reproduction Number

The basic reproductive number, R_0, of an infectious agent such as rabies virus is defined as the average number of secondary infections produced by an infected individual in an otherwise susceptible host population [59]. The R_0 can not be determined from the structure of the mathematical model alone but depends on the definition of infected and uninfected compartments. Let

$$x = (x_1, \ldots, x_n)^T,$$

where $x_i\,(i = 1, \ldots, n)$ represents the number of individuals in the compartment i. The basic reproduction number will be determined from the definition of infected and uninfected compartments. We define X^s as the set of all disease-free states

$$X^s = \{x \geq 0 : x_i = 0,\ i = 1, \ldots, m\},$$

where m is the number of the first compartments that correspond to the infected individuals. Let $F_i(x)$ be the rate of appearance of new infections in compartment i, V_i^+ be the rate of transfer of individuals out of compartment i and V_i^- be the rate of transfer of individuals into compartment i by all other means.

It is assumed that each function is continuously differentiable at least twice in each variable. The disease transmission model consists of non-negative initial conditions together with the following system of equations

$$\dot{x}_i = f_i(x) = F_i(x) - V_i(x),\ i = 1, \ldots, n, \tag{4.7}$$

where $V_i = V_i^- - V_i^+$ and the functions satisfy the following assumptions **A.1**–**A.5**

A.1 Each function represents a directed transfer of individuals, so they are all non-negative. Mathematically

$$x_i \geq 0 \Longrightarrow F_i, V_i^-, V_i^+ \geq 0,\ \forall i = 1, \ldots, n. \tag{4.8}$$

A.2 If there is an empty compartment, there can be no transfer of individuals out of the compartment by death, infection or any other means. Mathematically

$$x_i = 0 \Longrightarrow V_i^- = 0, \forall i = 1, \ldots, n. \tag{4.9}$$

A.3 Consider the disease transmission model given by (4.7), with : f_i, $i = 1, \ldots, n$, satisfying the conditions **A.1** and **A.2**. If $x_i = 0$, so $f_i(x) \geq 0$, that is, the non-negative cone ($x_i \geq 0$, $i = 1, \ldots, n$) is forward invariant. According to the theorem of Wiggins [60] for each non-negative initial condition, there is a unique non-negative solution. The following condition follows from the simple fact that the incidence of infection for the uninfected compartments is zero.

$$F_i = 0, \text{ if } i > m. \tag{4.10}$$

A.4 To ensure that the disease-free subspace is invariant, we assume that if the population is disease free, then the population will remain disease-free. That is, there is no (independent of density) immigration of infectious agents. This condition is stated as follows

$$x \in X^s \Longrightarrow F_i(x) = V_i^+(x) = 0, \forall i = 1, \ldots, m. \tag{4.11}$$

A.5 The remaining condition is based on derivatives near a point of DFE. We define a DFE of (4.7) as a locally asymptotically stable equilibrium solution of the disease-free model, that is, (4.7) restricted to X^s.

We consider a population close to an equilibrium point without disease x^e. If the population remains close to a DFE (i.e. if the introduction of a few infectious individuals does not result in an outbreak), then the population will return to a DFE according to the following linear system

$$\dot{x} = Df(x^e)(x - x^e), \tag{4.12}$$

where $Df(x^e)$ is the Jacobian matrix $\left(\frac{\partial f_i}{\partial x_j}\right)$ evaluated at a DFE x^e. Here, some derivatives are one-sided, since x^e is at the boundary of the domain. We limit our attention to systems in which a DFE is stable in the absence of new infection. That is, if $F(x)$ is set to zero, then all eigenvalues of $Df(x^e)$ have negative real parts.

Lemma 4.1. *[61] If x^e is a DFE of* (4.7) *and the function $f(x)$ satisfies the assumptions **A.1**–**A.5**, then the derivatives and are partitioned as*

$$DF(x^e) = \begin{pmatrix} F_1 & 0 \\ 0 & 0 \end{pmatrix}, \; DV(x^e) = \begin{pmatrix} J_1 & 0 \\ J_3 & J_4 \end{pmatrix},$$

where F_1 and J_1 are the $m \times m$ matrices defined by

$$F_1 = \left[\frac{\partial F_i}{\partial x_j}(x^e)\right] \text{ and } J_1 = \left[\frac{\partial V_i}{\partial x_j}(x^e)\right], \text{ with } 1 \leq i,\ j \leq m.$$

Definition 4.1. *Let λ_i, $i = 1, \ldots, l$, $l \leq m$ be the eigenvalues of the matrix $F_1 J_1^{-1}$. We call spectral radius of the matrix $F_1 J_1^{-1}$ the quantity*

$$\rho\left(F_1 J_1^{-1}\right) = \max\{|\lambda_i|, i = 1, \ldots, l,\ l \leq m\}.$$

Definition 4.2. *[61] The matrix $F_1 J_1^{-1}$ is called the next generation matrix for the model* (4.7) *and the base reproduction number is given by*

$$R_0 = \rho\left(F_1 J_1^{-1}\right). \tag{4.13}$$

Following the method of van den Driessche [61], presented previously, one easily compute the following basic reproduction number:

$$R_0 = \frac{\beta\,\gamma\,b}{(\alpha + b)\,(\delta + b)\,(\gamma + b)}. \tag{4.14}$$

The reader interested in the details of the algorithm according to which the basic reproduction number (4.14) is computed, is referred to the open access article [62].

4.2.4 Stability of the Normalized SEIQRP Delayed Model

Now, we prove some sufficient conditions for the local asymptotic stability of the DFE, Σ_0, and the endemic equilibrium point, Σ^+, for any time delay $\tau \geq 0$.

Consider the following coordinate transformation: $x_1(t) = s(t) - \bar{s}$, $x_2(t) = e(t) - \bar{e}$, $x_3(t) = i(t) - \bar{i}$, $x_4(t) = q(t) - \bar{q}$, $x_5(t) = r(t) - \bar{r}$, and $x_6(t) = p(t) - \bar{p}$, where $(\bar{s}, \bar{r}, \bar{i}, \bar{q}, \bar{r}, \bar{p})$ denotes any equilibrium point of system (4.3). The linearized system of (4.3) takes the form

$$\dot{X}(t) = A_0\, X(t) + A_1\, X(t - \tau), \tag{4.15}$$

where $X = (x_1, x_2, x_3, x_4, x_5, x_6)^T$,

$$A_0 = \begin{pmatrix} -\alpha - b & 0 & 0 & 0 & 0 & 0 \\ 0 & -\gamma - b & 0 & 0 & 0 & 0 \\ 0 & \gamma & -\delta - b & 0 & 0 & 0 \\ 0 & 0 & \delta & -\lambda - b & 0 & 0 \\ 0 & 0 & 0 & \lambda & -b & 0 \\ \alpha & 0 & 0 & 0 & 0 & -b \end{pmatrix},$$

and

$$A_1 = \begin{pmatrix} -\beta\,\bar{i} & 0 & -\beta\,\bar{s} & 0 & 0 & 0 \\ \beta\,\bar{i} & 0 & \beta\,\bar{s} & 0 & 0 & 0 \\ 0 & 0 & 0 & 0 & 0 & 0 \\ 0 & 0 & 0 & 0 & 0 & 0 \\ 0 & 0 & 0 & 0 & 0 & 0 \\ 0 & 0 & 0 & 0 & 0 & 0 \end{pmatrix}.$$

The characteristic equation of system (4.3), for any equilibrium point, is given by

$$\Delta(y) = |y\,Id_{6\times 6} - A_0 - A_1\,e^{-\tau\,y}|. \tag{4.16}$$

We are now in a position to prove our first two results.

Theorem 4.1 (Stability of the DFE of System (4.3))**.** *If $R_0 < 1$, then the DFE Σ_0 is locally asymptotically stable for any time-delay $\tau \geq 0$. If $R_0 > 1$, then the DFE Σ_0 is unstable for any time-delay $\tau \geq 0$.*

Proof. The characteristic equation of (4.3), at the DFE Σ_0, is given by

$$P(y,\tau) = (y+b)^2\,(y+\alpha+b)\,(y+\lambda+b)\,(y^2+\Lambda_1\,y+\Lambda_2(y)) = 0, \tag{4.17}$$

where $\Lambda_1 = \delta + 2\,b + \gamma$ and $\Lambda_2(y) = (\delta+b)\,(\gamma+b) - \dfrac{\beta\,\gamma\,b}{\alpha+b}e^{-\tau\,y}$.

Let $R_0 < 1$. We divide the proof into non-delayed and delayed cases.

(i) Let $\tau = 0$. In this case, the Equation (4.17) becomes

$$P(y,0) = (y+b)^2\,(y+\alpha+b)\,(y+\lambda+b)\,\left(y^2+\Lambda_1\,y+(\delta+b)\,(\gamma+b) - \frac{\beta\,\gamma\,b}{\alpha+b}\right) = 0\,. \tag{4.18}$$

We need to prove that all roots of the characteristic Equation (4.18) have negative real parts. It is easy to see that $y_1 = -b$, $y_2 = -\alpha - b$ and $y_3 = -\lambda - b$ are roots of Equation (4.18) and all of them are real negative roots. Thus, we just need to analyze the fourth term of (4.18), here denoted by P_1, that is,

$$P_1(y,0) := y^2 + \Lambda_1\,y + (\delta+b)\,(\gamma+b) - \frac{\beta\,\gamma\,b}{\alpha+b}.$$

Using the Routh–Hurwitz Criterion [63], we know that all roots of $P_1(y,0)$ have negative real parts if, and only if, the coefficients of $P_1(y,0)$ are strictly positive. In this case, we have $\Lambda_1 = \delta + 2\,b + \gamma > 0$ and

$$(\delta+b)\,(\gamma+b) - \frac{\beta\,\gamma\,b}{\alpha+b} > 0 \quad \text{ if and only if } \quad R_0 = \frac{\beta\,\gamma\,b}{(\delta+b)\,(\gamma+b)\,(\alpha+b)} < 1.$$

Therefore, we have just proved that the DFE, Σ_0, is locally asymptotically stable for $\tau = 0$, whenever $R_0 < 1$.

(ii) Let $\tau > 0$. In this case, we will use Rouché's Theorem [64], [65] to prove that all roots of the characteristic Equation (4.17) cannot intersect the imaginary axis, i.e., the characteristic equation cannot have pure imaginary roots. Suppose the contrary, that is, suppose there exists $w \in \mathbb{R}$ such that $y = w\,i$ is a solution of (4.17). Replacing y in the fourth term of (4.17), we get that

$$-w^2 + (\delta + 2\,b + \gamma)\,w\,i + (\delta + b)\,(\gamma + b) - \frac{\beta\,\gamma\,b}{\alpha + b}\,(\cos(\tau\,w) - i\,\sin(\tau\,w)) = 0.$$

Then,

$$\begin{cases} -w^2 + (\delta + b)\,(\gamma + b) = \dfrac{\beta\,\gamma\,b}{\alpha + b}\,\cos(\tau\,w), \\ (\delta + 2\,b + \gamma)\,w = -\dfrac{\beta\,\gamma\,b}{\alpha + b}\,\sin(\tau\,w)\,. \end{cases}$$

By adding up the squares of both equations, and using the fundamental trigonometric formula, we obtain that

$$w^4 + \left((\delta + b)^2 + (\gamma + b)^2\right) w^2 + (\delta + b)^2\,(\gamma + b)^2 - \left(\frac{\beta\,\gamma\,b}{\alpha + b}\right)^2 = 0,$$

which is equivalent to

$$w^2 = \frac{1}{2}\sqrt{\left((\delta + b)^2 - (\gamma + b)^2\right)^2 + 4\,\left(\frac{\beta\,\gamma\,b}{\alpha + b}\right)^2} - \frac{1}{2}\left((\delta + b)^2 + (\gamma + b)^2\right). \quad (4.19)$$

If $R_0 < 1$, then $(\delta + b)^2\,(\gamma + b)^2 - \left(\dfrac{\beta\,\gamma\,b}{\alpha + b}\right)^2 > 0$, and

$$\left((\delta + b)^2 + (\gamma + b)^2\right)^2 - 4\left((\delta + b)^2\,(\gamma + b)^2 - \left(\frac{\beta\,\gamma\,b}{\alpha + b}\right)^2\right) < \left((\delta + b)^2 + (\gamma + b)^2\right)^2,$$

so that

$$\sqrt{\left((\delta + b)^2 - (\gamma + b)^2\right)^2 + 4\,\left(\frac{\beta\,\gamma\,b}{\alpha + b}\right)^2} < (\delta + b)^2 + (\gamma + b)^2\,.$$

Hence, we have $w^2 < 0$, which is a contradiction. Therefore, we have proved that whenever $R_0 < 1$, the characteristic Equation (4.17) cannot have pure imaginary roots and the DFE Σ_0 is locally asymptotically stable, for any strictly positive time-delay τ.

(iii) Suppose now that $R_0 > 1$. We know that the characteristic Equation (4.17) has three real negative roots $y_1 = -b$, $y_2 = -\alpha - b$, and $y_3 = -\lambda - b$. Thus, we need to check if the remaining roots of

$$q(y) := y^2 + \Lambda_1\,y + \Lambda_2(y) \quad (4.20)$$

have negative real parts. It is easy to see that $q(0) = \Lambda_2(0) < 0$ because we are assuming $R_0 > 1$. On the other hand, $\lim_{y\to+\infty} q(y) = +\infty$. Therefore, by continuity of $q(y)$, there is at least one positive root of the characteristic Equation (4.17). Hence, we conclude that Σ_0 is unstable when $R_0 > 1$.

The proof is complete. □

Theorem 4.2 (Stability of the EE of System (4.3))**.** *Let $\tau = 0$. If $R_0 > 1$, then the EE point Σ^+ is locally asymptotically stable. When $\tau > 0$, the EE Σ^+ is locally asymptotically stable if the basic reproduction number R_0 satisfies the following relations:*

$$1 < R_0 < \min\left(3, 1 + \frac{\sqrt{(\alpha+b)^2 + (\delta+b)^2 + (\gamma+b)^2}}{\alpha+b}\right) \tag{4.21}$$

and

$$M_1 R_0^2 + M_2 R_0 + M_3 > 0, \tag{4.22}$$

where

$$\begin{aligned}
M_1 &= -(\alpha+b)^2\,\left((\delta+b)^2 + (\gamma+b)^2\right),\\
M_2 &= 2\,(\alpha+b)^2\left((\delta+\gamma+2\,b)^2 - 3\,(\delta+b)\,(\gamma+b)\right)\\
&\quad + 2\,(\alpha+b)\,(\delta+b)\,(\gamma+b)\,(\delta+\gamma+2\,b),\\
M_3 &= 2\,(\alpha+b)\,(\delta+b)\,(\gamma+b)\,(\alpha-\delta-\gamma-b)\,.
\end{aligned}$$

Proof. The characteristic Equation (4.16), computed at the EE Σ^+, is given by

$$\tilde{P}(y,\tau) = (y+b)^2\,(y+\lambda+b)\,(y^3 + \Delta_1(y)\,y^2 + \Delta_2(y)\,y + \Delta_3(y)) = 0\,, \tag{4.23}$$

where $\Delta_1(y) = L_1 + \bar{L}_1\,e^{-\tau\,y}$, $\Delta_2(y) = L_2 + \bar{L}_2\,e^{-\tau\,y}$, and $\Delta_3(y) = L_3 + \bar{L}_3\,e^{-\tau\,y}$ with

$$\begin{aligned}
L_1 &= \alpha+\delta+\gamma+3\,b,\\
\bar{L}_1 &= \frac{\beta\,\gamma\,b - (\delta+b)\,(\gamma+b)\,(\alpha+b)}{(\delta+b)\;(\gamma+b)},\\
L_2 &= (\gamma+2\,b+\delta)\,(\alpha+b) + (\gamma+b)\,(\delta+b),\\
\bar{L}_2 &= (\gamma+2\,b+\delta)\,(\alpha+b)\,(R_0-1) - (\gamma+b)\,(\delta+b),\\
L_3 &= (\alpha+b)\,(\gamma+b)\,(\delta+b),\\
\bar{L}_3 &= \beta\,\gamma\,b - 2\,(\alpha+b)\,(\gamma+b)\,(\delta+b).
\end{aligned}$$

(i) Let $\tau = 0$. In this case, the Equation (4.23) becomes

$$\tilde{P}(y,0) = (y+b)^2\,(y+\lambda+b)\,(y^3 + \tilde{\Delta}_1\,y^2 + \tilde{\Delta}_2\,y + \tilde{\Delta}_3) = 0, \tag{4.24}$$

where $\tilde{\Delta}_1 = L_1 + \bar{L}_1$, $\tilde{\Delta}_2 = L_2 + \bar{L}_2$ and $\tilde{\Delta}_3 = L_3 + \bar{L}_3$. We need to prove that all the roots of the characteristic Equation (4.24) have negative real parts. It is easy

to see that $y_1 = -b$ and $y_2 = -\lambda - b$ are roots of (4.24) and both are real negative roots. Thus, we just need to consider the third term of the above equation. Let

$$\tilde{P}_3(y,0) := y^3 + \tilde{\Delta}_1\, y^2 + \tilde{\Delta}_2\, y + \tilde{\Delta}_3 = 0\,. \tag{4.25}$$

Using the Routh–Hurwitz Criterion [63], we know that all roots of $\tilde{P}_3(y,0)$ have negative real parts if, and only if, the coefficients of $\tilde{P}_3(y,0)$ are strictly positive and $\tilde{\Delta}^* = \tilde{\Delta}_1\,\tilde{\Delta}_2 - \tilde{\Delta}_3 > 0$. If $R_0 > 1$, then

$$\begin{aligned}
\tilde{\Delta}_1 &= \alpha + \delta + \gamma + 3\,b + (\alpha + b)\,(R_0 - 1) > 0,\\
\tilde{\Delta}_2 &= (\delta + \gamma + 2\,b)\,(\alpha + b)\,R_0 > 0,\\
\tilde{\Delta}_3 &= (\alpha + b)\,(\delta + b)\,(\gamma + b)\,(R_0 - 1) > 0,\\
\tilde{\Delta}^* &= (\alpha + b)\,(\alpha + b)\,(\delta + \gamma + 2\,b)\,R_0^2\\
&\quad + (\alpha + b)\,(\delta^2 + 3\,b\,(\delta + b) + \gamma\,(\delta + \gamma + 3\,b))\,R_0\\
&\quad + (\alpha + b)\,(\delta + b)\,(\gamma + b) > 0.
\end{aligned}$$

(ii) Let $\tau > 0$. Using Rouché's Theorem, we prove that all the roots of the characteristic Equation (4.23) cannot intersect the imaginary axis, i.e., the characteristic equation cannot have pure imaginary roots. Suppose the opposite, that is, assume there exists $w \in \mathbb{R}$ such that $y = w\,i$ is a solution of (4.23). Replacing y into the third term of (4.23), we get that

$$-w^3\,i - L_1\,w^2 + L_2\,w\,i + L_3 + (-\bar{L}_1\,w^2 + \bar{L}_2\,w\,i + \bar{L}_3)\,(\cos(\tau\,w) - i\,\sin(\tau\,w)) = 0.$$

Then,

$$\begin{cases}
-L_1\,w^2 + L_3 = (\bar{L}_1\,w^2 - \bar{L}_3)\,\cos(\tau\,w) - \bar{L}_2\,w\,\sin(\tau\,w),\\
-w^3 + L_2\,w = -\bar{L}_2\,w\,\cos(\tau\,w) - (\bar{L}_1\,w^2 - \bar{L}_3)\,\sin(\tau\,w)\,.
\end{cases}$$

By adding up the squares of both equations, and using the fundamental trigonometric formula, we obtain that

$$w^6 + K_1\,w^4 + K_2\,w^2 + K_3 = 0,$$

where

$$\begin{aligned}
K_1 &= L_1^2 - \bar{L}_1^2 - 2\,L_2,\\
K_2 &= 2\,\bar{L}_1\,\bar{L}_3 - 2\,L_1\,L_3 + L_2^2 - \bar{L}_2^2,\\
K_3 &= L_3^2 - \bar{L}_3^2.
\end{aligned}$$

Assume that the basic reproduction number R_0 satisfies relations (4.21) and (4.22) with the following condition:

$$\min\left(3, 1+\frac{\sqrt{(\alpha+b)^2+(\delta+b)^2+(\gamma+b)^2}}{\alpha+b}\right)=1+\frac{\sqrt{(\alpha+b)^2+(\delta+b)^2+(\gamma+b)^2}}{\alpha+b}. \tag{4.26}$$

Then,

$$K_1=(\delta+b)^2+(\gamma+b)^2+(\alpha+b)^2\left(1-(R_0-1)^2\right)>0.$$

In contrast, if R_0 satisfies relations (4.21) and (4.22) with the condition

$$\min\left(3, 1+\frac{\sqrt{(\alpha+b)^2+(\delta+b)^2+(\gamma+b)^2}}{\alpha+b}\right)=3\,, \tag{4.27}$$

then we have

$$1<R_0<3<1+\frac{\sqrt{(\alpha+b)^2+(\delta+b)^2+(\gamma+b)^2}}{\alpha+b},$$

which is equivalent to

$$\begin{aligned}
&0<R_0-1<2<\frac{\sqrt{(\alpha+b)^2+(\delta+b)^2+(\gamma+b)^2}}{\alpha+b},\\
&1-\left(\frac{(\alpha+b)^2+(\delta+b)^2+(\gamma+b)^2}{(\alpha+b)^2}\right)<1-(R_0-1)^2<1,\\
&-(\delta+b)^2-(\gamma+b)^2<(\alpha+b)^2\left(1-(R_0-1)^2\right)<(\alpha+b)^2.
\end{aligned}$$

Thus,

$$K_1>0.$$

Under the assumption that the basic reproduction number R_0 satisfies relations (4.21) and (4.22), we have

$$K_2=M_1R_0^2+M_2R_0+M_3>0\,.$$

Therefore, if we assume that the basic reproduction number R_0 satisfies relations (4.21) and (4.22) with condition (4.27), then

$$K_3=(\alpha+b)^2(\delta+b)^2(\gamma+b)^2\left(1-(R_0-2)^2\right)>0;$$

if R_0 satisfies relations (4.21) and (4.22) with condition (4.26), then we have

$$1<R_0<1+\frac{\sqrt{(\alpha+b)^2+(\delta+b)^2+(\gamma+b)^2}}{\alpha+b}<3,$$

which is equivalent to

$$-1<R_0-2<-1+\frac{\sqrt{(\alpha+b)^2+(\delta+b)^2+(\gamma+b)^2}}{\alpha+b}<1,$$

and also equivalent to

$$1 - (R_0 - 2)^2 > 0.$$

Thus,

$$K_3 > 0\,.$$

We conclude that the left side of equation (4.23) is strictly positive, which implies that this equation is not possible. Therefore, (4.24) does not have imaginary roots, which implies that Σ^+ is locally asymptotically stable for any time delay $\tau > 0$.

The proof is complete. □

It should be noted that Theorem 4.2 is not trivial, and it is not easy to give a biological/medical interpretation to the relations (4.21) and (4.22).

4.3 The Delayed SEIQRPW Model with Vaccination

Let us introduce in the model (4.2) a constant u and an extra variable $W(t)$, $t \in [0, t_f]$, representing the fraction of susceptible individuals that are vaccinated and the number of vaccines used, respectively, with

$$\dot{W}(t) = u\, S(t), \tag{4.28}$$

subject to the initial condition $W(0) = 0$. Note that (4.28) is just the production rate of vaccinated.

The model with vaccination is given by the following system of seven nonlinear delayed differential equations:

$$\begin{cases} \dot{S}(t) = bN(t) - \frac{\beta\, S(t-\tau)\, I(t-\tau)}{N(t)} - (\alpha + u + \mu)\; S(t)\,, \\ \dot{E}(t) = \frac{\beta\, S(t-\tau)\, I(t-\tau)}{N(t)} - (\gamma + \mu) E(t)\,, \\ \dot{I}(t) = \gamma E(t) - (\delta + \mu) I(t)\,, \\ \dot{Q}(t) = \delta I(t) - (\lambda + \mu) Q(t)\,, \\ \dot{R}(t) = \lambda Q(t) - \mu R(t)\,, \\ \dot{P}(t) = \alpha S(t) - \mu P(t)\,, \\ \dot{W}(t) = u\, S(t) - \mu W(t)\,, \end{cases} \tag{4.29}$$

where the total population $N(t)$ is given by

$$N(t) = S(t) + E(t) + I(t) + Q(t) + R(t) + P(t) + W(t)\,, \quad \forall\, t \in [0, T]\,. \tag{4.30}$$

The state variables are subject to the following initial conditions: $S(\theta) = S_0$, $\theta \in [-\tau, 0]$, $E(0) = E_0$, $I(\theta) = I_0$, $\theta \in [-\tau, 0]$, $Q(0) = Q_0$, $R(0) = R_0$, $P(0) = P_0$, and $W(0) = 0$.

Note that in model (4.29) we do not vaccinate the insusceptible/protected individuals $P(t)$, assumed protected through precautionary measures with a protection rate α. Moreover, the fraction of susceptible individuals that are vaccinated is u. A schematic diagram of our system is given in Figure 4.2.

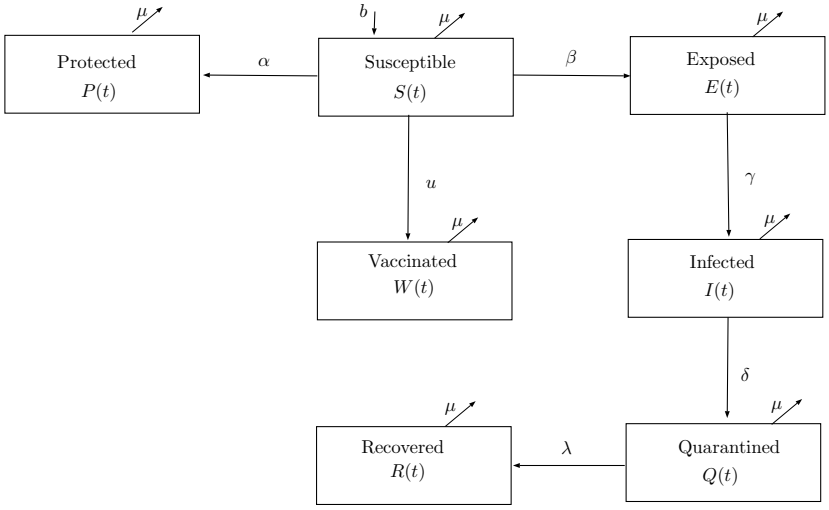

Figure 4.2: Schematic diagram of the generalized SEIQRPW delayed model (4.29).

4.3.1 Normalized SEIQRPW Delayed Model with Vaccination

Analogously to Section 4.2, we consider the proportions of each compartment of individuals in the population, namely $s(t) = \frac{S(t)}{N(t)}$, $e(t) = \frac{E(t)}{N(t)}$, $i(t) = \frac{I(t)}{N(t)}$, $q(t) = \frac{Q(t)}{N(t)}$, $r(t) = \frac{R(t)}{N(t)}$, $p(t) = \frac{P(t)}{N(t)}$, and $w(t) = \frac{W(t)}{N(t)}$. According to Equation (4.30), we have $\dot{N}(t) = (b - \mu)N(t)$. Therefore, the normalized SEIQRP delayed model is given by

$$\begin{cases} \dot{s}(t) = b - \beta\, s(t-\tau)\, i(t-\tau) - (\alpha + u + b)\, s(t), \\ \dot{e}(t) = \beta\, s(t-\tau)\, i(t-\tau) - (\gamma + b)\, e(t), \\ \dot{i}(t) = \gamma\, e(t) - (\delta + b)\, i(t), \\ \dot{q}(t) = \delta\, i(t) - (\lambda + b)\, q(t), \\ \dot{r}(t) = \lambda\, q(t) - b\, r(t), \\ \dot{p}(t) = \alpha\, s(t) - b\, p(t), \\ \dot{w}(t) = u\, s(t) - b\, w(t)\,. \end{cases} \tag{4.31}$$

The state variables for system (4.31) are subject to the following initial conditions: $s(\theta) = \dfrac{S_0}{N(0)}$, $\theta \in [-\tau, 0]$, $e(0) = \dfrac{E_0}{N(0)}$, $i(\theta) = \dfrac{I_0}{N(0)}$, $\theta \in [-\tau, 0]$, $q(0) = \dfrac{Q_0}{N(0)}$, $r(0) = \frac{R_0}{N(0)}$, $p(0) = \dfrac{P_0}{N(0)}$, and $w(0) = 0$, with $s(t)+e(t)+i(t)+q(t)+r(t)+p(t)+w(t) = 1$.

4.3.2 Equilibrium Points

The DFE and EE of model (4.31) can be obtained by equating the right-hand side of Equation (4.31) to zero, hence satisfying

$$\begin{aligned}
b - \beta\, s(t-\tau)\, i(t-\tau) - (\alpha + u + b)\, s(t) &= 0\,,\\
\beta\, s(t-\tau)\, i(t-\tau) - (\gamma + b)\, e(t) &= 0\,,\\
\gamma e(t) - (\delta + b) i(t) &= 0\,,\\
\delta i(t) - (\lambda + b) q(t) &= 0\,,\\
\lambda\, q(t) - b\, r(t) &= 0\,,\\
\alpha s(t) - b p(t) &= 0\,,\\
u\, s(t) - b\, w(t) &= 0\,.
\end{aligned}$$

The DFE of model (4.31), Σ_1, is given by

$$\Sigma_1 = (s_0, e_0, i_0, q_0, r_0, p_0, w_0) = \left(\frac{b}{\alpha + u + b}, 0, 0, 0, 0, \frac{\alpha}{\alpha + u + b}, \frac{u}{\alpha + u + b} \right)\,, \quad (4.32)$$

while the EE point for system (4.31), Σ_V^+, is given by

$$\Sigma_V^+ = (s^*, e^*, i^*, q^*, r^*, p^*, w^*)\,, \quad (4.33)$$

where

$$\begin{aligned}
s^* &= \frac{(\delta + b)\ (\gamma + b)}{\beta\, \gamma},\\
e^* &= \frac{\beta\, s^+\, i^+}{(\gamma + b)},\\
i^* &= \frac{\beta\, \gamma\, b - (\delta + b)\, (\gamma + b)\, (\alpha + u + b)}{\beta\ (\delta + b)\ (\gamma + b)},\\
q^* &= \frac{\beta\, \gamma\, b\, \delta - \delta\ (\delta + b)\, (\gamma + b)\, (\alpha + u + b)}{\beta\ (\lambda + b)\ (\delta + b)\ (\gamma + b)},\\
r^* &= \frac{\lambda\, \delta\, \beta\, \gamma\, b - \lambda\, \delta\ (\delta + b)\, (\gamma + b)\, (\alpha + u + b)}{b\, \beta\ (\lambda + b)\ (\delta + b)\ (\gamma + b)},\\
p^* &= \frac{\alpha\ (\delta + b)\ (\gamma + b)}{b\, \beta\, \gamma},\\
w^* &= \frac{u\ (\delta + b)\ (\gamma + b)}{b\, \beta\, \gamma}.
\end{aligned}$$

4.3.3 Basic reproduction number

The progression of a person from compartment e to i is not considered a new infection. Then

$$F = \begin{pmatrix} 0 \\ \beta\, s(t-\tau)\, i(t-\tau) \\ 0 \\ 0 \\ 0 \\ 0 \\ 0 \end{pmatrix} \text{ and } V = \begin{pmatrix} -b + \beta\, s(t-\tau)\, i(t-\tau) + (\alpha + u + b)\, s(t) \\ +(\gamma + b)\, e(t) \\ -\gamma\, e(t) + (\delta + b)\, i(t) \\ -\delta\, i(t) + (\lambda + b)\, q(t) \\ -\lambda\, q(t) + b\, r(t) \\ -\alpha\, s(t) + b\, p(t) \\ -u\, s(t) + b\, w(t) \end{pmatrix}.$$

The infected compartments are e and i, which gives $m = 2$. The point of equilibrium without disease Σ_0 is given by (4.32), then we have:

$$F_1 = \begin{pmatrix} 0 & \frac{\beta b}{\alpha+u+b} \\ 0 & 0 \end{pmatrix},\ J_1 = \begin{pmatrix} \gamma + b & 0 \\ -\gamma & \delta + b \end{pmatrix},$$

the eigenvalues of the matrix $F_1\, J_1^{-1}$ are

$$0 \ \text{ and } \ \frac{\beta\, \gamma\, b}{(\alpha + u + b)\,(\delta + b)\,(\gamma + b)},$$

so

$$\tilde{R}_0 = \frac{\beta\, \gamma\, b}{(\alpha + u + b)\,(\delta + b)\,(\gamma + b)}\,. \tag{4.34}$$

4.3.4 Stability of the Normalized SEIQRPW Delayed Model with Vaccination

Consider the following coordinate transformation: $x_1(t) = s(t) - \bar{s}$, $x_2(t) = e(t) - \bar{e}$, $x_3(t) = i(t) - \bar{i}$, $x_4(t) = q(t) - \bar{q}$, $x_5(t) = r(t) - \bar{r}$, $x_6(t) = p(t) - \bar{p}$, and $x_7(t) = w(t) - \bar{w}$, where $(\bar{s}, \bar{e}, \bar{i}, \bar{q}, \bar{r}, \bar{p}, \bar{w})$ denotes an equilibrium point of system (4.31). The linearized system of (4.31) takes the form

$$\dot{X}(t) = \tilde{A}_0\, X(t) + \tilde{A}_1\, X(t-\tau), \tag{4.35}$$

where $X = (x_1, x_2, x_3, x_4, x_5, x_6, x_7)^T$,

$$\tilde{A}_0 = \begin{pmatrix} -\alpha - u - b & 0 & 0 & 0 & 0 & 0 & 0 \\ 0 & -\gamma - b & 0 & 0 & 0 & 0 & 0 \\ 0 & \gamma & -\delta - b & 0 & 0 & 0 & 0 \\ 0 & 0 & \delta & -\lambda - b & 0 & 0 & 0 \\ 0 & 0 & 0 & \lambda & -b & 0 & 0 \\ \alpha & 0 & 0 & 0 & 0 & -b & 0 \\ u & 0 & 0 & 0 & 0 & 0 & -b \end{pmatrix},$$

$$\tilde{A}_1 = \begin{pmatrix} -\beta\,\bar{i} & 0 & -\beta\,\bar{s} & 0 & 0 & 0 & 0 \\ \beta\,\bar{i} & 0 & \beta\,\bar{s} & 0 & 0 & 0 & 0 \\ 0 & 0 & 0 & 0 & 0 & 0 & 0 \\ 0 & 0 & 0 & 0 & 0 & 0 & 0 \\ 0 & 0 & 0 & 0 & 0 & 0 & 0 \\ 0 & 0 & 0 & 0 & 0 & 0 & 0 \\ 0 & 0 & 0 & 0 & 0 & 0 & 0 \end{pmatrix}.$$

The characteristic equation of system (4.31) is given by

$$\tilde{\Gamma}(y) = |y\,Id_{7\times 7} - \tilde{A}_0 - \tilde{A}_1\,e^{-\tau\,y}|. \tag{4.36}$$

We are also able to prove stability results for the normalized SEIQRPW delayed model with vaccination.

Theorem 4.3 (Stability of the DFE of System (4.31))**.** *If $\tilde{R}_0 < 1$, then the DFE Σ_1 is locally asymptotically stable for any time-delay $\tau \geq 0$. If $\tilde{R}_0 > 1$, then the DFE is unstable for any time-delay $\tau \geq 0$.*

Proof. The characteristic Equation (4.36) at the DFE, Σ_1, is given by

$$P^*(y,\tau) = (y+b)^3\,(y+\alpha+u+b)\,(y+\lambda+b)\,(y^2+\Gamma_1\,y+\Gamma_2(y)) = 0, \tag{4.37}$$

where $\Gamma_1 = \delta + 2\,b + \gamma$ and $\Gamma_2(y) = (\delta+b)\,(\gamma+b) - \dfrac{\beta\,\gamma\,b}{\alpha+u+b}e^{-\tau\,y}$.

(i) Let $\tau = 0$. In this case, the Equation (4.37) becomes

$$P^*(y,0) = (y+b)^3\,(y+\alpha+u+b)\,(y+\lambda+b) \left(y^2+\Gamma_1\,y+(\delta+b)\,(\gamma+b) - \frac{\beta\,\gamma\,b}{\alpha+u+b}\right) = 0\,. \tag{4.38}$$

We need to prove that all roots of the characteristic Equation (4.38) have negative real parts. It is easy to see that $y_1 = -b$, $y_2 = -\alpha - u - b$ and $y_3 = -\lambda - b$ are roots of Equation (4.38) and the three are real and negative. Thus, we just need to consider the fourth term of Equation (4.38). Let

$$P_3^*(y,0) := y^2 + \Gamma_1\,y + (\delta+b)\,(\gamma+b) - \frac{\beta\,\gamma\,b}{\alpha+u+b}.$$

Using the Routh–Hurwitz Criterion [63], we know that all roots of $P_3^*(y,0)$ have negative real parts if, and only if, the coefficients of $P_3^*(y,0)$ are strictly positive. In this case, $\Gamma_1 = \delta + 2\,b + \gamma > 0$ and

$$(\delta+b)\,(\gamma+b) - \frac{\beta\,\gamma\,b}{\alpha+u+b} > 0 \text{ if, and only if, } \tilde{R}_0 = \frac{\beta\,\gamma\,b}{(\alpha+u+b)\;(\delta+b)\;(\gamma+b)} < 1.$$

Therefore, we have proved that the DFE, Σ_1, is locally asymptotically stable for $\tau = 0$, whenever $\tilde{R}_0 < 1$.

(ii) Let $\tau > 0$. Using Rouché's Theorem, we prove that all roots of the characteristic Equation (4.37) can not have pure imaginary roots. Suppose the contrary, i.e., that there exists $w \in \mathbb{R}$ such that $y = w\,i$ is a solution of (4.37). Replacing y in the fourth term of (4.37), we get

$$-w^2 + (\delta + 2\,b + \gamma)\,w\,i + (\delta + b)\,(\gamma + b) - \frac{\beta\,\gamma\,b}{\alpha + u + b}\,(\cos(\tau\,w) - i\,\sin(\tau\,w)) = 0\,.$$

Then,

$$\begin{cases} -w^2 + (\delta + b)\,(\gamma + b) = \dfrac{\beta\,\gamma\,b}{\alpha + u + b}\,\cos(\tau\,w), \\ (\delta + 2\,b + \gamma)\,w = -\dfrac{\beta\,\gamma\,b}{\alpha + u + b}\,\sin(\tau\,w)\,. \end{cases}$$

By adding up the squares of both equations and using the fundamental trigonometric formula, one has

$$w^4 + \left((\delta + b)^2 + (\gamma + b)^2\right) w^2 + (\delta + b)^2\,(\gamma + b)^2 - \left(\frac{\beta\,\gamma\,b}{\alpha + u + b}\right)^2 = 0,$$

which is equivalent to

$$w^2 = \frac{1}{2}\sqrt{\left((\delta + b)^2 - (\gamma + b)^2\right)^2 + 4\left(\frac{\beta\,\gamma\,b}{\alpha + u + b}\right)^2} - \frac{1}{2}\left((\delta + b)^2 + (\gamma + b)^2\right). \tag{4.39}$$

If $\tilde{R}_0 < 1$, then $(\delta + b)^2\,(\gamma + b)^2 - \left(\dfrac{\beta\,\gamma\,b}{\alpha + u + b}\right)^2 > 0$, and

$$\left((\delta + b)^2 + (\gamma + b)^2\right)^2 - 4\left((\delta + b)^2\,(\gamma + b)^2 - \left(\frac{\beta\,\gamma\,b}{\alpha + u + b}\right)^2\right) < \left((\delta + b)^2 + (\gamma + b)^2\right)^2,$$

so that

$$\sqrt{\left((\delta + b)^2 - (\gamma + b)^2\right)^2 + 4\left(\frac{\beta\,\gamma\,b}{\alpha + u + b}\right)^2} < (\delta + b)^2 + (\gamma + b)^2\,.$$

Hence, we have $w^2 < 0$, which is a contradiction. Therefore, we have proved that if $\tilde{R}_0 < 1$, then the characteristic Equation (4.37) cannot have pure imaginary roots and the DFE Σ_1 is locally asymptotically stable, for any strictly positive time delay τ.

(iii) Suppose now that $\tilde{R}_0 > 1$. We know that the characteristic Equation (4.37) has three real negative roots $y_1 = -b, y_2 = -\alpha - u - b$ and $y_3 = -\lambda - b$. Thus, we need to check if the remaining roots of

$$q^*(y) := y^2 + \Gamma_1\,y + \Gamma_2(y) \tag{4.40}$$

have negative real parts. It is easy to see that $q(0) = \Gamma_2(0) < 0$, because we are assuming $\tilde{R}_0 > 1$. On the other hand, $\lim_{y \to +\infty} q^*(y) = +\infty$. Therefore, by continuity of $q^*(y)$, there is at least one positive root of the characteristic Equation (4.37). Hence, we conclude that Σ_1 is unstable, for any $\tau \geq 0$.

The proof is complete. □

Theorem 4.4 (Stability of the EE point of System (4.31))**.** *Let $\tau = 0$. If $\tilde{R}_0 > 1$, then the EE Σ_V^+ is locally asymptotically stable. When $\tau > 0$, the EE Σ_V^+ is locally asymptotically stable if the basic reproduction number $\tilde{R}_0$ satisfies the following relations:*

$$1 < \tilde{R}_0 < \min\left(3, 1 + \frac{\sqrt{(\alpha+u+b)^2 + (\delta+b)^2 + (\gamma+b)^2}}{\alpha+u+b}\right) \tag{4.41}$$

and

$$M_1^* \tilde{R}_0^2 + M_2^* \tilde{R}_0 + M_3^* > 0\,, \tag{4.42}$$

where

$$\begin{aligned} M_1^* &= -(\alpha+u+b)^2 \left((\delta+b)^2 + (\gamma+b)^2\right), \\ M_2^* &= 2\,(\alpha+u+b)^2 \left((\delta+\gamma+2\,b)^2 - 3\,(\delta+b)\,(\gamma+b)\right) \\ &\quad + 2\,(\alpha+u+b)\,(\delta+b)\,(\gamma+b)\,(\delta+\gamma+2\,b), \\ M_3^* &= 2\,(\alpha+u+b)\,(\delta+b)\,(\gamma+b)\,(\alpha+u-\delta-\gamma-b)\,. \end{aligned} \tag{4.43}$$

Proof. The characteristic Equation (4.36), computed at the EE Σ_V^+, is given by

$$\tilde{P}^*(y,\tau) = (y+b)^3\,(y+\lambda+b)\,(y^3 + \Omega_1(y)\,y^2 + \Omega_2(y)\,y + \Omega_3(y)) = 0\,, \tag{4.44}$$

where $\Omega_1(y) = L_1^* + \bar{L}_1^*\,e^{-\tau\,y}$, $\Omega_2(y) = L_2^* + \bar{L}_2^*\,e^{-\tau\,y}$, and $\Omega_3(y) = L_3^* + \bar{L}_3^*\,e^{-\tau\,y}$ with

$$\begin{aligned} L_1^* &= \alpha+u+\delta+\gamma+3\,b, \\ \bar{L}_1^* &= \frac{\beta\,\gamma\,b - (\delta+b)\,(\gamma+b)\,(\alpha+u+b)}{(\delta+b)\,(\gamma+b)}, \\ L_2^* &= (\gamma+2\,b+\delta)\,(\alpha+u+b) + (\gamma+b)\,(\delta+b), \\ \bar{L}_2^* &= (\gamma+2\,b+\delta)\,(\alpha+u+b)\,(\tilde{R}_0-1) - (\gamma+b)\,(\delta+b), \\ L_3^* &= (\alpha+u+b)\,(\gamma+b)\,(\delta+b), \\ \bar{L}_3^* &= \beta\,\gamma\,b - 2\,(\alpha+u+b)\,(\gamma+b)\,(\delta+b). \end{aligned}$$

(i) Let $\tau = 0$. In this case, Equation (4.44) becomes

$$\tilde{P}^*(y,0) = (y+b)^3\,(y+\lambda+b)\left(y^3 + \tilde{\Omega}_1\,y^2 + \tilde{\Omega}_2\,y + \tilde{\Omega}_3\right) = 0\,, \tag{4.45}$$

where $\tilde{\Omega}_1 = L_1^* + \bar{L}_1^*$, $\tilde{\Omega}_2 = L_2^* + \bar{L}_2^*$ and $\tilde{\Omega}_3 = L_3^* + \bar{L}_3^*$. Looking at the roots of the characteristic Equation (4.45), it is easy to see that $y_1 = -b$ and $y_2 = -\lambda - b$ are real negative roots of (4.45). Considering the third term of the above equation, let

$$\tilde{P}_3^*(y,0) := y^3 + \tilde{\Omega}_1\,y^2 + \tilde{\Omega}_2\,y + \tilde{\Omega}_3 = 0\,. \tag{4.46}$$

Using the Routh–Hurwitz Criterion [63], we know that all roots of $\tilde{P}_3^*(y,0)$ have negative real parts if, and only if, the coefficients of $\tilde{P}_3^*(y,0)$ are strictly positive and

$$\tilde{\Omega}^* = \tilde{\Omega}_1\,\tilde{\Omega}_2 - \tilde{\Omega}_3 \;> 0.$$

If $\tilde{R}_0 > 1$, then

$$\begin{aligned}
\tilde{\Omega}_1 &= \alpha + u + \delta + \gamma + 3\,b + (\alpha + u + b)\;(\tilde{R}_0 - 1) > 0,\\
\tilde{\Omega}_2 &= (\delta + \gamma + 2\,b)\,(\alpha + u + b)\,\tilde{R}_0 > 0,\\
\tilde{\Omega}_3 &= (\alpha + u + b)\,(\delta + b)\,(\gamma + b)\,(\tilde{R}_0 - 1) > 0,\\
\tilde{\Omega}^* &= (\alpha + u + b)\,(\delta + \gamma + 2\,b)\,\tilde{R}_0^2 + (\alpha + u + b)\,(\delta^2 + 3\,b\,(\delta + b) + \gamma\,(\delta + \gamma + 3\,b))\,\tilde{R}_0\\
&\quad + (\alpha + u + b)\,(\delta + b)\,(\gamma + b) > 0.
\end{aligned}$$

(ii) Let $\tau > 0$. By Rouché's theorem, we prove that all roots of the characteristic Equation (4.44) cannot intersect the imaginary axis, i.e., the characteristic equation cannot have pure imaginary roots. Suppose the opposite, i.e., that there exists $w \in \mathbb{R}$ such that $y = w\,i$ is a solution of (4.44). Replacing y in the third term of (4.44), we get

$$-w^3\,i - L_1^*\,w^2 + L_2^*\,w\,i + L_3^* + (-\bar{L}_1^*\,w^2 + \bar{L}_2^*\,w\,i + \bar{L}_3^*)\;(\cos(\tau\,w) - i\,\sin(\tau\,w)) = 0.$$

Then,

$$\begin{cases}
-L_1^*\,w^2 + L_3^* = (\bar{L}_1^*\,w^2 - \bar{L}_3^*)\;\cos(\tau\,w) - \bar{L}_2^*\,w\;\sin(\tau\,w)\,,\\
-w^3 + L_2^*\,w = -\bar{L}_2^*\,w\;\cos(\tau\,w) - (\bar{L}_1^*\,w^2 - \bar{L}_3^*)\;\sin(\tau\,w)\,.
\end{cases}$$

By adding up the squares of both equations and using the fundamental trigonometric formula, we obtain that

$$w^6 + K_1^*\,w^4 + K_2^*\,w^2 + K_3^* = 0,$$

where

$$\begin{aligned}
K_1^* &= (L_1^*)^2 - (\bar{L}_1^*)^2 - 2\,L_2^*,\\
K_2^* &= 2\,\bar{L}_1^*\,\bar{L}_3^* - 2\,L_1^*\,L_3^* + (L_2^*)^2 - (\bar{L}_2^*)^2,\\
K_3^* &= (L_3^*)^2 - (\bar{L}_3^*)^2.
\end{aligned}$$

Assume that the basic reproduction number $\tilde{R}_0$ satisfies relations (4.41) and (4.42) with the condition

$$\begin{aligned}
\min\left(3, 1 + \frac{\sqrt{(\alpha + u + b)^2 + (\delta + b)^2 + (\gamma + b)^2}}{\alpha + b}\right)&\\
= 1 + \frac{\sqrt{(\alpha + u + b)^2 + (\delta + b)^2 + (\gamma + b)^2}}{\alpha + u + b}.&\quad (4.47)
\end{aligned}$$

Then,

$$K_1^* = (\delta + b)^2 + (\gamma + b)^2 + (\alpha + u + b)^2 \left(1 - \left(\tilde{R}_0 - 1\right)^2\right) > 0.$$

In contrast, if $\tilde{R}_0$ satisfies relations (4.41) and (4.42) under the condition

$$\min\left(3, 1 + \frac{\sqrt{(\alpha + u + b)^2 + (\delta + b)^2 + (\gamma + b)^2}}{\alpha + u + b}\right) = 3, \tag{4.48}$$

then we have

$$1 < \tilde{R}_0 < 3 < 1 + \frac{\sqrt{(\alpha + u + b)^2 + (\delta + b)^2 + (\gamma + b)^2}}{\alpha + u + b},$$

which is equivalent to

$$\begin{aligned}
&0 < \tilde{R}_0 - 1 < 2 < \frac{\sqrt{(\alpha + u + b)^2 + (\delta + b)^2 + (\gamma + b)^2}}{\alpha + u + b}, \\
&1 - \left(\frac{(\alpha + u + b)^2 + (\delta + b)^2 + (\gamma + b)^2}{(\alpha + u + b)^2}\right) < 1 - (\tilde{R}_0 - 1)^2 < 1, \\
&-(\delta + b)^2 - (\gamma + b)^2 < (\alpha + u + b)^2 \left(1 - (\tilde{R}_0 - 1)^2\right) < (\alpha + u + b)^2.
\end{aligned}$$

Thus,

$$K_1^* > 0.$$

Under the assumption that the basic reproduction number $\tilde{R}_0$ satisfies relations (4.41) and (4.42), we have

$$K_2^* = M_1^* \tilde{R}_0^2 + M_2^* \tilde{R}_0 + M_3^* > 0\,. \tag{4.49}$$

Therefore, if we assume that the basic reproduction number $\tilde{R}_0$ satisfies relations (4.41) and (4.42) with condition (4.48), then

$$K_3^* = (\alpha + u + b)^2 (\delta + b)^2 (\gamma + b)^2 \left(1 - \left(\tilde{R}_0 - 2\right)^2\right) > 0; \tag{4.50}$$

if $\tilde{R}_0$ satisfies (4.41) and (4.42) with condition (4.47), then we have

$$1 < \tilde{R}_0 < 1 + \frac{\sqrt{(\alpha + u + b)^2 + (\delta + b)^2 + (\gamma + b)^2}}{\alpha + u + b} < 3\,,$$

which is equivalent to

$$-1 < \tilde{R}_0 - 2 < -1 + \frac{\sqrt{(\alpha + u + b)^2 + (\delta + b)^2 + (\gamma + b)^2}}{\alpha + u + b} < 1,$$

and also equivalent to

$$1 - \left(\tilde{R}_0 - 2\right)^2 > 0\,.$$

Thus,

$$K_3^* > 0.$$

We have just proved that the left hand-side of Equation (4.44) is strictly positive, which implies that this equation is not possible. Therefore, (4.45) does not have imaginary roots, and Σ_V^+ is locally asymptotically stable, for any time delay $\tau > 0$, whenever $\tilde{R}_0$ satisfies conditions (4.41) and (4.42).

The proof is complete. □

It should be noted that Theorem 4.3 is not trivial, and it is not easy to give a biological/medical interpretation to the relations (4.41) and (4.42).

4.4 Numerical Simulations and Discussion

In this section, we investigate, numerically, the local stability of the normalized SEIQRP and SEIQRPW models, illustrating our results from Sections 4.2 and 4.3. All numerical computations were performed in the numeric computing environment MATLAB R2019b using the medium-order method and numerical interpolation [66].

4.4.1 Local Stability of the Delayed SEIQRP Model

Consider the normalized delayed SEIQRP model (4.3), proposed in Section 4.2. Take the initial conditions

$$(s_0, e_0, i_0, q_0, r_0, p_0) = (0.7, 0.05, 0.05, 0.1, 0.05, 0.05)$$

and the parameter values as given in Table 4.1.

Parameter	Value	Units	Ref
b	1		Assumed
μ	1		Assumed
δ	1	day^{-1}	Assumed
α	1	day^{-1}	Assumed
β	12	day^{-1}	Assumed
γ	1	day^{-1}	Assumed
λ	1	day^{-1}	Assumed
t_f	30	day	Assumed

Table 4.1: Parameter values used in the simulations of Section 4.4.1.

In Figure 4.3, we present the numerical solutions to the delayed model (4.3) in the time interval $[0, 30]$ days.

Considering the parameter values from Table 4.1, we have the following value for the basic reproduction number R_0 of Section 4.2: $R_0 = 1.5$. From Theorem 4.2, $R_0 = 1.5$

satisfies the conditions (4.21) and (4.22), so the EE $EE = (\frac{1}{3}, \frac{1}{6}, \frac{1}{12}, \frac{1}{24}, \frac{1}{24}, \frac{1}{3})$ of system (4.3) is locally asymptotically stable for any time delay $\tau \geq 0$.

In Figure 4.4, we observe the effect of the time delays: $\tau = 0, \ldots, 6$ on the classes e of exposed and i of infectious. The presence of waves is due to the presence of the time delay and is related to the emergence of the COVID-19 waves. For the study of multiple epidemic waves in the context of COVID-19, we refer the interested reader to [67].

4.4.2 Delayed SEIQRPW Model with Vaccination: COVID-19 in Italy

Now, we study, numerically, the stability of the spread of the epidemic of COVID-19 in Italy for the period of three months starting from 18 October 2020, using the delayed model (4.31) that we proposed in Section 4.3. The preliminary conditions and real data were taken and computed from the database `https://raw.githubusercontent.com/pcm-dpc/COVID-19/master/dati-regioni/dpc-covid19-ita-regioni.csv` (accessed on 14 August 2021). We consider the initial conditions

$$(s_0, e_0, i_0, q_0, r_0, p_0, w_0) = \frac{1}{N}(59769273, 403601, 8837, 44098, 254058, 133, 0)$$

with $N = 60480000$ [68], and the parameter values as given in Table 4.2, which are obtained using the nonlinear least-squares solver [69]. The reader is interested in the details of the nonlinear least-squares solver, according to which the parameters of the delayed model (4.31) are computed, is referred to as the open-access article [69].

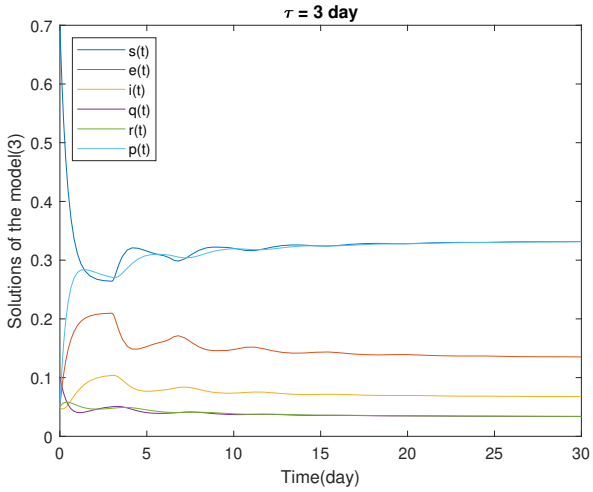

Figure 4.3: Dynamics of model (4.3) with $\tau = 3$ days. Parameter values as in Table 4.1.

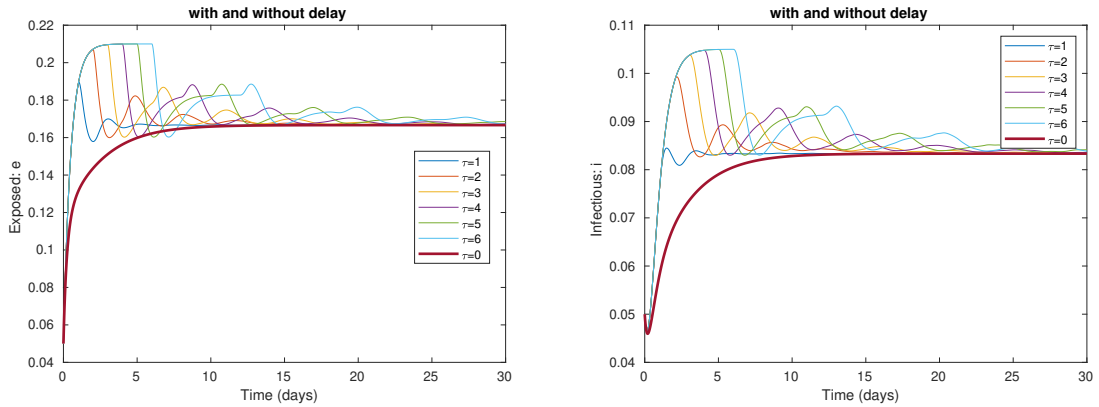

Figure 4.4: Dynamics of model (4.3) with $\tau \in [0, 6]$ days. Parameter values as in Table 4.1.

Parameter	Value	Units	Ref
b	7.391‰		[68]
μ	10.658‰		[68]
α	1.1775	day^{-1}	[69]
β	3.97	day^{-1}	[69]
γ	0.0048	day^{-1}	[69]
λ	0.0182256	day^{-1}	[69]
δ	0.1432	day^{-1}	[69]
t_f	90	day	Assumed

Table 4.2: Parameter values used in the simulations of Section 4.4.2, modeling the spread of the epidemic of COVID-19 in Italy for the period of three months starting 18 October 2020.

In Figures 4.5 and 4.6, we present numerical solutions to the delayed model (4.31) in the time interval $t \in [0, 90]$ days, $t = 0$ representing 18 October 2020, and considering two cases:

- Case 1: $\tau = 0$ days (without delay), with different percentages of susceptible individuals being vaccinated — $u = 0\%$, $u = 20\%$, $u = 40\%$ and $u = 60\%$ (Figure 4.5).
- Case 2: $u = 20\%$ (fixed), with different delays — $\tau = 0$ days, $\tau = 3$ days, and $\tau = 6$ days (Figure 4.6).

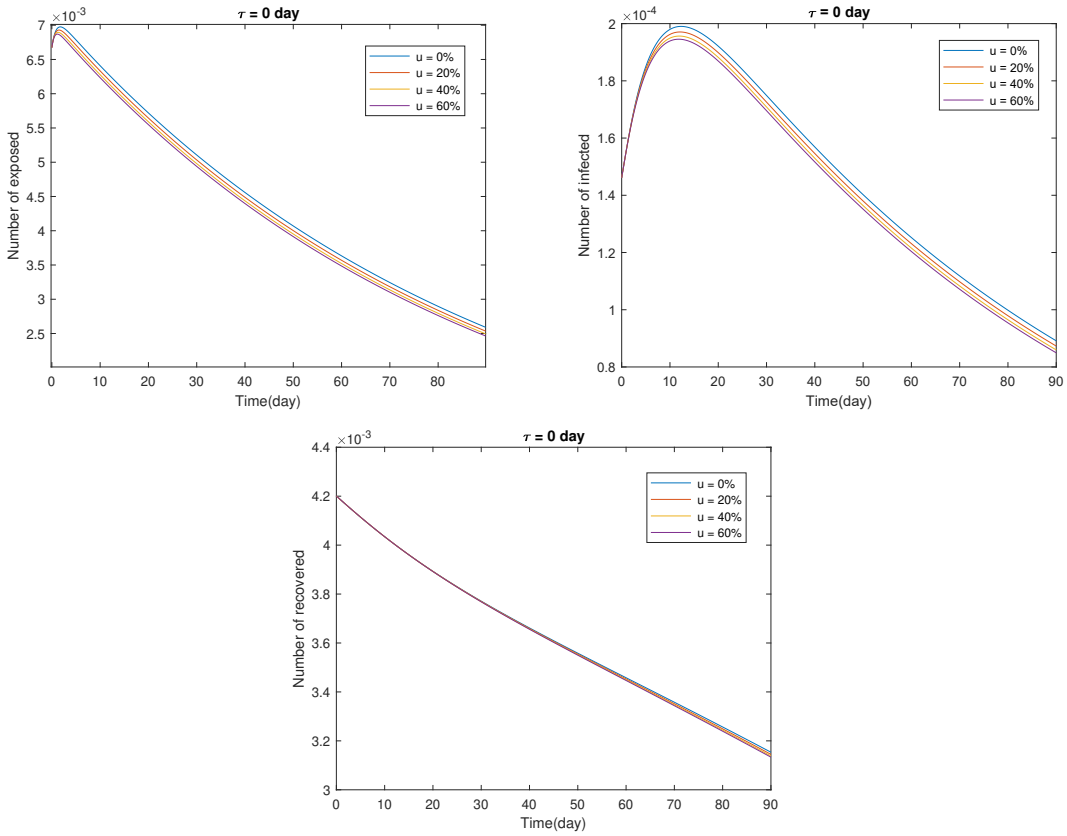

Figure 4.5: Predictions for Italy from the delayed model (4.31) with $\tau = 0$ and $u \in \{0\%, 20\%, 40\%, 60\%\}$, between 18 October 2020, and 19 January 2021.

Considering the parameter values from Table 4.2, and $u = 0$, $u = 20\%$, $u = 40\%$, $u = 60\%$, we have the following values for the basic reproduction number $\tilde{R}_0$ of Section 4.3: $\tilde{R}_0 = 0.0647$, $\tilde{R}_0 = 0.0554$, $\tilde{R}_0 = 0.0484$, and $\tilde{R}_0 = 0.043$, respectively. From Theorem 4.3, the DFE Σ_1 of system (4.31) is locally asymptotically stable for the time delay $\tau = 0$. From Theorem 4.4, the EE Σ_V^+ of system (4.31) is unstable for the time delay $\tau = 0$.

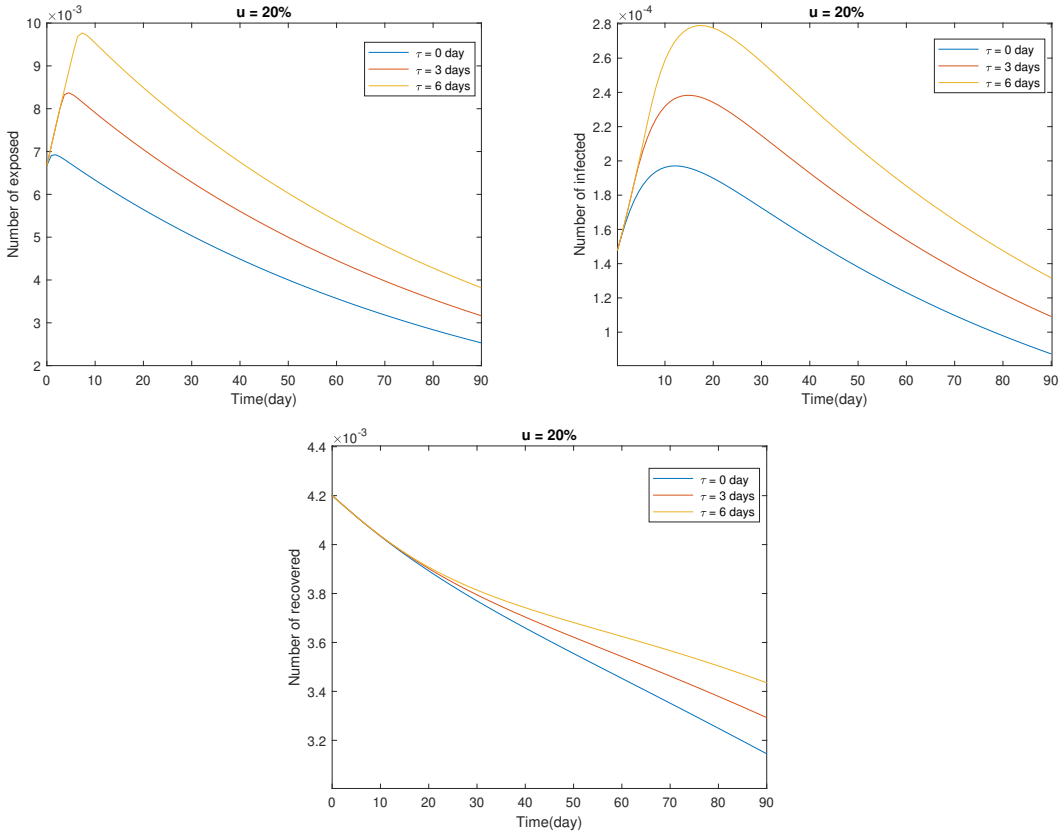

Figure 4.6: Predictions for Italy from the delayed model (4.31) with $u = 20\%$ and $\tau \in \{0, 3, 6\}$ days, between 18 October 2020, and 19 January 2021.

4.5 Conclusion

There is an inverse proportional relationship between the fraction u of susceptible individuals that are vaccinated and the number of exposed, infected, and recovered individuals: the greater the fraction of susceptible individuals that are vaccinated, the smaller the number of exposed, infected, and recovered individuals would be, and vice versa (see Figure 4.5). Moreover, there is a directly proportional relationship between the transfer time delay τ from the class of susceptible individuals to the class of infected individuals and the number of exposed, infected, and recovered individuals: the greater the time delay, the greater the number of exposed, infected, and recovered individuals would be, and vice versa (see Figure 4.6).

CHAPTER 5

Optimal Control to Limit the Spread of COVID-19

.

5.1 Introduction

A severe outbreak of respiratory illness started in Wuhan, a city of eleven million people in central China, in December 2019. The causative agent was the novel severe acute respiratory syndrome coronavirus 2, which was identified and isolated from a single patient in early January 2020 and subsequently verified in sixteen additional patients. The virus is believed to have a zoonotic origin. In particular, the Huanan Seafood Market, a live animal and seafood wholesale market in Wuhan, was regarded as a primary source of this epidemic, as it was found that 55% of the first four hundred twenty-five confirmed cases were linked to the marketplace. Meanwhile, recent comparisons of the genetic sequences of this virus and bat coronaviruses show a 96% similarity [70]. In [28], a generalized SEIR model is presented to analyze the COVID-19 epidemic based on a dynamic mechanism that incorporates the intrinsic impact of hidden latent and infectious cases on the entire process of the virus transmission. The model of [28] has shown to be a good model to describe the reality of China. Its weakness is that it just tries to describe a reality without controlling it. Our main purpose and contribution here is to include control measures that allow us to interfere with reality. Moreover, we want to illustrate the validity of the model in a different context. For this reason, we have considered real data on COVID-19 from Italy instead of China. We modify the model analyzed in [28] in order to consider optimal control problems. Secondly, we analyze a concrete optimal control problem, solving it analytically through the

celebrated PMP [1]. Moreover, we perform numerical simulations of the spread of COVID-19 in Italy.

This chapter is organized as follows. In Section 5.2, we recall the generalized SEIR model of [28]. Our original results begin with Section 5.3, where we introduce a generalized SEIR control system. An optimal control problem is posed and solved analytically in Section 5.4. Then, in Section 5.5, we estimate the parameters of the model using real data of COVID-19 from Italy, and we illustrate the usefulness of the proposed optimal control problem through numerical simulations. Our results show that the generalized SEIR model of [28], originally considered for China, is also effective with respect to Italy, being able to model well-available real data, while our optimal control approach shows clearly the positive and crucial effects of social distancing, preventive means, and treatment in the combat of COVID-19. We end with Section 5.6 of conclusions.

The results presented in this chapter have been published in [71]

5.2 A generalized SEIR-type model

The classical SEIR model consists of four compartments: susceptible individuals $S(t)$, exposed individuals $E(t)$, infected individuals $I(t)$ and recovered individuals $R(t)$. This SEIR model is too simplistic to describe COVID-19 epidemic and new classes need to be included, e.g., Deaths and Quarantined individuals, in order to describe the reality. A generalized SEIR-type model for COVID-19 is proposed by Peng et al. [28], being expressed by a seven-dimensional dynamical system as follows:

$$\begin{cases} \dot{S}(t) = -\dfrac{\beta S(t) I(t)}{N} - \alpha S(t), \\ \dot{E}(t) = \dfrac{\beta S(t) I(t)}{N} - \gamma E(t), \\ \dot{I}(t) = \gamma E(t) - \delta I(t), \\ \dot{Q}(t) = \delta I(t) - \lambda(t) Q(t) - \kappa(t) Q(t), \\ \dot{R}(t) = \lambda(t) Q(t), \\ \dot{D}(t) = \kappa(t) Q(t), \\ \dot{P}(t) = \alpha S(t), \end{cases} \tag{5.1}$$

subject to fixed initial conditions

$$\begin{aligned} S(0) = S_0,\ E(0) = E_0,\ I(0) = I_0,\ Q(0) = Q_0, \\ R(0) = R_0,\ D(0) = D_0,\ P(0) = P_0. \end{aligned} \tag{5.2}$$

Here, the population is divided into susceptible individuals $S(t)$, exposed individuals $E(t)$, infected individuals $I(t)$, quarantined/hospitalized individuals (confirmed and infected) $Q(t)$, recovered individuals $R(t)$, death individuals $D(t)$, and insusceptible individuals (protected population) $P(t)$. It follows from (5.1) that

$$\dot{S}(t) + \dot{E}(t) + \dot{I}(t) + \dot{Q}(t) + \dot{R}(t) + \dot{D}(t) + \dot{P}(t) = 0,$$

so that

$$S(t) + E(t) + I(t) + Q(t) + R(t) + D(t) + P(t)$$

is constant along time t. This constant will be denoted by N, being determined by the initial conditions (5.2):

$$N := S_0 + E_0 + I_0 + Q_0 + R_0 + D_0 + P_0.$$

The constant parameters α, β, γ and δ represent, respectively, the protection rate, infection rate, the inverse of the average latent time, and the rate at which infectious people enter in quarantine, and they have the dimension of time^{-1} (day^{-1}). The recovery and mortality rates, respectively λ and κ, are time-dependent analytical functions defined by

$$\lambda(t) := \frac{\lambda_1}{1 + e^{-\lambda_2(t-\lambda_3)}} \tag{5.3}$$

and

$$\kappa(t) := \frac{\kappa_1}{e^{\kappa_2(t-\kappa_3)} + e^{-\kappa_2(t-\kappa_3)}}, \tag{5.4}$$

where the parameters λ_1, λ_2, λ_3, κ_1, κ_2 and κ_3 are determined empirically from real data. Note that λ_1, λ_2, κ_1 and κ_2 have the dimension of time^{-1} (day^{-1}), while λ_3 and κ_3 have the dimension of time (day).

Remark 5.1. *The basic reproduction number is usually computed for autonomous systems when the right-hand side of the system does not depend explicitly on time t [61], [72]. Here, system* (5.1) *depends on* (5.3) *and, therefore, it is a non-autonomous system. In this case, we are not aware of a valid method to compute the basic reproduction number.*

5.3 Formulation of the Problem

We introduce three time-dependent controls to model (5.1) of [28]:

1. Control $u_1(t)$, representing the effect of social distancing;
2. Control $u_2(t)$, representing the effect of preventive means;
3. Control $u_3(t)$, representing the effect of treatment.

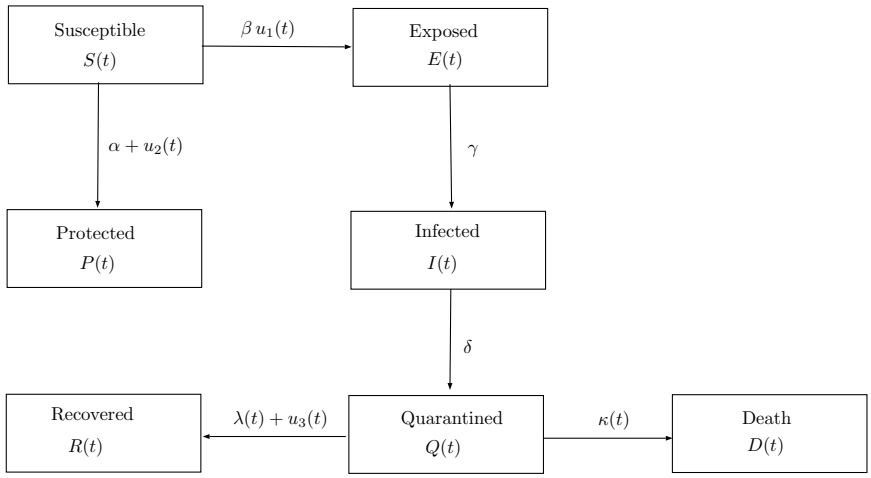

Figure 5.1: Schematic diagram of the generalized SEIR-type control system (5.5).

Mathematically, we have the control system

$$\begin{cases} \dot{S}(t) = -\dfrac{\beta u_1(t) S(t) I(t)}{N} - (\alpha + u_2(t)) S(t), \\ \dot{E}(t) = \dfrac{\beta u_1(t) S(t) I(t)}{N} - \gamma E(t), \\ \dot{I}(t) = \gamma E(t) - \delta I(t), \\ \dot{Q}(t) = \delta I(t) - (\lambda(t) + u_3(t)) Q(t) - \kappa(t) Q(t), \\ \dot{R}(t) = (\lambda(t) + u_3(t)) Q(t), \\ \dot{D}(t) = \kappa(t) Q(t), \\ \dot{P}(t) = (\alpha + u_2(t)) S(t), \end{cases} \tag{5.5}$$

subject to initial conditions (5.2). We call (5.5) the generalized SEIR-type control model. A schematic diagram of our control system is given in Figure 5.1.

5.4 Optimal Control

We consider the generalized SEIR control model (5.5) and formulate an optimal control problem to determine the strategy $u(t) = (u_1(t), u_2(t), u_3(t))$, over a fixed interval of time $[0, t_f]$, that minimizes the cost functional

$$J(u) \quad = \quad \int_0^{t_f} \left(w_1 \frac{\beta u_1 S(t) I(t)}{N} - w_2 R(t) - w_3 P(t) + v_1 \frac{u_1^2}{2} + v_2 \frac{u_2^2}{2} + v_3 \frac{u_3^2}{2} \right) dt, \tag{5.6}$$

where t_f represents the final time of the period under study and the constants w_1, w_2, w_3, v_1, v_2 and v_3 represent the weights associated with the total number of new infections, the number of recovered individuals, the number of insusceptible individuals, and the costs associated with the controls u_1, u_2 and u_3, respectively. The controls u are Lebesgue measurable and bounded:

$$u(t) \in \Gamma := \left\{ \mu = (\mu_1, \mu_2, \mu_3) \in \mathbb{R}^3 : u_{i\,\min} \leq \mu_i \leq u_{i\,\max},\ i = 1, 2, 3 \right\}. \tag{5.7}$$

The intervals $[u_{i\,\min}, u_{i\,\max}]$ also translate the fact that there are limitations to the effects of social distancing, the preventive means and the treatment rate. Let

$$\begin{aligned} x(t) &= (x_1(t), \ldots, x_7(t)) \\ &= (S(t), E(t), I(t), Q(t), R(t), D(t), P(t)) \in \mathbb{R}^7. \end{aligned}$$

The optimal control problem consists of finding the optimal trajectory $\tilde{x}$ associated with the optimal control $\tilde{u} \in L^1$, $\tilde{u}(t) \in \Gamma$, satisfying the control system (5.5), the initial conditions

$$x(0) = (S_0, E_0, I_0, Q_0, R_0, D_0, P_0) \tag{5.8}$$

and giving minimum value to (5.6).

The existence of an optimal control $\tilde{u}$ and associated optimal trajectory $\tilde{x}$ comes from the convexity of the integrand of the cost functional (5.6) with respect to control u and the Lipschitz property of the state system with respect to state variables x (see [73] for existence results of optimal solutions). According to the PMP [1], if $\tilde{u} \in L^1$ is optimal for problem (5.5)–(5.8) and fixed final time t_f, then there exists

$$\psi \in AC([0, t_f]; \mathbb{R}^7),\ \psi(t) = (\psi_1(t), \ldots, \psi_7(t)),$$

called the adjoint vector, such that

$$\begin{cases} \dot{x} = \dfrac{\partial H}{\partial \psi}, \\ \dot{\psi} = -\dfrac{\partial H}{\partial x}, \end{cases}$$

where the Hamiltonian H is defined by

$$\begin{aligned} H(x, u, \psi) = \frac{w_1 u_1 \beta x_1 x_3}{N} - w_2 x_5 - w_3 x_7 + \sum_{i=1}^{3} v_i \frac{u_i^2}{2} \\ + \psi^T \left(Ax + \left(\sum_{i=1}^{2} b_i \Lambda_i x \Phi_i + f(x)^T \Phi_3 \right) u \right) \end{aligned}$$

with

$$
\begin{aligned}
f(x) &= (f_1(x)\ f_2(x)\ \ 0\ \ 0\ \ 0\ \ 0\ \ 0), \\
f_1(x) &= \frac{-\beta x_1 x_3}{N}, \\
f_2(x) &= \frac{\beta x_1 x_3}{N}, \\
b_1 &= (-1\ 0\ 0\ 0\ 0\ 0\ 1)^T, \\
b_2 &= (0\ 0\ \ 0\ \ -1\ 1\ 0\ 0)^T, \\
\Lambda_1 &= (1\ 0\ 0\ 0\ 0\ 0\ 0), \\
\Lambda_2 &= (0\ 0\ 0\ 1\ 0\ 0\ 0), \\
\Phi_1 &= (0\ 1\ 0), \\
\Phi_2 &= (0\ 0\ 1), \\
\Phi_3 &= (1\ 0\ 0),
\end{aligned}
$$

$$
A = \begin{pmatrix}
-\alpha & 0 & 0 & 0 & 0 & 0 & 0 \\
0 & -\gamma & 0 & 0 & 0 & 0 & 0 \\
0 & \gamma & -\delta & 0 & 0 & 0 & 0 \\
0 & 0 & \delta & -\lambda(t) - \kappa(t) & 0 & 0 & 0 \\
0 & 0 & 0 & \lambda(t) & 0 & 0 & 0 \\
0 & 0 & 0 & \kappa(t) & 0 & 0 & 0 \\
\alpha & 0 & 0 & 0 & 0 & 0 & 0
\end{pmatrix}.
$$

The minimality condition

$$
H(\tilde{x}(t), \tilde{u}(t), \tilde{\psi}(t)) = \min_{u \in \Gamma} H(\tilde{x}(t), u, \tilde{\psi}(t)) \tag{5.9}
$$

holds almost everywhere on $[0, t_f]$. Moreover, the transversality conditions of PMP, we get:

$$
\tilde{\psi}_i(t_f) = 0, \quad i = 1, \ldots, 7,
$$

hold. Solving the minimality condition (5.9) on the interior of the set of admissible controls, Γ gives

$$
\tilde{u}(t) = \left(\frac{\beta \tilde{x}_1(t) \tilde{x}_3(t) \left(\tilde{\psi}_1(t) - \tilde{\psi}_2(t) - w_1 \right)}{N v_1}, \frac{\tilde{x}_1(t) \left(\tilde{\psi}_1(t) - \tilde{\psi}_7(t) \right)}{v_2}, \frac{\tilde{x}_4(t) \left(\tilde{\psi}_4(t) - \tilde{\psi}_5(t) \right)}{v_3} \right),
$$

where the adjoint functions satisfy

$$\begin{cases} \dot{\tilde{\psi}}_1 = -\dfrac{\tilde{u}_1\beta\tilde{x}_3}{N^2}\left(\tilde{x}_2+\tilde{x}_3+\tilde{x}_4+\tilde{x}_5+\tilde{x}_6+\tilde{x}_7\right)\times\left(w_1-\tilde{\psi}_1+\tilde{\psi}_2\right)+(\alpha+\tilde{u}_2)(\tilde{\psi}_1-\tilde{\psi}_7), \\ \dot{\tilde{\psi}}_2 = \dfrac{\tilde{u}_1\beta\tilde{x}_1\tilde{x}_3\left(w_1-\tilde{\psi}_1+\tilde{\psi}_2\right)}{N^2}+\gamma(\tilde{\psi}_2-\tilde{\psi}_3), \\ \dot{\tilde{\psi}}_3 = -\dfrac{\tilde{u}_1\beta\tilde{x}_1}{N^2}\left(\tilde{x}_2+\tilde{x}_3+\tilde{x}_4+\tilde{x}_5+\tilde{x}_6+\tilde{x}_7\right)\times\left(w_1-\tilde{\psi}_1+\tilde{\psi}_2\right)+\delta(\tilde{\psi}_3-\tilde{\psi}_4), \\ \dot{\tilde{\psi}}_4 = \dfrac{\tilde{u}_1\beta\tilde{x}_1\tilde{x}_3\left(w_1-\tilde{\psi}_1+\tilde{\psi}_2\right)}{N^2}+\kappa(t)(\tilde{\psi}_4-\tilde{\psi}_6)+\left(\lambda(t)+\tilde{u}_3\right)(\tilde{\psi}_4-\tilde{\psi}_5), \\ \dot{\tilde{\psi}}_5 = \dfrac{\tilde{u}_1\beta\tilde{x}_1\tilde{x}_3(w_1-\tilde{\psi}_1+\tilde{\psi}_2)}{N^2}+w_2, \\ \dot{\tilde{\psi}}_6 = \dfrac{\tilde{u}_1\beta\tilde{x}_1\tilde{x}_3(w_1-\tilde{\psi}_1+\tilde{\psi}_2)}{N^2}, \\ \dot{\tilde{\psi}}_7 = \dfrac{\tilde{u}_1\beta\tilde{x}_1\tilde{x}_3(w_1-\tilde{\psi}_1+\tilde{\psi}_2)}{N^2}+w_3. \end{cases} \tag{5.10}$$

Note that we have obtained an analytical explicit expression for the controls $\tilde{u}_1(t), \tilde{u}_2(t)$ and $\tilde{u}_3(t)$,

$$\begin{aligned} \tilde{u}_1(t) &= \frac{\beta\tilde{x}_1(t)\tilde{x}_3(t)\left(\tilde{\psi}_1(t)-\tilde{\psi}_2(t)-w_1\right)}{Nv_1}, \\ \tilde{u}_2(t) &= \frac{\tilde{x}_1(t)\left(\tilde{\psi}_1(t)-\tilde{\psi}_7(t)\right)}{v_2}, \\ \tilde{u}_3(t) &= \frac{\tilde{x}_4(t)\left(\tilde{\psi}_4(t)-\tilde{\psi}_5(t)\right)}{v_3}, \end{aligned} \tag{5.11}$$

but we do not have the controls in open-loop (because they depend on the state variables $\tilde{x}$ and adjoint variables $\tilde{\psi}$). To plot $\tilde{u}(t)$ as a function of t we need to solve numerically system (5.5) and (5.10) to know the expressions for $\tilde{x}$ and $\tilde{\psi}$ and be able to obtain the controls u_i, $i = 1, 2, 3$, in agreement with (5.11). This is done numerically in the next section. For more on numerical approaches to solve optimal control problems, we refer the reader to [33], [74] and references therein.

5.5 Numerical Results

Now, our aim is to find optimal controls to limit the spread of the epidemic of COVID-19 in Italy, by reducing the number of new infections and by increasing insusceptible individuals and the percentage of those recovered, while reducing the cost during the period of three months starting from September 1, 2020. All numerical computations were performed in the numeric computing environment MATLAB R2019b using the medium-order method and numerical interpolation [66]. The rest of the preliminary conditions and real data were taken and computed from the database `https://raw.githubusercontent.com/pcm-dpc/`

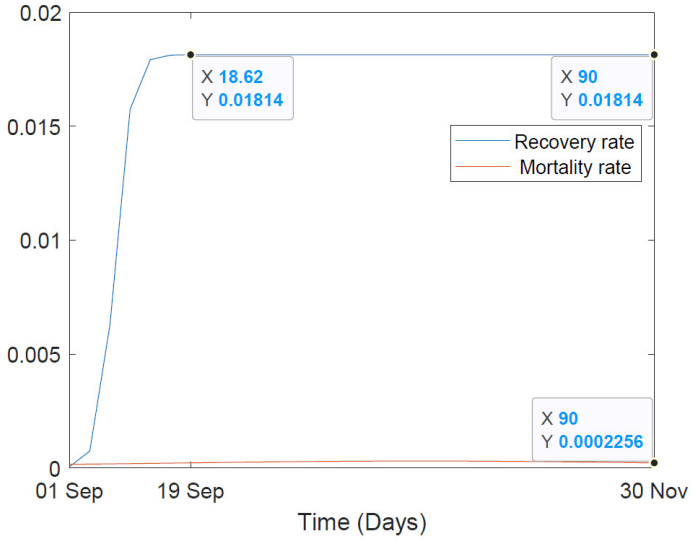

Figure 5.2: The recovery and mortality rates (5.3) and (5.4) for the case of Italy (Section 5.5).

`COVID-19/master/dati-regioni/dpc-covid19-ita-regioni.csv`. The real data for the COVID-19 pandemic in Italy, for September and October 2020, is summarized in appendix: see Appendix A for recovered individuals, Appendix B for deaths, and Appendix C for quarantined individuals.

The parameters α, β, γ, δ, $(\kappa_1, \kappa_2, \kappa_3)$ and $(\lambda_1, \lambda_2, \lambda_3)$ were fitted in the least square sense. The parameter values as given in Table 5.1.

Parameter	Initial value	Estimated value
α	0.06	1.1775×10^{-7}
β	1	3.97
γ	5	0.0048
δ	0.5	0.1432
$(\lambda_1, \lambda_2, \lambda_3)$	$(0.01, 0.1, 10)$	$(0.0181, 0.8111, 6.9882)$
$(\kappa_1, \kappa_2, \kappa_3)$	$(0.001, 0.001, 10)$	$(0.00062, 0.0233, 54.0351)$

Table 5.1: Parameter values used in the simulations of system (5.5).

The parameters of the generalized SEIR model (5.5) were calculated simultaneously by the nonlinear least squares method [69]. These parameters have been presented in the same table 5.1. In Figure 5.2, we plot functions $\lambda(t)$ (5.3) and $\kappa(t)$ (5.4). For the optimal control problem of Section 5.4, we further fixed $w_i = v_i = 1$, $u_{1\,\min} = 0.1$, $u_{j\,\min} = 0$, $u_{i\,\max} = 1$, $i = 1, 2, 3$, $j = 1, 2$.

In Figures 5.3 and 5.4, we present plots with the numerical solutions to the nonlinear differential equations of the generalized SEIR model (5.1), in red color; to the nonlinear differential equations of the generalized SEIR control system (5.5) under optimal controls,

in the sense of Section 5.4, in green color; and the real data of the quarantined cases, the number of recovered individuals, and the number of deaths from September 1 to October 31, 2020, in orange. The computed optimal controls for Italy from September 1 to November 30, 2020, which give rise to the green curves in the plots of Figures 5.3 and 5.4, are shown in Figure 5.5. The obtained simulations allow us to predict the results of the decisions taken in Italy, as well to give the best decisions for Italy, according to our generalized SEIR control system and optimal control problem.

The orange curves in Figures 5.3e and 5.3f and Figure 5.4 represent the real data on quarantine, recovered, and death cases in Italy from September 1 to October 31, 2020. The red curves simulate what happens from the beginning of September to the end of November following the generalized SEIR model (5.1), when the number of quarantined, recovered, and deaths increases, and reach, respectively, two million three hundred eighty-eight thousand (2388000), nine hundred six thousand three hundred (906300), and forty-five thousand seven hundred (45700) cases.

The red curves in Figures 5.3c, 5.3d and 5.3a simulate what happens from the beginning of September to the end of November, according with the generalized SEIR model, when the number of infected, exposed and insusceptible cases reach, respectively, one million one hundred forty-six thousand (1146000), forty-one million two hundred fifty-thousand (41250000) and five hundred twenty-eight (528) cases.

The green curves in Figures 5.3 and 5.4 show what happens from September 1 to November 30, 2020, under optimal control measures, when the number of infected (Figure 5.3c) and recovered (Figure 5.3f) cases increase and reach six hundred and fifty (650) and two hundred forty-nine thousand four hundred (249400) cases, respectively, while the number of exposed (Figure 5.3d), insusceptible (Figure 5.3a), and quarantined (Figure 5.3e) cases reach eighteen thousand four hundred ninety (18490), sixty million one hundred eighty thousand (60180000), and one hundred twenty-eight (128) cases, respectively. Deaths remain stable during the entire period, precisely, thirty-five thousand five hundred (35500) cases (Figure 5.4).

The curves in Figure 5.5 show the optimal controls that need to be implemented in order to reduce the overall burden of COVID-19 in Italy and obtain the best possible situation given by the green curves in Figures 5.3 and 5.4, which takes into account the cost reduction resulting from the controls u_1, u_2 and u_3. The effect of social distancing is equal to the minimum value of its constraint ($u_1 = 0.1$), see Figure 5.5a, and this corresponds to the application of social distancing among the entire population. The effect of preventive measures is equal to the maximum value of its constraint until September 19 ($u_2 = 1$), see Figure 5.5b, then decreases gradually until it reaches zero ($u_2 = 0$) on November 30, 2020, see Figure 5.5c. The effect of treatment takes the maximum value of its constraint until November 29, 2020 ($u_3 = 1$), then decreases

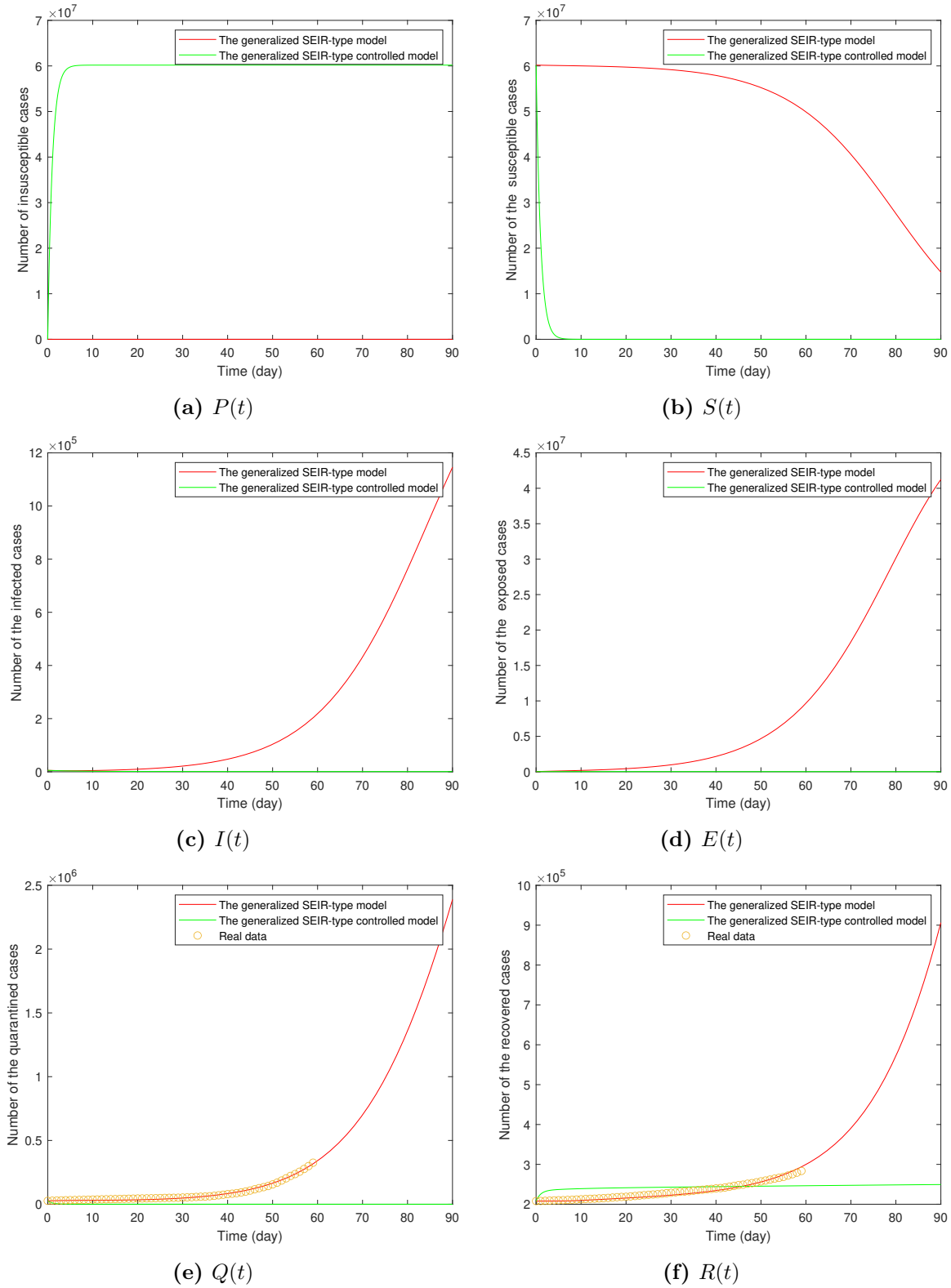

Figure 5.3: Predictions for Italy from the generalized SEIR model (5.1), in red, the generalized SEIR control system (5.5) under optimal controls, in green, between Sept. 1 and Nov. 30, 2020, versus available real data of quarantined and recovered from Sept. 1 to Oct. 31, 2020, in orange.

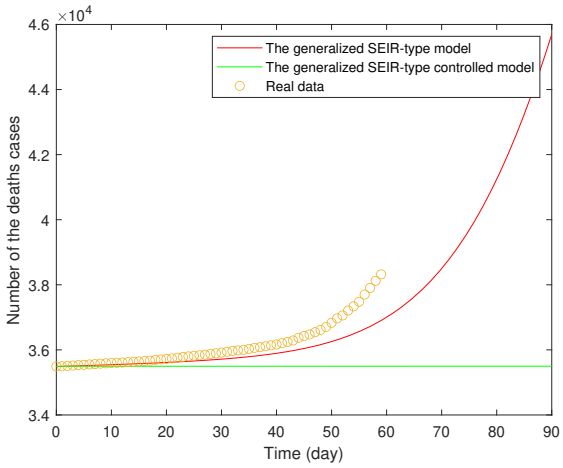

Figure 5.4: Predictions for Italy from the generalized SEIR model (5.1), in red, the generalized SEIR control system (5.5) under optimal controls, in green, between Sept. 1 and Nov. 30, 2020, versus available real data of deaths from Sept. 1 to Oct. 31, 2020, in orange.

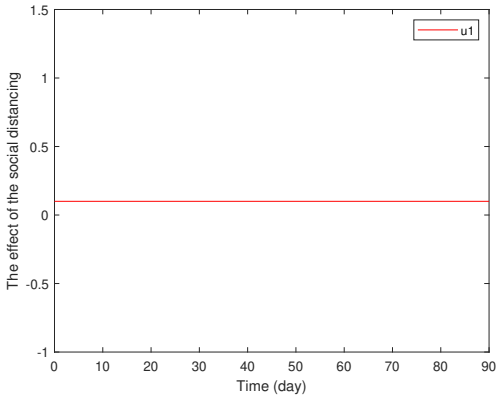

(a) $u_1(t)$ (social distancing)

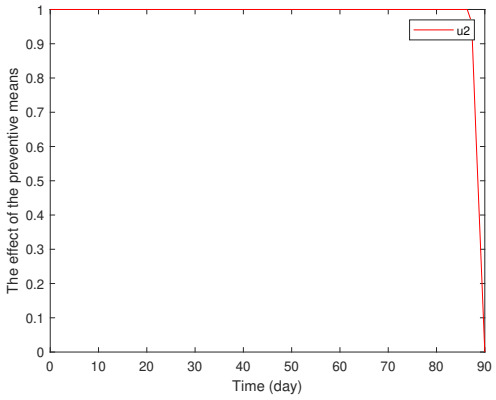

(b) $u_2(t)$ (preventive means)

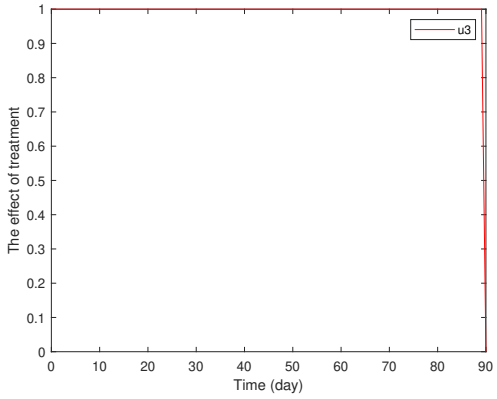

(c) $u_3(t)$ (treatment)

Figure 5.5: The Pontryagin extremal controls of the optimal control problem of Section 5.4 for the case of Italy between Sept. 1 and Nov. 30, 2020.

to zero on November 30, 2020, ($u_3 = 0$), meaning a decrease in the pressure on the health sector. Note that by taking preventive measures (u_1, u_2, u_3), we limit the spread of COVID-19 and we have better results. This means that, with the help of optimal control theory, what happened in Italy would have been less dramatic.

5.6 Conclusion

Recent results have shown how the theory of optimal control is an important tool to combat COVID-19 in a community: in [75] for a controlled sanitary deconfinement in Portugal; in [76] from a more theoretical point of view; here for the case of Italy. We proposed a simple SEIR-type control system, showing its effectiveness with respect to real data from Italy in the period from Sept. 1 to Nov. 30, 2020. While the real data (see Appendices A–B–C) is consistent with the generalized SEIR model (5.1), because the goal of this model is to describe the COVID-19 reality, our new SEIR control system (5.5) simulates what would happen if we took into account the values of the three control functions, as described in Section 5.3. In agreement, the situations obtained with controls are better then the situations obtained without controls. More precisely, by considering the proposed controls, we show how optimal control theory could have drastically diminish the burden of COVID-19 in the period under study while taking into account the resulting cost reduction. In concrete, if it would have been possible to implement optimality, in the sense of optimal control theory and Pontryagin's optimality conditions, the control measures of social distancing as in Figure 5.5a, preventive means as in Figure 5.5b, and treatment as in Figure 5.5c, then it would have been possible to decrease significantly the number of deaths (cf. Figure 5.4 and Tables B.1 and B.2, which accounts for a decrease of 7.36% of deaths in Italy by the end of October 2020 under optimal control) with much less quarantined individuals (see Figure 5.3e and Tables C.1 and C.2, which accounts a decrease of 99.96% of quarantined individuals in Italy by the end of Oct. 2020 under optimal control theory). Thus, one can say that the approach proposed by the theory of optimal control is very effective, simultaneously from health and economic points of view, being far from trivial. Note that by PMP one obtains an increase in the number of recovered individuals in the first period, up to 14-Oct-2020, and, after this date, a decrease in the number of recovered (cf. Figure 5.3f and Tables A.1 and A.2), caused by the drastic reduction on the number of susceptible and infected (see Figures 5.3b and 5.3c, respectively). While our aim here was to study the effect of controls, guided by the application of the PMP and showing how they can help to decrease the spread of COVID-19, other aspects remain open for further research. In particular, it remains open to the theoretical study of the stability of the models. In this direction, the recent results of [77], [78] may be useful.

CHAPTER 6

Transport and Optimal Control of Vaccination Dynamics for COVID-19

6.1 Introduction

BNT162b2 is an mRNA-based vaccine candidate against SARS-CoV-2, currently being developed by Pfizer and BioTech [79]. As announced on 9$^{\text{th}}$ November 2020, BNT162b2 shows an efficacy against COVID-19 in patients without prior evidence of SARS-CoV-2 infection. A first interim efficacy analysis was conducted by an external, independent Data Monitoring Committee from the Phase 3 clinical study, and the case split, between vaccinated individuals and those who received the placebo indicates a vaccine efficacy rate above 90%, at seven days after the second dose, of the 94 cases reviewed [80].

The major obstacle that must be overcome is related to the process of transporting the vaccine, which must be stored at -70^oC [81]. Pfizer indicates that the vaccine will be distributed from its factories in the USA, Belgium and Germany. The American Wall Street Journal revealed that Pfizer has developed a special box packed with dry ice and a GPS tracker, which can hold 5000 doses of the vaccine under the right conditions for 10 days. Moreover, there is another obstacle related to the cost of the transportation boxes, where a similar box of 1200 doses in -8^oC costs 6868 USD, which is very expensive.

The transport of the vaccine must comply with the general standards for drug storage and the recommended conditions. Although many transport vehicles are equipped with refrigeration devices, assuring recommended storage conditions, simple insulated transport boxes are often used. In this study, we use the heat diffusion equation

and assume that the shape of the vaccine bottle is cylindrical [82]. We perform the calculations to find out an initial temperature that ensures the arrival of the vaccine while fulfilling the required condition of -70^oC, by using insulated transfer boxes with the internal temperature at 0^oC [83].

This chapter is organized as follows. We begin by formulating the vaccination transport model in Section 6.2. In Section 6.3, we recall the generalized SEIR model. Then, in Section 6.4, we formulate the generalized SEIR model with vaccination as an optimal control problem. The obtained optimal control problem is solved numerically in Section 6.5. In Section 6.6, we present a discussion concerning the spread of COVID-19 in Italy during three months, starting from 1$^{\text{st}}$ November 2020. We end with Section 6.7 of conclusion, including some future research directions.

The results presented in this chapter have been published in [84]

6.2 Vaccine transport model

In this section, we present a model to maintain the effectiveness of the vaccine while transporting it from the factory storage area to the desired destination. The aim is to know the initial temperature that maintains the effectiveness of the vaccine, less than -70^o, and this by using the available mobile boxes at 0^oC. Thus, we propose the following mathematical model:

$$\begin{cases} \dfrac{\partial T(t,x,y,z)}{\partial t} - \alpha \nabla^2 T(t,x,y,z) = 0, & \text{on } \ [0,t_*] \times \Omega, \\ T(t_*,x,y,z) = -70^oC, & \forall (x,y,z) \in \Omega, \\ T(t,x,y,z) = 0^oC, & \forall (t,x,y,z) \in [0,t_*] \times \partial\Omega, \\ \Omega = \{(x,y,z) \in \mathbb{R}^3 : \ x^2+y^2 < r^2, \ 0 < z < h\}, \\ \partial\Omega = \{(x,y,z) \in \mathbb{R}^3 : \ x^2+y^2 = r^2, \ 0 \le z \le h\}, \end{cases} \tag{6.1}$$

where $T(t,x,y,z)$ represents the temperature of the vaccine at the point (x,y,z) and the time t; t_* is the arrival time of the vaccine; and 0^oC is the temperature inside the box. The sets Ω and $\partial\Omega$ represent the interior and the border of the bottle containing the vaccine, respectively, r and h are the radius and height of the bottle, respectively, and α is the thermal diffusivity defined by

$$\alpha = \frac{k}{\rho c_\rho}, \tag{6.2}$$

where k is the thermal conductivity, c_ρ is the specific heat capacity, and ρ is the density.

6.3 Initial mathematical model for COVID-19

The generalized SEIR model proposed by Peng et al. [28] is expressed by a seven-dimensional dynamical system defined by

$$\begin{cases} \dot{S}(t) = -\dfrac{\beta S(t) I(t)}{N} - \omega S(t), \\ \dot{E}(t) = \dfrac{\beta S(t) I(t)}{N} - \gamma E(t), \\ \dot{I}(t) = \gamma E(t) - \delta I(t), \\ \dot{Q}(t) = \delta I(t) - \lambda(t) Q(t) - \kappa(t) Q(t), \\ \dot{R}(t) = \lambda(t) Q(t), \\ \dot{D}(t) = \kappa(t) Q(t), \\ \dot{P}(t) = \omega S(t), \end{cases} \tag{6.3}$$

where the state variables are subjected to the following initial conditions:

$$S(0) = S_0,\ E(0) = E_0,\ I(0) = I_0,\ Q(0) = Q_0,\ R(0) = R_0,\ D(0) = D_0,\ P(0) = P_0.$$

In this model, the population is divided into the following compartments: susceptible individuals $S(t)$, exposed individuals $E(t)$, infected individuals $I(t)$, quarantined individuals $Q(t)$, recovered individuals $R(t)$, death individuals $D(t)$, and insusceptible/protected individuals $P(t)$. These variables, in total, constitute the whole population, denoted by N:

$$N = S(t) + E(t) + I(t) + Q(t) + R(t) + D(t) + P(t).$$

The parameters ω, β, γ, δ, $\lambda(t)$ and $\kappa(t)$ represent the protection rate, infection rate, inverse of the average latent time, rate at which infectious people enter in quarantine, time-dependent recovery rate, and the time-dependent mortality rate, respectively. The recovery $\lambda(t)$ and mortality $\kappa(t)$ rates are analytical functions of time, defined by

$$\lambda(t) = \frac{\lambda_1}{1 + \exp(-\lambda_2(t - \lambda_3))}, \tag{6.4}$$

$$\kappa(t) = \frac{\kappa_1}{\exp(\kappa_2(t - \kappa_3)) + \exp(-\kappa_2(t - \kappa_3))}, \tag{6.5}$$

where the parameters λ_1, λ_2, λ_3, κ_1, κ_2 and κ_3 are empirically determined in Section 6.6.

6.4 Mathematical model for COVID-19 with vaccination

We now introduce the vaccine for the susceptible population in order to control the spread of COVID-19. Let us introduce in model (6.3) a control function $u(t)$ and an

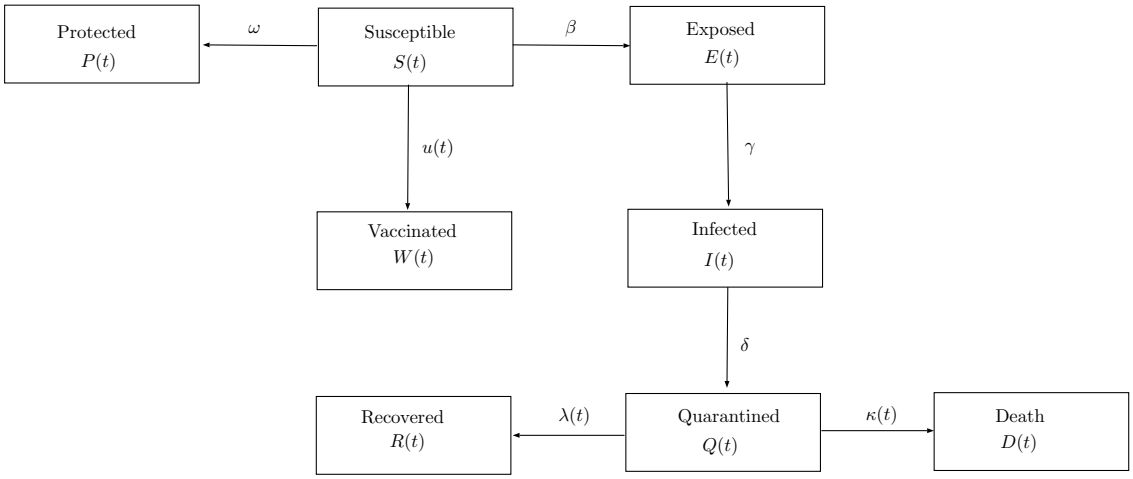

Figure 6.1: Schematic diagram of the generalized SEIR model with vaccination.

extra variable $W(t)$, $t \in [0, t_f]$, representing the percentage of susceptible individuals being vaccinated and the number of vaccines used, respectively, with

$$\frac{dW}{dt}(t) = u(t)S(t), \quad \text{subject to the initial condition } W(0) = 0, \tag{6.6}$$

where t_f represents the final time of the vaccination program. Hence, our model with vaccination is given by the following system of eight nonlinear ordinary differential equations:

$$\begin{cases} \dot{S}(t) = -\dfrac{\beta S(t)I(t)}{N} - \omega S(t) - u(t)S(t), \\ \dot{E}(t) = \dfrac{\beta S(t)I(t)}{N} - \gamma E(t), \\ \dot{I}(t) = \gamma E(t) - \delta I(t), \\ \dot{Q}(t) = \delta I(t) - \lambda(t)Q(t) - \kappa(t)Q(t), \\ \dot{R}(t) = \lambda(t)Q(t), \\ \dot{D}(t) = \kappa(t)Q(t), \\ \dot{P}(t) = \omega S(t), \\ \dot{W}(t) = u(t)S(t), \end{cases} \tag{6.7}$$

where the state variables are subject to the initial conditions:

$$S(0) = S_0,\ E(0) = E_0,\ I(0) = I_0,\ Q(0) = Q_0,$$
$$R(0) = R_0,\ D(0) = D_0,\ P(0) = P_0,\ W(0) = W_0 = 0.$$

A schematic diagram of model (6.7) is given in Figure 6.1.

6.5 Optimal Control

We consider the model with vaccination (6.7) and formulate an optimal control problem to determine the vaccination strategy u that minimizes the cost of treatment

and vaccination:

$$\min_u J(u) = \int_0^{t_f} \Big(w_1 I^2(t) + w_2 u^2(t) \Big)\, dt, \tag{6.8}$$

where w_1 and w_2 represent the weights associated with the cost of treatment and vaccination, respectively. We assume that the control function u takes values between 0 and 1. When $u(t) = 0$, no susceptible individual is vaccinated at time t and if $u(t) = 1$, then all susceptible individuals are vaccinated at time t. Let

$$\begin{aligned} x(t) &= (x_1(t), \ldots, x_8(t)) \\ &= (S(t), E(t), I(t), Q(t), R(t), D(t), P(t), W(t)) \in \mathbb{R}^8. \end{aligned}$$

The optimal control problem consists in finding the control $\tilde{u}$ and the associated optimal trajectory $\tilde{x}$, satisfying the control system (6.7) with the given initial conditions

$$x(0) = (S_0, E_0, I_0, Q_0, R_0, D_0, P_0, W_0), \tag{6.9}$$

where the control $\tilde{u} \in \Gamma$,

$$\Gamma = \{u(\cdot) \in L^\infty([0, t_f], \mathbb{R}) \ : \ 0 \le u(t) \le 1, \ t \in [0, t_f]\}, \tag{6.10}$$

minimizes the objective functional (6.8). With the new variables, problem (6.7)–(6.10) becomes

$$\begin{gathered} \min_{u \in \Gamma} J(u) = \int_0^{t_f} \Big(w_1 x_3^2(t) + w_2 u^2(t) \Big)\, dt, \\ \dot{x}(t) = A(t)x(t) + B(x(t))u(t) + f(x(t)), \quad x(0) = (S_0, E_0, I_0, Q_0, R_0, D_0, P_0, W_0), \end{gathered} \tag{6.11}$$

where

$$A(t) = \begin{pmatrix} -\omega & 0 & 0 & 0 & 0 & 0 & 0 & 0 \\ 0 & -\gamma & 0 & 0 & 0 & 0 & 0 & 0 \\ 0 & \gamma & -\delta & 0 & 0 & 0 & 0 & 0 \\ 0 & 0 & \delta & -\lambda(t) - \kappa(t) & 0 & 0 & 0 & 0 \\ 0 & 0 & 0 & \lambda(t) & 0 & 0 & 0 & 0 \\ 0 & 0 & 0 & \kappa(t) & 0 & 0 & 0 & 0 \\ \omega & 0 & 0 & 0 & 0 & 0 & 0 & 0 \\ 0 & 0 & 0 & 0 & 0 & 0 & 0 & 0 \end{pmatrix},$$

$$B(x) = (-x_1, \ 0, \ 0, \ 0, \ 0, \ 0, \ 0, \ x_1)^T,$$

$$f(x) = \left(-\frac{\beta x_1 x_3}{N}, \ \frac{\beta x_1 x_3}{N}, \ 0, \ 0, \ 0, \ 0, \ 0, \ 0 \right)^T.$$

The existence of the optimal control $\tilde{u}$ and the associated optimal trajectory $\tilde{x}$ comes from the convexity of the integrand of the cost functional (6.8) with respect to the

control u and the Lipschitz property of the state system with respect to the state vector $x(t)$ (see [73] for existence results of optimal solutions). According to the PMP [1], if $\tilde{u} \in \Gamma$ is optimal for the problem (6.11) with fixed final time t_f, then there exists

$$\psi \in AC([0, t_f], \mathbb{R}^8),\ \psi(t) = (\psi_1(t), \ldots, \psi_8(t)),$$

called the adjoint vector, such that

$$\dot{x} = \frac{\partial H}{\partial \psi} \ \text{ and } \ \dot{\psi} = -\frac{\partial H}{\partial x},$$

where the Hamiltonian H is defined by

$$H(t, x, \psi, u) = w_1 x_3^2 + w_2 u^2 + \psi^T \left(A(t)x + B(x)u + f(x)\right). \tag{6.12}$$

The adjoint functions satisfy

$$\dot{\psi} = -\frac{\partial H}{\partial x} = \bar{A}(t, x, u)\psi + \bar{B}(x), \tag{6.13}$$

where

$$\bar{A}(t, x, u) = \begin{pmatrix} \frac{\beta x_3}{N} + \omega + u & -\frac{\beta x_3}{N} & 0 & 0 & 0 & 0 & -\omega & -u \\ 0 & \gamma & -\gamma & 0 & 0 & 0 & 0 & 0 \\ \frac{\beta x_1}{N} & -\frac{\beta x_1}{N} & \delta & -\delta & 0 & 0 & 0 & 0 \\ 0 & 0 & 0 & \lambda(t) + \kappa(t) & -\lambda(t) & -\kappa(t) & 0 & 0 \\ 0 & 0 & 0 & 0 & 0 & 0 & 0 & 0 \\ 0 & 0 & 0 & 0 & 0 & 0 & 0 & 0 \\ 0 & 0 & 0 & 0 & 0 & 0 & 0 & 0 \\ 0 & 0 & 0 & 0 & 0 & 0 & 0 & 0 \end{pmatrix},$$

$$\bar{B}(x) = (0,\ 0,\ -2w_1 x_3,\ 0,\ 0,\ 0,\ 0,\ 0)^T.$$

The minimality condition

$$H(t, \tilde{x}(t), \tilde{\psi}(t), \tilde{u}(t)) = \min_{u \in \Gamma} H(t, \tilde{x}(t), \tilde{\psi}(t), u) \tag{6.14}$$

holds almost everywhere on $[0, t_f]$. Moreover, the transversality conditions assert that $\tilde{\psi}_i(t_f) = 0,\ i = 1, \ldots, 8$. It follows from Pontryagin's minimum principle that the extremal control $\tilde{u}^p$ is given by

$$\tilde{u}^p(t) = \begin{cases} \tilde{u}(t) & \text{if } \ 0 < \tilde{u}(t) < 1, \\ 0 & \text{if } \ \tilde{u}(t) \leq 0, \\ 1 & \text{if } \ \tilde{u}(t) \geq 1, \end{cases} \tag{6.15}$$

where

$$\tilde{u}(t) = \frac{\tilde{x}_1(t)\left(\tilde{\psi}_1(t) - \tilde{\psi}_8(t)\right)}{2w_2}. \tag{6.16}$$

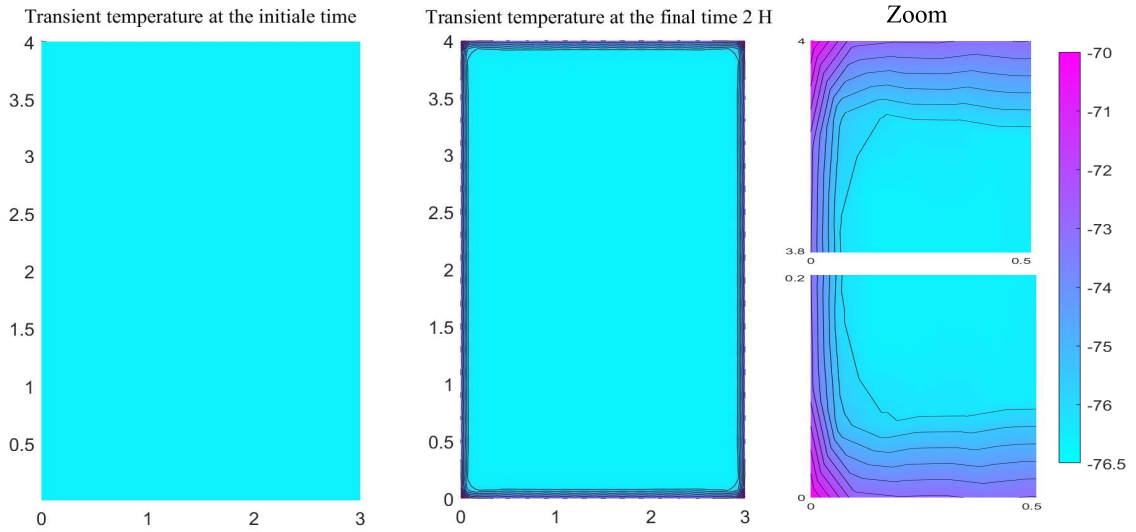

Figure 6.2: Numerical solution of the heat diffusion equation (6.1).

6.6 Numerical Results

The current study aims to find the initial temperature to maintain the effectiveness of the vaccine during the transportation process, as well as determining an optimal vaccination strategy to limit the spread of COVID-19 in Italy. For that, we reduce the costs of treatment and vaccination, during the three months starting from 1st November 2020. We use the MATLAB R2020b program to perform all numerical computations. The initial conditions and real data are taken from the public database *Dati COVID-19 Italia*, available from `https://github.com/pcm-dpc/COVID-19`.

We consider that the glass bottle of vaccine has a cylindrical shape with a radius $r = 1.5\ cm$ and a height $h = 4\ cm$ and the following values:

- The thermal conductivity of glass: $\kappa = 1\, W/(m\, K)$.
- The heat capacity of the vaccine: $c_\rho = 3700\ J/(kg^oC)$
- The density of the vaccine: $\rho = 1000\ kg/m^3$.

with the final time $t_* = 2\, hours$. In Figure 6.2 we present the numerical solution of the heat transfer equation (6.1), which gives the initial temperature equal to -76.5^oC. The parameter values as given in Table 6.1.

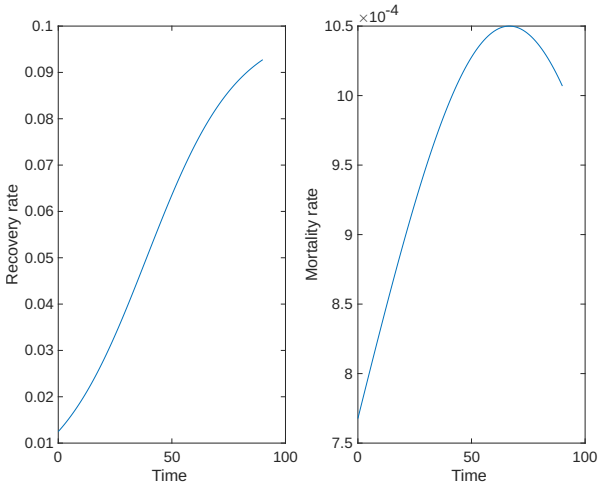

Figure 6.3: The recovery and mortality rates.

Parameter	Initial value	Estimated value
α	0.06	1.1775×10^{-7}
β	1	0.5425
γ	5	0.0873
δ	0.5	0.3425
ω	0.06	0.0547
$(\lambda_1, \lambda_2, \lambda_3)$	$(0.01, 0.1, 10)$	$(0.0999,\ 0.0501,\ 38.8542)$
$(\kappa_1, \kappa_2, \kappa_3)$	$(0.001, 0.001, 10)$	$(0.0021,\ 0.0125,\ 66.6652)$

Table 6.1: Parameter values used in the simulations of system (6.3).

The parameters of the generalized SEIR model (6.3) were calculated simultaneously by the nonlinear least squares method [69]. These parameters over the period starting from 1$^{\text{st}}$ November 2020 till 31$^{\text{th}}$ January 2021.

In Figure 6.3 we show the recovery rate $\lambda(t)$ and the mortality rate $\kappa(t)$.

We fixed $w_1 = w_2 = 1$. The numerical solutions to the nonlinear differential equations that represent the generalized SEIR model (6.3), the generalized SEIR model with vaccination (6.7), and the real data of the quarantined, recovered and death cases, from 1$^{\text{st}}$ November till 6$^{\text{th}}$ December 2021, are shown in Figure 6.4.

In Figure 6.5 we present the optimal control (6.15)–(6.16) and the number of vaccines used starting from 1$^{\text{st}}$ November 2020 till 31$^{\text{th}}$ January 2021.

The orange curves in Figure 6.4 represent the real data for the number of quarantine, recovery, and death cases in Italy starting from 1$^{\text{st}}$ November till 6$^{\text{th}}$ December 2020. The red curves in Figure 6.4 represent the solutions of the generalized SEIR model (6.3) without vaccination, and they simulate what happened from the beginning of November to the end of January. There is an increase in the number of the recovered, death and insusceptible cases that reach, respectively, 1830000, 74050 and 58130000

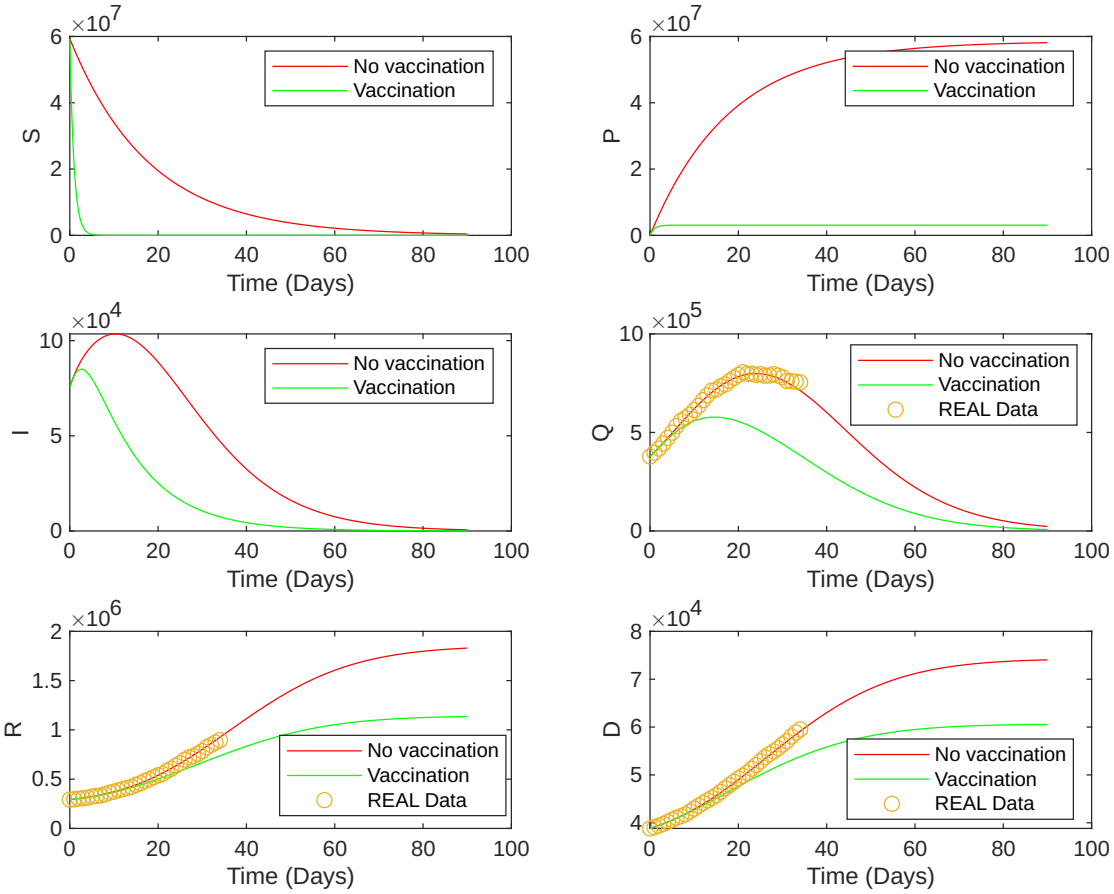

Figure 6.4: The solutions of the generalized SEIR models (6.3) and (6.7), respectively without and with vaccination, and real data of Italy from 1$^{\text{st}}$ November till 6$^{\text{th}}$ December 2021 with total population of $N = 60480000$.

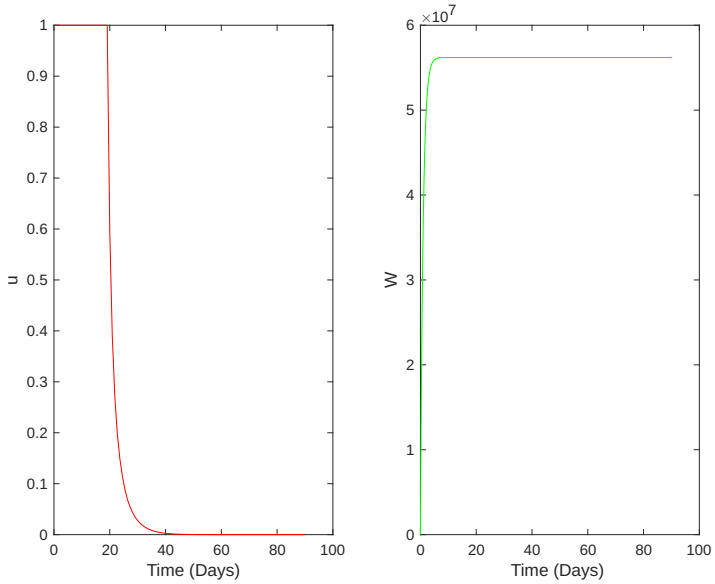

Figure 6.5: The optimal control $\tilde{u}$ (left) and the number of vaccines $W(t)$ (right).

cases. The red curves for both the number of infected and quarantined individuals have their higher limit values of 103500 cases on 11^{th} November and 798500 on 25^{th} November, respectively, reaching the values 614 and 22640 cases on 31^{th} January 2021, respectively. We note that the number of susceptible individuals gradually decrease, reaching 416600 cases at the end of January 2021.

The green curves in Figure 6.4 represent the solutions of the generalized SEIR model (6.7) with vaccination, and they simulate what happened from the beginning of November to the end of January. There is an increase in the number of recovered, death and insusceptible cases that reach, respectively, 1135000, 60560 and 3076000 cases. The green curves for both the number of infected and quarantined individuals have their higher limit values of 84800 cases on 4^{th} November and 577600 cases on 15^{th} November, respectively, reaching 55 and 7237 cases on 31^{th} January 2021, respectively. We note that the number of susceptible individuals decrease rapidly reaching 0 cases on 19^{th} November 2020.

The red curve in Figure 6.5 shows that the optimal vaccination of 100 percent of the susceptible individuals takes 19 days, followed by a rapid decrease in the number of susceptible individuals, which means they move to the class of vaccinated. The green curve in Figure 6.5 shows the necessary number of vaccines to eliminate COVID-19, which is estimated at 56200100 doses. The total number of vaccinated and insusceptible individuals equal to 59276100 of the total Italian population of 60480000.

6.7 Conclusion

Our results show the importance of the vaccine for COVID-19 control and also the best result that could be obtained if the number of available vaccines satisfies the needs of the population and are distributed according with the theory of optimal control.

In this chapter, our optimal control problem has only one control: the vaccine. In reality, there are several other factors to have into account and other variables to control. In a future work, we would like to use the support maximum principle [85], as well as the hybrid direction method [33], to elaborate a primal-dual method for solving a more realistic optimal control problem, in presence of multiple inputs [86].

References

[1] L. S. Pontryagin, V. G. Boltyanskii, R. V. Gamkrelidze, and E. F. Mishchenko, *The mathematical theory of optimal processes.* K. N. Trirogoff and L. W. Neustadt, Eds. Interscience Publishers John Wiley & Sons, Inc., New York-London, 1962.

[2] A. S. Evers, M. Maze, and E. D. Kharasch, *Anesthetic pharmacology: basic principles and clinical practice*. 2nd edition, Cambridge University Press, Cambridge, 2011.

[3] N. Singh *et al.*, "The effects of the type of anesthesia on outcomes of lower extremity infrainguinal bypass," *Journal of Vascular Surgery*, vol. 44, no. 5, pp. 964–970, 2006. DOI: https://doi.org/10.1016/j.jvs.2006.06.035.

[4] A. F. Merry and S. J. Mitchell, "Complications of anaesthesia," *Anaesthesia*, vol. 73, no. S1, pp. 7–11, 2018. DOI: https://doi.org/10.1111/anae.14135.

[5] C. L. Beck, "Modeling and control of pharmacodynamics," *European Journal of Control*, vol. 24, no. 2, pp. 33–49, 2015. DOI: https://doi.org/10.1016/j.ejcon.2015.04.006.

[6] H. Derendorf and B. Meibohm, "Modeling of pharmacokinetic/pharmacodynamic (PK/PD) relationships: Concepts and perspectives," *Pharm Res*, vol. 16, pp. 176–185, 1999. DOI: https://doi.org/10.1023/A:1011907920641.

[7] A. R. Absalom, V. Mani, T. D. Smet, and M. M. R. F. Struys, "Pharmacokinetic models for propofol defining and illuminating the devil in the detail," *Br. J. Anaesth.*, vol. 103, no. 1, pp. 26–37, 2009. DOI: https://doi.org/10.1093/bja/aep143.

[8] M. Enlund, "Tci : Target controlled infusion, or totally confused infusion? call for an optimised population based pharmacokinetic model for propofol," *Upsala J. Med. Sci.*, vol. 113, no. 2, pp. 161–170, 2008. DOI: https://doi.org/10.3109/2000-1967-222.

[9] T. A. Oshin, "Exploratory mathematical frameworks and design of control systems for the automation of propofol anesthesia," *Int. J. Dyn. Control*, vol. 10, no. 6, pp. 1858–1875, 2022. DOI: https://doi.org/10.1007/s40435-022-00953-1.

[10] X. Wu, H. Zhang, and J. Li, "An analytical approach of one-compartmental pharmacokinetic models with sigmoidal hill elimination," *Bull. Math. Biol.*, vol. 84, no. 2022, pp. 117–143, 2022. DOI: https://doi.org/10.1007/s11538-022-01078-4.

[11] C. K. Nanditha and M. P. Rajan, "An adaptive pharmacokinetic optimal control approach in chemotherapy for heterogeneous tumor," *J. Biol. Systems*, vol. 30, no. 3, pp. 529–551, 2022. DOI: https://doi.org/10.1142/S0218339022500188.

[12] J. J. Wang, Z. Dai, W. Zhang, and J. J. Shi, "Operating room scheduling for non-operating room anesthesia with emergency uncertainty," *Ann. Oper. Res.*, vol. 321, no. 1-2, pp. 565–588, 2023. DOI: https://doi.org/10.1007/s10479-022-04870-6.

[13] T. W. Schniderand, C. F. Minto, P. L. Gambus, *et al.*, "The influence of method of administration and covariates on the pharmacokinetics of propofol in adult volunteers," *Anesthesiology*, vol. 88, no. 5, pp. 1170–1182, 1998. DOI: https://doi.org/10.1097/00000542-199805000-00006.

[14] B. Marsh, M. White, N. Morton, and G. N. Kenny, "Pharmacokinetic model driven infusion of propofol in children," *Br. J. Anaesth.*, vol. 67, pp. 41–48, 1991. DOI: https://doi.org/10.1093/bja/67.1.41.

[15] S. Zabi, I. Queinnec, S. Tarbouriech, G. Garcia, and M. Mazerolles, "New approach for the control of anesthesia based on dynamics decoupling," *IFAC-PapersOnLine*, vol. 48, no. 20, pp. 511–516, 2015. DOI: https://doi.org/10.1016/j.ifacol.2015.10.192.

[16] S. Zabi, I. Queinnec, G. Garcia, and M. Mazerolles, "Time-optimal control for the induction phase of anesthesia," *IFAC-PapersOnLine*, vol. 50, no. 1, pp. 12 197–12 202, 2017. DOI: https://doi.org/10.1016/j.ifacol.2017.08.2279.

[17] M. Ilyas, A. Khan, M. A. Khan, W. Xie, R. A. Riaz, and Y. Khan, "Observer design estimating the propofol concentration in PK/PD model with feedback control of anesthesia administration," *Arch. Control Sci.*, vol. 32(68), no. 1, pp. 85–103, 2022. DOI: https://doi.org/10.24425/acs.2022.140866.

[18] P. Agarwal, J. J. Nieto, M. Ruzhansky, and D. F. M. Torres, *Analysis of Infectious Disease Problems (COVID-19) and Their Global Impact, Infosys Science Foundation Series in Mathematical Sciences*. Springer, Singapore, 2021. DOI: https://doi.org/10.1007/978-981-16-2450-6.

[19] D. K. Bagal, A. Rath, A. Barua, and D. Patnaik, "Estimating the parameters of susceptible–infected–recovered model of COVID-19 cases in india during lockdown periods," *Chaos Solitons Fractals*, vol. 140, p. 12, 2020. DOI: https://doi.org/10.1016/j.chaos.2020.110154.

[20] W. O. Kermack and A. G. McKendrick, "A contribution to the mathematical theory of epidemics," *Proc. R. Soc. Lond.*, vol. Ser. A 115, pp. 700–721, 1927. DOI: https://doi.org/10.1098/rspa.1927.0118.

[21] S. A. Lauer *et al.*, "The incubation period of coronavirus disease 2019 (COVID-19) from publicly reported confirmed cases: Estimation and application," *Annals of Internal Medicine*, vol. 172, no. 9, pp. 577–583, 2020. DOI: https://doi.org/10.7326/M20-0504.

[22] Q. Lin *et al.*, "A conceptual model for the coronavirus disease 2019 (COVID-19) outbreak in wuhan, china with individual reaction and governmental action," *International Journal of Infectious Diseases*, vol. 93, pp. 211–216, 2020. DOI: https://doi.org/10.1016/j.ijid.2020.02.058.

[23] A. Moussaoui and P. Auger, "Prediction of confinement effects on the number of COVID-19 outbreak in algeria," *Math. Model. Nat. Phenom.*, vol. 15, no. 37, p. 14, 2020. DOI: https://doi.org/10.1051/mmnp/2020028.

[24] Z. Zhao, X. Li, F. Liu, C. M. G. Zhu, and L. Wang, "Prediction of the COVID-19 spread in african countries and implications for prevention and control: A case study in south africa, egypt, algeria, nigeria, senegal and kenya," *Science of the Total Environment*, vol. 729, pp. 1–10, 2020. DOI: https://doi.org/10.1016/j.scitotenv.2020.138959.

[25] A. P. Lemos-Paião, C. J. Silva, and D. F. M. Torres, "A new compartmental epidemiological model for COVID-19 with a case study of portugal," *Ecological Complexity*, vol. 44, p. 8, 2020. DOI: https://doi.org/10.1016/j.ecocom.2020.100885.

[26] F. Ndaırou, I. Area, J. J. Nieto, C. J. Silva, and D. F. M. Torres, "Fractional model of COVID-19 applied to galicia, spain and portugal," *Chaos Solitons Fractals*, vol. 144, p. 7, 2021. DOI: https://doi.org/10.1016/j.chaos.2021.110652.

[27] H. Zine *et al.*, "A stochastic time-delayed model for the effectiveness of moroccan COVID-19 deconfinement strategy," *Math. Model. Nat. Phenom.*, vol. 15, no. 50, pp. 1–14, 2020. DOI: https://doi.org/10.1051/mmnp/2020040.

[28] L. Peng, W. Yang, D. Zhang, C. Zhuge, and L. Hong, "Epidemic analysis of COVID-19 in china by dynamical modeling," *preprint, arXiv:2002.06563v2*, vol. 1, pp. 1–11, 2020. DOI: https://doi.org/10.1101/2020.02.16.20023465.

[29] J. M. Bailey and W. M. Haddad, "Drug dosing control in clinical pharmacology," *IEEE Control Syst. Mag.*, vol. 25, no. 2, pp. 35–51, 2005. DOI: https://doi.org/10.1109/MCS.2005.1411383.

[30] W. P. T. James, "Research on obesity: A report of the dhss/mrc group," *Nutrition Bulletin*, vol. 4, no. 3, pp. 187–190, 1977. DOI: https://doi.org/10.1111/j.1467-3010.1977.tb00966.x.

[31] W. M. Haddad, V. Chellaboina, and Q. Hui, *Nonnegative and compartmental dynamical systems*. Princeton Univ. Press, Princeton, NJ, 2010.

[32] H. G. Bock and K. J. Plitt, "A multiple shooting algorithm for direct solution of optimal control problems," *IFAC Proceedings*, vol. 7, no. 2, pp. 1603–1608, 1984. DOI: https://doi.org/10.1016/S1474-6670(17)61205-9.

[33] M. A. Zaitri, M. O. Bibi, and M. Bentobache, "A hybrid direction algorithm for solving optimal control problems," *Cogent Math. Stat.*, vol. 6, no. 1, pp. 1–12, 2019. DOI: https://doi.org/10.1080/25742558.2019.1612614.

[34] P. Deuflhard, *Newton methods for nonlinear problems*. Springer Series in Computational Mathematics, Berlin, 2004.

[35] M. Elsisi and M. Soliman, "Optimal design of robust resilient automatic voltage regulators," *ISA Transactions*, vol. 108, pp. 257–268, 2021. DOI: https://doi.org/10.1016/j.isatra.2020.09.003.

[36] M. A. E. M. et al., "Optimal energy management solutions using artificial intelligence techniques for photovoltaic empowered water desalination plants under cost function uncertainties," *IEEE Access*, vol. 10, pp. 93 646–93 658, 2022. DOI: https://doi.org/10.1109/ACCESS.2022.3203692.

[37] V. F. Morales-Delgado, M. A. T.-H. C. Vargas-De-León, and J. F. Gómez-Aguilar, "Exact solutions to fractional pharmacokinetic models using multivariate mittag-leffler functions," *Chaos Solitons Fractals*, vol. 168, pp. 113–164, 2023. DOI: https://doi.org/10.1016/j.chaos.2023.113164.

[38] Y. Karaca and D. Baleanu, "Algorithmic complexity-based fractional-order derivatives in computational biology," in *Advances in Mathematical Modelling, Applied Analysis and Computation*, J. Singh, G. A. Anastassiou, D. Baleanu, C. Cattani, and D. Kumar, Eds., Singapore: Springer Nature Singapore, 2023, pp. 55–89.

[39] R. Magin, "Fractional calculus in bioengineering (part 1)," *Critical Reviews in Biomedical Engineering*, vol. 32, pp. 1–104, 2004. DOI: https://doi.org/10.1615/CritRevBiomedEng.v32.i1.10.

[40] A. A. Kilbas, H. M. . Srivastava, and J. J. Trujillo, *Theory and applications of fractional differential equations*. Elsevier Science Inc., New York, 2006, vol. 204.

[41] R. Almeida, "A caputo fractional derivative of a function with respect to another function," *Commun Nonlinear Sci Numer Simulats*, vol. 44, pp. 460–481, 2017. DOI: https://doi.org/10.1016/j.cnsns.2016.09.006.

[42] R. Gorenflo, A. A. Kilbas, F. Mainardi, and S. V. Rogosin, *Mittag–Leffler Functions and Related Topics and Applications*. Springer Berlin, Heidelberg, 2014. DOI: https://doi.org/10.1007/978-3-662-43930-2.

[43] S. Joshi, E. Mittal, and R. M. Pandey, "On euler type integrals involving extended mittag-leffler functions," *Bol. Soc. Parana. Mat.*, vol. 38, no. 2, pp. 125–134, 2017. DOI: https://doi.org/10.5269/bspm.v38i2.34829.

[44] F. Jarad and T. Abdeljawad, "Generalized fractional derivatives and laplace transform," *Discrete and Continuous Dynamical Systems*, vol. 13, no. 3, pp. 709–722, 2020. DOI: https://doi.org/10.3934/dcdss.2020039.

[45] J. Duan and L. Chen, "Solution of fractional differential equation systems and computation of matrix mittag-leffler functions," *Symmetry*, vol. 10, no. 10, No. 503, pp. 1–14, 2018. DOI: https://doi.org/10.3390/sym10100503.

[46] M. A. Zaitri, C. J. Silva, and D. F. M. Torres, "An analytic method to determine the optimal time for the induction phase of anesthesia," *Axioms*, vol. 9, no. 12, pp. 1–15, 2023. DOI: https://doi.org/10.3390/axioms12090867.

[47] J. Arino and P. van den Driessche, "Time delays in epidemic models, modeling and numerical considerations," *Delay Differential Equations and Applications*, pp. 539–578, 2006. DOI: https://doi.org/10.1007/1-4020-3647-7_13.

[48] C. J. Silva and H. Maurer, "Optimal control of hiv treatment and immunotherapy combination with state and control delays," *Optim. Control. Appl. Meth.*, vol. 41, pp. 537–554, 2020. DOI: https://doi.org/10.1002/oca.2558.

[49] C. J. Silva, H. Maurer, and D. F. M. Torres, "Optimal control of a tuberculosis model with state and control delays," *Math. Biosci. Eng.*, vol. 14, no. 1, pp. 321–337, 2017. DOI: https://doi.org/10.3934/mbe.2017021.

[50] S. Tipsri and W. Chinviriyasit, "The effect of time delay on the dynamics of an seir model with nonlinear incidence," *Chaos, Solitons & Fractals*, vol. 75, pp. 153–172, 2015. DOI: https://doi.org/10.1016/j.chaos.2015.02.017.

[51] P. E. Fine, "The interval between successive cases of an infectious disease," *Am. J. Epidemiol.*, vol. 158, pp. 1039–1047, 2003. DOI: https://doi.org/10.1093/aje/kwg251.

[52] X. He *et al.*, "Temporal dynamics in viral shedding and transmissibility of COVID-19," *Nat. Med.*, vol. 26, pp. 672–675, 2020. DOI: https://doi.org/10.1038/s41591-020-0869-5.

[53] H. Xin *et al.*, "Estimating the latent period of coronavirus disease 2019 (COVID-19)," *Clin. Infect. Dis.*, vol. 74, no. 9, pp. 1678–1681, 2022. DOI: https://doi.org/10.1093/cid/ciab746.

[54] W. H. O. WHO, "Novel coronavirus (2019-ncov): Situation report-7," 2020. DOI: https://apps.who.int/iris/handle/10665/330771.

[55] C. P. Muller, "Do asymptomatic carriers of SARS-COV-2 transmit the virus?" *The Lancet Regional Health - Europe*, vol. 4, 2021. DOI: https://doi.org/10.1016/j.lanepe.2021.100082.

[56] M. A. Zaitri, C. J. Silva, and D. Torres, "Stability analysis of delayed COVID-19 models," *Axioms*, vol. 11, no. 8, pp. 1–21, 2022. DOI: https://doi.org/10.3390/axioms11080400.

[57] G. Giordano *et al.*, "Modelling the COVID-19 epidemic and implementation of population-wide interventions in italy," *Nat. Med.*, vol. 26, pp. 855–860, 2020. DOI: https://doi.org/10.1038/s41591-020-0883-7.

[58] Z. Liu *et al.*, "A COVID-19 epidemic model with latency period," *Infectious Disease Modelling*, vol. 5, pp. 323–337, 2020. DOI: https://doi.org/10.1016/j.idm.2020.03.003.

[59] R. Anderson and R. May, *Infectious Diseases of Humans Dynamics and Control*. University Press, Oxford, 1991.

[60] S. Wiggins, *Introduction to Applied Nonlinear Dynamical Systems and Chaos*. Springer, Berlin, 1990.

[61] P. van den Driessche and J. Watmough, "Reproduction numbers and sub-threshold endemic equilibria for compartmental models of disease transmission," *Math. Biosci.*, vol. 180, no. 1–2, pp. 29–48, 2002. DOI: https://doi.org/10.1016/S0025-5564(02)00108-6.

[62] A. P. Lemos-Paião, C. J. Silva, and F. Torres, "A cholera mathematical model with vaccination and the biggest outbreak of world's history," *AIMS Mathematics*, vol. 3, no. 4, pp. 448–463, 2018. DOI: https://doi.org/10.3934/Math.2018.4.448.

[63] J. W. Rogers, "Locations of roots of polynomials," *SIAM Review*, vol. 25, no. 3, pp. 327–342, 1983. DOI: https://doi.org/10.1137/1025075.

[64] Y. Kuang, *Delay differential equations with applications in population dynamics*. Academic Press, 2012.

[65] S. I. Niculescu, *Delay effects on stability*. Lecture Notes in Control and Information Sciences,Springer-Verlag London, Ltd., 2001.

[66] L. F. Shampine and M. W. Reichelt, "The matlab ode suite," *SIAM J. Sci. Comput.*, vol. 18, no. 1, pp. 1–22, 1997. DOI: https://doi.org/10.1137/S1064827594276424.

[67] C. J. Silva *et al.*, "Complex network model for COVID-19: Human behavior, pseudo-periodic solutions and multiple epidemic waves," *J. Math. Anal. Appl.*, vol. 514, no. 2, p. 25, 2022. DOI: https://doi.org/10.1016/j.jmaa.2021.125171.

[68] U. Nations, "The 2022 revision of world population prospects," 2022. DOI: https://population.un.org/wpp/.

[69] E. Cheynet, "Generalized seir epidemic model (fitting and computation)," *Zenodo*, 2020. DOI: https://doi.org/10.5281/ZENODO.3911854.

[70] R. Lu *et al.*, "Genomic characterisation and epidemiology of 2019 novel coronavirus: Implications for virus origins and receptor binding," *The Lancet*, vol. 395, no. 10224, pp. 565–574, 2020. DOI: https://doi.org/10.1016/S0140-6736(20)30251-8.

[71] M. A. Zaitri, M. O. Bibi, and D. F. M. Torres, "Optimal control to limit the spread of COVID-19 in italy," *Kuwait J. Sci.*, vol. Special issue, pp. 1–14, 2021. DOI: https://doi.org/10.48129/kjs.splcov.13961.

[72] C. Barril, A. Calsina, S. Cuadrado, and J. Ripoll, "On the basic reproduction number in continuously structured populations," *Math. Methods Appl. Sci*, vol. 44, no. 1, pp. 799–812, 2021. DOI: https://doi.org/10.1002/mma.6787.

[73] M. Porta, *Optimization–theory and applications*. Springer-Verlag, 1983.

[74] M. Alipour, "Numerical study on multi-order multi-dimensional fractional optimal control problem in general form," *Kuwait J. Sci.*, vol. 44, no. 3, pp. 9–19, 2017. DOI: https://doi.org/10.48129/kjs.online..

[75] C. J. Silva *et al.*, "Optimal control of the COVID-19 pandemic: Controlled sanitary deconfinement in portugal," *Scientific Reports*, vol. 11, p. 15, 2021. DOI: https://doi.org/10.1038/s41598-021-83075-6.

[76] M. Zamir, T. Abdeljawad, F. Nadeem, A. Wahid, and A. Yousef, "An optimal control analysis of a COVID-19 model," *Alexandria Engineering Journal*, vol. 60, no. 3, pp. 2875–2884, 2021. DOI: https://doi.org/10.1016/j.aej.2021.01.022.

[77] A. Boukhouima *et al.*, "Stability analysis and optimal control of a fractional hiv-aids epidemic model with memory and general incidence rate," *Eur. Phys. J. Plus*, vol. 136, no. 130, pp. 1–20, 2021. DOI: https://doi.org/10.1140/epjp/s13360-020-01013-3.

[78] F. Ndaırou and D. F. M. Torres, "Mathematical analysis of a fractional COVID-19 model applied to wuhan, spain and portugale," *Axioms*, vol. 10, no. 3, pp. 1–13, 2021. DOI: https://doi.org/10.3390/axioms10030135.

[79] E. Edward *et al.*, "Safety and immunogenicity of two rna-based COVID-19 vaccine candidates," *N. Engl. J. Med.*, vol. 383, no. 25, pp. 2439–2450, 2020. DOI: https://doi.org/10.1056/NEJMoa2027906.

[80] F. P. Polack *et al.*, "Safety and efficacy of the bnt162b2 mrna COVID-19 vaccine," *N. Engl. J. Med.*, vol. 383, no. 16, pp. 2603–2615, 2020. DOI: https://doi.org/10.1056/NEJMoa2034577.

[81] A. B. Vogel *et al.*, "A prefusion sars-cov-2 spike rna vaccine is highly immunogenic and prevents lung infection in non-human primates," *bioRxiv*, 2020. DOI: https://doi.org/10.1101/2020.09.08.280818.

[82] M. O. Necati, *Heat Conduction*. Interscience Publishers John Wiley & Sons, Inc. New York, 1993.

[83] M. Shashkov and S. Steinberg, "Solving diffusion equations with rough coefficients in rough grids," *Journal of Computational Physics*, vol. 129, no. 2, pp. 383–405, 1996. DOI: https://doi.org/10.1006/jcph.1996.0257.

[84] M. A. Zaitri, M. O. Bibi, and D. F. M. Torres, *Transport and optimal control of vaccination dynamics for COVID-19*. Chapter of Book : Mathematical Analysis of Infectious Diseases, 1 st Edition, ELSEVIER, 2022, pp. 27–39. DOI: https://doi.org/10.1016/B978-0-32-390504-6.00007-3.

[85] M. O. Bibi, *Methods for solving linear-quadratic problems of optimal control, PhD thesis in Applied Mathematics*. University of Minsk, 1985.

[86] N. Khimoum and M. O. Bibi, "Primal-dual method for solving a linear-quadratic multi-input optimal control problem," *Optimization Letters*, vol. 14, pp. 653–669, 2020. DOI: https://doi.org/10.1007/s11590-018-1375-2.

APPENDIX A

Recovered individuals

In Tables A.1 and A.2 we show the real data of recovered individuals from COVID-19 in Italy, in September and October 2020, respectively, versus the number of recovered individuals predicted by the model of Peng et al. [28] and the improvement one could have done by introducing suitable controls as explained in Section 5.3 and using the theory of optimal control as in Section 5.4.

Table A.1: Real data of Recovered individuals ($R(t)$) from COVID-19, Italy, September 2020 versus number of $R(t)$ predicted by SEIR-type model (5.1) and controlled model (5.5). We also indicate the percentage of relative error η_R between real data and the one predicted by model (5.1); and the improvement $\mathcal{I}_R$ (increase of recovered individuals with respect to real data) by introducing controls u_1, u_2 and u_3 as in (5.5) in an optimal control way.

Day	Real R	R by (5.1)	R by(5.5)	η_R	$\mathcal{I}_R$
01	207944	207944	207944	0%	0%
02	208201	207947	225126	0.12 %	08.12%
03	208490	207953	231873	0.25%	11.21%
04	209027	207966	234737	0.50%	12.29%
05	209610	207996	236134	0.77%	12.65%
06	210015	208060	236956	0.93%	12.82%
07	210238	208187	237538	0.97%	12.98%
08	210801	208409	238005	1.13%	12.90%
09	211272	208744	238409	1.19%	12.84%
10	211885	209176	238769	1.27%	12.68%
11	212432	209672	239096	1.29%	12.55%
12	213191	210206	239395	1.40%	12.29%
13	213634	210759	239672	1.34%	12.18%
14	213950	211324	239930	1.22%	12.14%
15	214645	211897	240170	1.28%	11.89%
16	215265	212477	240396	1.29%	11.67%
17	215954	213063	240609	1.33%	11.41%
18	216807	213657	241003	1.45%	11.16%
19	217716	214260	241186	1.58%	10.78%
20	218351	214873	241363	1.59%	10.53%
21	218703	215498	241696	1.46%	10.51%
22	219670	216136	241855	1.60%	10.09%
23	220665	216790	242009	1.75%	9.67%
24	221762	217460	242160	1.93%	9.19%
25	222716	218150	242306	2.05%	8.79%
26	223693	218861	242450	2.16%	8.38%
27	224417	219596	242591	2.14%	8.09%
28	225190	220358	242730	2.14%	7.78%
29	226506	221149	242866	2.36%	7.22%
30	227704	221973	243000	2.51%	6.71%

Table A.2: Real data of Recovered individuals ($R(t)$) from COVID-19, Italy, October 2020 versus number of $R(t)$ predicted by SEIR-type model (5.1) and controlled model (5.5). We also indicate the percentage of relative error η_R between real data and the one predicted by model (5.1); and the improvement $\mathcal{I}_R$ (increase of recovered individuals with respect to real data) by introducing controls u_1, u_2 and u_3 as in (5.5) in an optimal control way.

Day	Real R	R by (5.1)	R by (5.5)	η_R	$\mathcal{I}_R$
01	222832	224334	243132	0.67%	9.11%
02	229970	223731	243263	2.71%	5.78%
03	231217	224672	243392	2.83%	5.26%
04	231914	225662	243520	2.69%	5.00%
05	232681	226703	243647	2.56%	4.71%
06	234099	227801	243772	2.69%	4.13%
07	235303	228961	243896	2.69%	3.65%
08	236363	230188	244019	2.61%	3.23%
09	237549	231490	244141	2.55%	2.77%
10	238525	232871	244263	2.37%	2.40%
11	239709	234341	244383	2.23%	1.94%
12	240600	235905	244503	1.95%	1.62%
13	242028	237573	244622	1.84%	1.07%
14	244065	239353	244740	1.93%	0.27%
15	245964	241255	244857	1.91%	0.45%
16	247872	243290	244974	1.84%	1.16%
17	249127	245468	245089	1.46%	1.62%
18	251461	247802	245205	1.45%	2.48%
19	252959	250305	245319	1.04%	3.02%
20	255005	252990	245433	0.79%	3.75%
21	257374	255872	245547	0.58%	4.59%
22	259456	258968	245659	0.18%	5.31%
23	261808	262296	245771	0.18%	6.12%
24	264117	265872	245883	0.66%	6.90%
25	266203	269718	245994	1.32%	7.59%
26	268626	273855	246104	1.94%	8.38%
27	271988	278306	246214	2.32%	9.47%
28	275404	283094	246324	2.79%	10.55%
29	279282	288247	246401	3.21%	11.77%

APPENDIX B

Deaths

In Tables B.1 and B.2 we show the real data of death individuals from COVID-19 in Italy, in September and October 2020, respectively, versus the number of death individuals predicted by the model of Peng et al. [28] and the improvement one could have done by introducing suitable controls as explained in Section 5.3 and using the theory of optimal control as in Section 5.4.

Table B.1: Real data of Death individuals ($D(t)$) from COVID-19, Italy, September 2020 versus number of $D(t)$ predicted by SEIR-type model (5.1) and controlled model (5.5). We also indicate the percentage of relative error η_D between real data and the one predicted by model (5.1); and the improvement $\mathcal{I}_D$ (decrease of death individuals with respect to real data) by introducing controls u_1, u_2 and u_3 as in (5.5) in an optimal control way.

Day	Real D	D by (5.1)	D by (5.5)	η_D	$\mathcal{I}_D$
01	35491	35491	35491	0%	0%
02	35497	35495	35493	0.005%	0.01%
03	35518	35500	35494	0.05%	0.06%
04	35533	35505	35495	0.07%	0.07%
05	35541	35510	35495	0.08%	0.12%
06	35553	35515	35495	0.10%	0.16%
07	35563	35521	35495	0.11%	0.19%
08	35577	35526	35496	0.14%	0.22%
09	35587	35532	35496	0.15%	0.25%
10	35597	35538	35496	0.16%	0.28%
11	35603	35544	35496	0.16%	0.30%
12	35610	35550	35496	0.16%	0.32%
13	35624	35556	35496	0.19%	0.35%
14	35633	35563	35496	0.19%	0.38%
15	35645	35570	35496	0.21%	0.41%
16	35658	35576	35496	0.22$	0.45%
17	35668	35583	35496	0.23%	0.48%
18	35692	35591	35496	0.28%	0.54%
19	35707	35598	35496	0.30%	0.59%
20	35724	35606	35496	0.33%	0.63%
21	35738	35614	35496	0.34%	0.67%
22	35758	35622	35496	0.38%	0.73%
23	35781	35630	35496	0.42%	0.79%
24	35801	35640	35496	0.44%	0.85%
25	35818	35648	35496	0.47%	0.89%
26	35835	35658	35496	0.49%	0.94%
27	35851	35668	35496	0.51%	0.99%
28	35875	35680	35497	0.54%	1.05%
29	35894	35690	35497	0.56%	1.10%
30	35918	35702	35497	0.60%	1.17%

Table B.2: Real data of Death individuals ($D(t)$) from COVID-19, Italy, October 2020 versus number of $D(t)$ predicted by SEIR-type model (5.1) and controlled model (5.5). We also indicate the percentage of relative error η_D between real data and the one predicted by model (5.1); and the improvement $\mathcal{I}_D$ (decrease of death individuals with respect to real data) by introducing controls u_1, u_2 and u_3 as in (5.5) in an optimal control way.

Day	Real D	D by (5.1)	D by (5.5)	η_D	$\mathcal{I}_D$
01	35941	35715	35497	0%	0%
02	35968	35728	35497	0.66%	1.30%
03	35986	35742	35497	0.67%	1.35%
04	36002	35757	35497	0.68%	1.40%
05	36030	35773	35497	0.71%	1.47%
06	36061	35790	35497	0.75%	1.56%
07	36083	35808	35497	0.76%	1.62%
08	36111	35827	35497	0.78%	1.70%
09	36140	35848	35497	0.80%	1.77%
10	36166	35870	35497	0.81%	1.84%
11	36205	35894	35497	0.85%	1.95%
12	36246	35920	35497	0.89%	2.06%
13	36289	35947	35497	0.94%	2.18%
14	36372	35976	35497	1.08%	2.40%
15	36427	36008	35497	1.15%	2.55%
16	36474	36042	35497	1.18%	2.67%
17	36543	36078	35497	1.27%	2.86%
18	36616	36118	35497	1.36%	3.05%
19	36705	36160	35497	1.48%	3.29%
20	36832	36206	35497	1.69%	3.62%
21	36968	36255	35497	1.92%	3.97%
22	37059	36307	35497	2.02%	4.21%
23	37210	36364	35497	2.27%	4.60%
24	37338	36425	35497	2.44%	4.93%
25	37479	36491	35497	2.63%	5.28%
26	37700	36638	35497	2.81%	5.84%
27	37905	36720	35498	3.12%	6.35%
28	38122	36902	35498	3.20%	6.88%
29	38321	37003	35498	3.43%	7.36%

APPENDIX C

Quarantine

In Tables C.1 and C.2 we show the real data of quarantined individuals from COVID-19 in Italy, in September and October 2020, respectively, versus the number of quarantined individuals predicted by the model of Peng et al. [28] and the improvement one could have done by introducing suitable controls as explained in Section 5.3 and using the theory of optimal control as in Section 5.4.

Table C.1: Real data of Quarantined individuals ($Q(t)$) from COVID-19, Italy, September 2020 versus number of $Q(t)$ predicted by SEIR-type model (5.1) and controlled model (5.5). We also indicate the percentage of relative error η_Q between real data and the one predicted by model (5.1); and the improvement $\mathcal{I}_Q$ (decrease of quarantined individuals with respect to real data) by introducing controls u_1, u_2 and u_3 as in (5.5) in an optimal control way.

Day	Real Q	Q by (5.1)	Q by (5.5)	η_Q	$\mathcal{I}_Q$
01	26754	26754	26754	0 %	0 %
02	27817	27472	10292	01.24%	63.00%
03	28915	28120	4188	02.74%	85.51%
04	30099	28715	1901	04.59%	93.68%
05	31194	29264	1023	06.18%	96.69%
06	32078	29763	668	07.21%	97.91%
07	32993	30197	509	08.47%	98.45%
08	33789	30789	426	08.87%	98.73%
09	34734	30964	374	10.85%	98.92%
10	35708	31105	337	12.89%	99.05%
11	36767	31246	307	15.01%	99.16%
12	37503	31412	282	16.24%	99.24%
13	38509	31617	261	17.89%	99.32%
14	39187	31872	244	18.66%	99.37%
15	39712	32183	228	18.95%	99.42%
16	40532	32557	215	19.67%	99.46%
17	41413	33000	203	20.31%	99.50%
18	42457	33519	193	21.05%	99.54%
19	43161	34119	184	20.94%	99.57%
20	44098	34808	176	21.06%	99.60%
21	45079	35593	169	21.04%	99.62%
22	45489	36480	163	19.80%	99.64%
23	46114	37479	158	18.72%	99.65%
24	46780	38599	153	17.48%	99.67%
25	47718	39848	149	16.49%	99.68%
26	48593	41237	145	15.13%	99.70%
27	49618	42777	142	13.78%	99.71%
28	50323	44480	139	11.61%	99.72%
29	50630	46359	137	08.43%	99.72%
30	51263	48428	134	05.53%	99.73%

Table C.2: Real data of Quarantined individuals ($Q(t)$) from COVID-19, Italy, October 2020 versus number of $Q(t)$ predicted by SEIR-type model (5.1) and controlled model (5.5). We also indicate the percentage of relative error η_Q between real data and the one predicted by model (5.1); and the improvement $\mathcal{I}_Q$ (decrease of quarantined individuals with respect to real data) by introducing controls u_1, u_2 and u_3 as in (5.5) in an optimal control way.

Day	Real Q	Q by (5.1)	Q by (5.5)	η_Q	$\mathcal{I}_Q$
01	52647	50023	130	04.98%	99.75%
02	53997	53197	129	01.48%	99.76%
03	55566	55931	127	00.65%	99.77%
04	57429	58922	126	02.59%	99.78%
05	58903	62193	124	05.58%	99.78%
06	60134	65764	123	09.36%	99.79%
07	62576	69659	122	11.31%	99.80%
08	59526	73904	121	24.15%	99.79%
09	70110	78527	120	12.00%	99.82%
10	74829	83557	119	11.63%	99.84%
11	79075	89027	118	12.58%	99.85%
12	82764	94972	118	14.75%	99.85%
13	87193	101428	117	16.32%	99.86%
14	92445	108435	117	17.29%	99.87%
15	99266	116035	116	16.89%	99.88%
16	107312	124275	115	15.80%	99.89%
17	116935	133204	114	13.91%	99.90%
18	126237	142876	114	13.18%	99.90%
19	134003	153344	113	14.43%	99.91%
20	142739	164668	112	15.36%	99.92%
21	155442	176913	112	13.81%	99.92%
22	169302	190145	111	12.31%	99.93%
23	186002	204439	111	09.91%	99.94%
24	203182	219871	110	08.21%	99.94%
25	222241	236520	109	06.42%	99.95%
26	236684	254470	109	07.51%	99.95%
27	255090	273812	108	07.33%	99.95%
28	276457	294640	107	06.57%	99.96%
29	299191	317055	107	05.97%	99.96%